

JAERI - M  
91-011

NEANDC(J)-157/U  
INDC(JPN)-145/L

EVALUATION OF NEUTRON NUCLEAR DATA OF  
NATURAL SILVER AND ITS ISOTOPES

February 1991

LIU Ting-jin\*, Keiichi SHIBATA and Tsuneo NAKAGAWA

日本原子力研究所  
Japan Atomic Energy Research Institute

JAERI-M レポートは、日本原子力研究所が不定期に公刊している研究報告書です。  
入手の問合せは、日本原子力研究所技術情報部情報資料課（〒319-11茨城県那珂郡東海村）あて、お申しこしください。なお、このほかに財團法人原子力弘済会資料センター（〒319-11 茨城県那珂郡東海村日本原子力研究所内）で複写による実費頒布をおこなっております。

JAERI-M reports are issued irregularly.  
Inquiries about availability of the reports should be addressed to Information Division  
Department of Technical Information, Japan Atomic Energy Research Institute, Tokaimura,  
Naka-gun, Ibaraki-ken 319-11, Japan.

Evaluation of Neutron Nuclear Data of  
Natural Silver and Its Isotopes

LIU Ting-jin\*, Keiichi SHIBATA and Tsuneo NAKAGAWA

Department of Physics  
Tokai Research Establishment  
Japan Atomic Energy Research Institute  
Tokai-mura, Naka-gun, Ibaraki-ken

(Received January 24, 1991)

Neutron nuclear data of natural silver and its isotopes ( $^{107}\text{Ag}$  and  $^{109}\text{Ag}$ ) have been evaluated in the energy range from  $10^{-5}$  eV to 20 MeV. Evaluated quantities are the total, elastic and inelastic scattering, capture,  $(n,2n)$ ,  $(n,3n)$ ,  $(n,p)$ ,  $(n,\alpha)$ ,  $(n,np)$ ,  $(n,n\alpha)$  reaction and gamma-ray production cross sections, the resonance parameters and the angular and energy distributions of emitted neutrons and gamma-rays. The evaluation is based on available experimental data and theoretical calculations. The experimental data were carefully examined and selected. Multi-step Hauser-Feshbach calculation played an important role in the determination of the reaction cross sections. The precompound process was taken into account above 5 MeV, in addition to the compound one. The evaluated data have been compiled into JENDL-3 in the ENDF-5 format.

Keywords: Evaluation, Silver, Neutron Nuclear Data, JENDL-3,  
Hauser-Feshbach Calculation, Cross Section, Resonance  
Parameter, Angular Distribution, Energy Distribution

---

\* Institute of Atomic Energy, Beijing, The People's Republic of China

天然銀およびその同位元素の中性子核データの評価

日本原子力研究所東海研究所物理部  
劉 廷進\*・柴田 恵一・中川 庸雄

(1991年1月24日受理)

天然銀およびその同位元素 ( $^{107}\text{Ag}$  と  $^{109}\text{Ag}$ ) の中性子核データを,  $10^{-5}\text{eV}$  から  $20\text{MeV}$  までのエネルギー範囲で評価した。評価した物理量は、全断面積、弾性・非弾性散乱断面積、捕獲反応断面積、 $(n,2n)$  反応断面積、 $(n,3n)$  反応断面積、 $(n,p)$  反応断面積、 $(n\alpha)$  反応断面積、 $(n,np)$  反応断面積、 $(n,n\alpha)$  反応断面積、ガンマ線生成断面積、共鳴パラメータそして放出中性子とガンマ線の角度およびエネルギー分布である。本評価は、利用可能な実験値及び理論値を基に行った。実験値は、慎重に吟味、選別した。また、多段階 Hauser-Feshbach 理論による計算は、反応断面積を決定する上で重要な役割を果たした。 $5\text{ MeV}$  以上のエネルギーでは、複合核過程に加えて前平衡過程も考慮して計算を行った。評価済みデータは、ENDF-5 フォーマットで編集し、JENDL-3 に収納した。

## Contents

1. Introduction .....	1
2. Status of Experimental Data .....	2
2.1 Total Cross Section .....	2
2.2 Capture Cross Section .....	2
2.3 Inelastic Scattering Cross Section .....	2
2.4 ( $n,2n$ ) and ( $n,3n$ ) Reaction Cross Sections .....	3
2.5 ( $n,p$ ) Reaction Cross Section .....	3
2.6 ( $n,\alpha$ ) Reaction Cross Section .....	4
3. Theoretical Calculation .....	4
3.1 Computational Methods and Procedures .....	4
3.2 Parameter Determination .....	4
3.2.1 Optical-Model Potentials .....	4
3.2.2 Discrete Levels and Level Density .....	5
3.2.3 Giant Dipole Resonances .....	6
3.3 Calculated Results .....	6
4. Evaluated Data .....	7
4.1 Resonance Parameters .....	7
4.2 Cross Sections Above Resonance Region .....	8
4.3 Other Quantities .....	9
4.3.1 Energy and Angular Distributions of Emitted Neutrons ...	9
4.3.2 Gamma-Ray Production Cross Sections .....	9
5. Concluding Remarks .....	10
Acknowledgments .....	10
References .....	11

## 目 次

1.はじめに.....	1
2.実験データの現状.....	2
2.1 全断面積 .....	2
2.2 捕獲断面積 .....	2
2.3 非弾性散乱断面積 .....	2
2.4 $(n, 2n), (n, 3n)$ 反応断面積 .....	3
2.5 $(n, p)$ 反応断面積 .....	3
2.6 $(n, \alpha)$ 反応断面積 .....	4
3.理論計算.....	4
3.1 計算方法 .....	4
3.2 パラメータの決定 .....	4
3.2.1 光学ポテンシャル .....	4
3.2.2 離散準位と準位密度 .....	5
3.2.3 巨大双極子共鳴 .....	6
3.3 計算結果 .....	6
4.評価値.....	7
4.1 共鳴パラメータ .....	7
4.2 共鳴領域以上の断面積 .....	8
4.3 他の物理量 .....	9
4.3.1 放出中性子の角度及びエネルギー分布 .....	9
4.3.2 ガンマ線生成断面積 .....	9
5.緒言.....	10
謝辞.....	10
参考文献.....	11

## 1. Introduction

Neutron nuclear data of silver are important for nuclear applications. Stable isotopes  $^{107}\text{Ag}$  and  $^{109}\text{Ag}$  are formed as fission products in fission reactors. The threshold reactions such as ( $n,2n$ ) and ( $n,p$ ) are useful for dosimetry in fusion reactors. The second version of Japanese Evaluated Nuclear Data Library (JENDL-2) contains  $^{107}\text{Ag}$  and  $^{109}\text{Ag}$  data in the fission-product file. In the JENDL-2 evaluation, much emphasis was placed on the low-energy portion of isotopic data, and the accuracy of the cross sections in the MeV region is rather poor. Furthermore, JENDL-2 did not include the cross sections for the threshold reactions on silver.

The present work was attempted for the third version of JENDL (JENDL-3), which is applicable to fusion reactor calculation as well as thermal reactor, fast reactor and shielding calculation. Evaluated are the total, elastic and inelastic scattering, capture, ( $n,2n$ ), ( $n,3n$ ), ( $n,p$ ), ( $n,\alpha$ ), ( $n,np$ ), ( $n,n\alpha$ ) reaction and gamma-ray production cross sections, the resonance parameters and the angular and energy distributions of emitted neutrons and gamma-rays. The target nuclides considered here are natural silver and its stable isotopes, i.e.,  $^{107}\text{Ag}$  and  $^{109}\text{Ag}$ , while the data of natural silver were not contained in JENDL-2. The Q-values of the various reactions were calculated from the mass table of Wapstra and Bos<sup>1)</sup>, and are given in Table 1, together with the isotopic abundances<sup>2)</sup> of  $^{107}\text{Ag}$  and  $^{109}\text{Ag}$ .

The present evaluation is based on recent experimental data and theoretical calculations. Chapter 2 deals with the status of experimental data above the keV region. The elastic scattering cross section is omitted in Chap. 2, since it is evaluated by subtracting all the other cross sections from the total cross section. The ( $n,np$ ) and ( $n,n\alpha$ ) reactions are also omitted in Chap. 2, because the measurements are very few. In Chap. 3, described is the theoretical calculation. Discussion is made on how the evaluated data file is constructed in Chap. 4.

The essence of the present evaluation was already published<sup>3)</sup>. This report is intended to provide more complete information for users of JENDL-3. The status of the presently evaluated quantities is given in Table 2.

## 2. Status of Experimental Data

### 2.1 Total Cross Section

For natural silver, there are more than twenty sets of experimental data. Transmission measurements were performed by Foster, Jr. and Glasgow<sup>4)</sup> and by Poenitz and Whalen<sup>5)</sup> in the energy ranges from 47 keV to 20 MeV and from 2 MeV to 15 MeV, respectively. Both measurements are consistent with each other in the overlapping energy region. In the range from 7 keV to 100 keV, there are four sets<sup>5-8)</sup> of measured data. The data of Newson et al.<sup>8)</sup> are lower than those of the others, as seen in Fig. 1. The measurements of Selove<sup>9)</sup> are also inconsistent with the those of Newson et al. around 5 keV. Moreover, the average cross section of the fine-resolution data of Garg et al.<sup>10)</sup> around 4 keV was found to be much larger than the data of Newson et al. Therefore, we disregarded the data of Newson et al. in the present evaluation.

Very scarce are the isotopic data. Smith et al.<sup>11)</sup> measured the total cross section of <sup>107</sup>Ag in the energy range from 250 keV to 4.5 MeV. The 14-MeV cross sections of both isotopes were measured by Dukarevich et al.<sup>12)</sup>

### 2.2 Capture Cross Section

There are more than twenty measurements of natural silver available for the evaluation up to 3 MeV. We selected fifteen sets<sup>13-27)</sup> of experimental data. The data of Diven et al.<sup>15)</sup> were renormalized by using the <sup>235</sup>U fission cross section of ENDF/B-V.

Eight sets<sup>20,27-33)</sup> of experimental data were selected for <sup>107</sup>Ag below 4 MeV. The data of Johnsrud et al.<sup>30)</sup> were renormalized, because they were obtained by using a value of 45 barns for the thermal capture cross section of <sup>107</sup>Ag, but its latest recommended value<sup>34)</sup> is 37.6 barns. As for <sup>109</sup>Ag, we selected the experimental data of Mizumoto et al.<sup>27)</sup> and Macklin<sup>33)</sup> in the energy range from 4 keV to 2 MeV.

### 2.3 Inelastic Scattering Cross Section

Experimental data on the inelastic scattering are very scarce. Nishimura et al.<sup>35)</sup> measured the (n,n'γ) cross sections of natural

silver in the energy range from 300 keV to 1 MeV. Augustyniak et al.<sup>36)</sup> measured the excitation curves for population of the isomeric state in the  $^{109,107}\text{Ag}(n,n')$  reactions for 3 - 18 MeV. The 14-MeV activation cross section of the  $^{107}\text{Ag}(n,n')$  $^{107m}\text{Ag}$  reaction was obtained by Wagner et al.<sup>37)</sup> The differential inelastic scattering cross sections of  $^{107}\text{Ag}$  were obtained by Smith et al.<sup>11)</sup> using the time-of-flight technique between 1.5 MeV and 4 MeV.

#### 2.4 (n,2n) and (n,3n) Reaction Cross Sections

There are about thirty measurements of the  $^{107}\text{Ag}(n,2n)$  reaction. However, most of them were given at about 14 MeV as the activation cross sections to the ground state or to the isomeric state. Only three measurements<sup>38-40)</sup> deduced the cross sections to both the ground state and isomeric state. Averaging all the existing experimental data, we obtained a value of  $1358 \pm 57$  mb for the total (n,2n) reaction cross section at 14.5 MeV. As for  $^{109}\text{Ag}$ , available experimental data are only for the ground state, and there exist no data for the isomeric state and for the total (n,2n) reaction cross section. Thus, we deduced a average value of  $826 \pm 45$  mb for the ground state at 14.5 MeV from ten sets<sup>36,38,39,41-47)</sup> of experimental data. The average total (n,2n) cross section of  $^{109}\text{Ag}$  was found to be  $1387 \pm 170$  mb by assuming that the cross section to the isomeric state is 561 mb which is obtained for  $^{107}\text{Ag}$ .

Concerning the (n,3n) reaction, available are only the measurements of Liskien<sup>48)</sup> and Bayhurst et al.<sup>49)</sup> for  $^{107}\text{Ag}$ .

#### 2.5 (n,p) Reaction Cross Section

There are very few experimental data for natural silver and  $^{107}\text{Ag}$ . On the other hand, several data<sup>37,50-54)</sup> are available for  $^{109}\text{Ag}$ , but they are discrepant with one another around 14 MeV. Thus, we investigated systemtatics of the 14-MeV cross section around mass number of 110, and obtained a value of  $14 \pm 5$  mb for both isotopes at 14 MeV. Recently, after the present evaluation, Ryves et al.<sup>55)</sup> gave a value of  $15.4 \pm 0.8$  mb for the (n,p) reaction cross section of  $^{107}\text{Ag}$  at 14.3 MeV. This value is in good agreement with our value obtained above.

## 2.6 ( $n,\alpha$ ) Reaction Cross Section

There are very few experimental data on the ( $n,\alpha$ ) reaction cross section. Therefore, we investigated systematics at 14 MeV like the ( $n,p$ ) cross section mentioned above. A value of  $3.0 \pm 1.5$  mb was obtained for both isotopes from the systematics.

## 3. Theoretical Calculation

### 3.1 Computational Methods and Procedures

The multi-step Hauser-Feshbach code TNG<sup>56,57)</sup> was mainly used for calculating the neutron-induced reaction cross sections of both isotopes. The precompound process was taken into account above an incident energy of 5 MeV, in addition to the compound one. Calculated are the total, elastic and inelastic scattering, non-elastic, capture, ( $n,2n$ ), ( $n,3n$ ), ( $n,p$ ), ( $n,\alpha$ ), ( $n,np$ ) and ( $n,n\alpha$ ) reaction cross sections, angular distributions of neutrons and energy distributions of neutrons and gamma-rays.

The k factor, which represents a magnitude of the residual two-body interaction in the precompound mode, was deduced to be 600 MeV<sup>3</sup> through a comparison of the calculated neutron emission spectra with the experimental data. Angular distributions of the neutrons inelastically scattered to the continuum levels of <sup>107,109</sup>Ag were calculated and compared with the available experimental data in order to check the applicability of TNG.

TNG was not capable of calculating the angular distributions for the shape elastic scattering. Thus, they were calculated by using the CASTHY code<sup>58)</sup> with the same optical-model parameters as those for TNG.

### 3.2 Parameter Determination

#### 3.2.1 Optical-Model Potentials

The spherical optical model was used to calculate particle transmission coefficients, which were needed in the Hauser-Feshbach formalism. Concerning neutrons, Smith et al.<sup>59)</sup> obtained the parameters for natural silver in the energy range from 1.5 to 4 MeV. Parameter search was performed using their parameters as initial values so as to reproduce the experimental total cross sections. The

## 2.6 ( $n,\alpha$ ) Reaction Cross Section

There are very few experimental data on the ( $n,\alpha$ ) reaction cross section. Therefore, we investigated systematics at 14 MeV like the ( $n,p$ ) cross section mentioned above. A value of  $3.0 \pm 1.5$  mb was obtained for both isotopes from the systematics.

## 3. Theoretical Calculation

### 3.1 Computational Methods and Procedures

The multi-step Hauser-Feshbach code TNG<sup>56,57)</sup> was mainly used for calculating the neutron-induced reaction cross sections of both isotopes. The precompound process was taken into account above an incident energy of 5 MeV, in addition to the compound one. Calculated are the total, elastic and inelastic scattering, non-elastic, capture, ( $n,2n$ ), ( $n,3n$ ), ( $n,p$ ), ( $n,\alpha$ ), ( $n,np$ ) and ( $n,n\alpha$ ) reaction cross sections, angular distributions of neutrons and energy distributions of neutrons and gamma-rays.

The k factor, which represents a magnitude of the residual two-body interaction in the precompound mode, was deduced to be 600 MeV<sup>3</sup> through a comparison of the calculated neutron emission spectra with the experimental data. Angular distributions of the neutrons inelastically scattered to the continuum levels of <sup>107,109</sup>Ag were calculated and compared with the available experimental data in order to check the applicability of TNG.

TNG was not capable of calculating the angular distributions for the shape elastic scattering. Thus, they were calculated by using the CASTHY code<sup>58)</sup> with the same optical-model parameters as those for TNG.

### 3.2 Parameter Determination

#### 3.2.1 Optical-Model Potentials

The spherical optical model was used to calculate particle transmission coefficients, which were needed in the Hauser-Feshbach formalism. Concerning neutrons, Smith et al.<sup>59)</sup> obtained the parameters for natural silver in the energy range from 1.5 to 4 MeV. Parameter search was performed using their parameters as initial values so as to reproduce the experimental total cross sections. The

potential thus obtained has an energy-dependent imaginary term, while the original one of Smith et al.<sup>59)</sup> has no such a term. The final parameters for neutrons are given in Table 3. Figure 2 shows the calculated non-elastic scattering cross section of natural silver, together with the experimental data<sup>60-65)</sup>. The calculated cross section is in good agreement with the measured data up to 20 MeV.

As for charged particles, several sets of global potentials were examined. For protons, the parameters obtained by Perey<sup>66)</sup> and by Arthur and Young<sup>67)</sup> gave too large (n,p) reaction cross sections as compared with the experimental data. Then, the parameters were adjusted so as to reproduce the (n,p) reaction cross section, and the best values were obtained. For  $\alpha$ -particles, we employed the parameters of Arthur and Young<sup>67)</sup> which were determined by modifying Lemos' potential<sup>68)</sup>. These parameters are also given in Table 3.

### 3.2.2 Discrete Levels and Level Density

In the present calculation, it is necessary to input the discrete levels and level density parameters of fourteen nuclei, i.e.,  $^{103}\text{Rh}$ ,  $^{104}\text{Rh}$ ,  $^{105}\text{Rh}$ ,  $^{106}\text{Rh}$ ,  $^{106}\text{Pd}$ ,  $^{107}\text{Pd}$ ,  $^{108}\text{Pd}$ ,  $^{109}\text{Pd}$ ,  $^{105}\text{Ag}$ ,  $^{106}\text{Ag}$ ,  $^{107}\text{Ag}$ ,  $^{108}\text{Ag}$ ,  $^{109}\text{Ag}$  and  $^{110}\text{Ag}$ . The discrete levels were taken from the Nuclear Data Sheets<sup>69-76)</sup>, as well as the gamma-ray branching ratios between the discrete levels. The levels used in the present calculation are listed in Tables 4-10. For calculation of the capture gamma-ray spectra, s-wave branching ratios for primary transitions from the capturing state to the low-lying discrete levels of the compound nuclei were also obtained from the compilation works.<sup>74,76)</sup>

Concerning the level density, the composite formula of Gilbert and Cameron<sup>77)</sup> was used throughout. All pairing energy corrections  $\Delta$  were taken from their table. For the spin cut-off factor, we employed the following expression given by Facchini and Saetta-Menichella<sup>78)</sup>:

$$\sigma^2(E) \equiv ct = 0.146aA^{2/3}t, \quad (1)$$

where  $A$  is the mass number and  $t$  the thermodynamic temperature defined by Gilbert and Cameron<sup>77)</sup>. When  $E$  is less than the matching energy  $E_x$ , the spin cut-off factor is calculated from the relation

$$\sigma^2(E) = \sigma^2(E_c) + [\sigma^2(E_x) - \sigma^2(E_c)] \cdot E/E_x, \quad (2)$$

where  $E_c$  is the continuum cut-off energy. Here  $\sigma^2(E_x)$  is obtained from Eq.(1), and  $\sigma^2(E_c)$  is given by

$$\sigma^2(E_c) = \left[ \sum_{i=1}^M (J_i + 1/2)^2 \right] / 2M, \quad (3)$$

where  $J_i$  is the spin of the  $i$ -th excited state and  $M$  the number of the discrete levels considered in the calculation. The level density parameters were taken from the work of Iijima et al.<sup>79)</sup> at first. During the course of the calculation, however, the parameters were modified so as to reproduce experimental cross-section data. The LEVDENS code<sup>80)</sup> was used to obtain sets of consistent parameters since all the parameters are not independent of one another. The parameters thus determined are given in Table 11.

### 3.2.3 Giant Dipole Resonances

The gamma-ray transmission coefficient was calculated with the giant dipole model. The absorption cross section for the giant dipole resonance was assumed to have a two-component Lorentzian shape, i.e.,

$$\sigma^{E1}(E_\gamma) = \sum_{i=1}^2 \sigma_{mi} E_\gamma^2 \Gamma_i^2 / [(E_\gamma^2 - E_{mi}^2)^2 + E_\gamma^2 \Gamma_i^2], \quad (4)$$

where  $E_\gamma$  is the gamma-ray energy. The symbols  $E_{mi}$ ,  $\sigma_{mi}$  and  $\Gamma_i$  are the resonance energy, peak cross section and full width at half maximum, respectively. As to  $E_{mi}$ ,  $\sigma_{mi}$  and  $\Gamma_i$ , the following empirical formulas<sup>81)</sup> were used for all nuclei except  $^{108}\text{Ag}$  and  $^{110}\text{Ag}$ :

$$\begin{aligned} \sigma_{m1} &= 168NZ/(\pi A\Gamma_1) \quad (\text{mb}), & \sigma_{m2} &= 0.0 \quad (\text{mb}), \\ E_{m1} &= 163(NZ)^{1/2} A^{4/3} \quad (\text{MeV}), & E_{m2} &= 0.0 \quad (\text{MeV}), \\ \Gamma_1 &= 5.0 \quad (\text{MeV}), & \Gamma_2 &= 0.0 \quad (\text{MeV}), \end{aligned}$$

where  $Z$  is the atomic number and  $N=A-Z$ . On the other hand, the parameters for  $^{108}\text{Ag}$  and  $^{110}\text{Ag}$  were derived so as to reproduce experimental capture cross sections, and they are given as follows:

$$\begin{aligned} \sigma_{m1} &= 120.0 \quad (\text{mb}), & \sigma_{m2} &= 100.0 \quad (\text{mb}), \\ E_{m1} &= 17.5 \quad (\text{MeV}), & E_{m2} &= 21.5 \quad (\text{MeV}), \\ \Gamma_1 &= 5.0 \quad (\text{MeV}), & \Gamma_2 &= 5.0 \quad (\text{MeV}). \end{aligned}$$

### 3.3 Calculated Results

The inelastic scattering cross sections of  $^{107}\text{Ag}$  and  $^{109}\text{Ag}$  are shown in Figs. 3 and 4, respectively. The present calculations for  $^{107}\text{Ag}$  are almost consistent with the experimental data of Nishimura et al.<sup>35)</sup> and Smith et al.<sup>11)</sup>

The  $(n,2n)$  and  $(n,3n)$  reaction cross sections are illustrated in Figs. 5-10. The average 14-MeV cross section for the  $^{107}\text{Ag}(n,2n)$  reaction, which was obtained in this work, is well reproduced by the theoretical calculations, as seen in Fig. 6. The calculated  $(n,3n)$  reaction cross section of  $^{107}\text{Ag}$  is in good agreement with the experimental data of Liskien<sup>48)</sup> and Bayhurst et al.<sup>49)</sup>

Figures 11-13 show the  $(n,p)$  reaction cross sections. It is found from Fig. 13 that the present calculations for  $^{109}\text{Ag}$  reproduce the average behavior of experimental data, while the ENDF/B-V data have a somewhat strange structure as compared with the experimental data.

The calculated  $(n,\alpha)$  reaction cross sections are shown in Figs. 14-16. As for  $^{107}\text{Ag}$ , it is found from Fig. 15 that the ENDF/B-V data give much larger cross section than our calculations and the measured data of Bormann et al.<sup>82)</sup> Recently, Kneff et al.<sup>83)</sup> have reported a value of  $7.6 \pm 0.6$  mb for the helium production cross section of natural silver at 14.8 MeV, and thus the present calculation for  $^{107}\text{Ag}$  seems reasonable. As for  $^{109}\text{Ag}$ , the ENDF/B-V data are in better agreement with the experimental data than the present calculation.

The  $(n,n\alpha)$  and  $(n,np)$  reaction cross sections are illustrated in Figs. 17-22, although the experimental data are very few.

Neutron and gamma-ray emission spectra from natural silver are shown in Figs. 23 and 24, respectively. The agreement between the calculations and the experimental data<sup>84-86)</sup> is quite satisfactory in both cases.

Angular distributions of continuum neutrons coming from the compound and precompound processes are shown in Fig. 25, where a symbol  $E'$  stands for the outgoing energy. The calculations reproduce the measured forward-peaked distributions. A forward peaking increases with outgoing energies, which means that the precompound mode becomes remarkable in the higher energy region.

#### 4. Evaluated Data

##### 4.1 Resonance Parameters

Resonance parameters were given in the energy range below 100 keV. The energy range was divided into the resolved resonance region below 7 keV and the unresolved resonance region from 7 keV to 100 keV.

The  $(n,2n)$  and  $(n,3n)$  reaction cross sections of are illustrated in Figs. 5-10. The average 14-MeV cross section for the  $^{107}\text{Ag}(n,2n)$  reaction, which was obtained in this work, is well reproduced by the theoretical calculations, as seen in Fig. 6. The calculated  $(n,3n)$  reaction cross section of  $^{107}\text{Ag}$  is in good agreement with the experimental data of Liskien<sup>48)</sup> and Bayhurst et al.<sup>49)</sup>

Figures 11-13 show the  $(n,p)$  reaction cross sections. It is found from Fig. 13 that the present calculations for  $^{109}\text{Ag}$  reproduce the average behavior of experimental data, while the ENDF/B-V data have a somewhat strange structure as compared with the experimental data.

The calculated  $(n,\alpha)$  reaction cross sections are shown in Figs. 14-16. As for  $^{107}\text{Ag}$ , it is found from Fig. 15 that the ENDF/B-V data give much larger cross section than our calculations and the measured data of Bormann et al.<sup>82)</sup> Recently, Kneff et al.<sup>83)</sup> have reported a value of  $7.6 \pm 0.6$  mb for the helium production cross section of natural silver at 14.8 MeV, and thus the present calculation for  $^{107}\text{Ag}$  seems reasonable. As for  $^{109}\text{Ag}$ , the ENDF/B-V data are in better agreement with the experimental data than the present calculation.

The  $(n,n\alpha)$  and  $(n,np)$  reaction cross sections are illustrated in Figs. 17-22, although the experimental data are very few.

Neutron and gamma-ray emission spectra from natural silver are shown in Figs. 23 and 24, respectively. The agreement between the calculations and the experimental data<sup>84-86)</sup> is quite satisfactory in both cases.

Angular distributions of continuum neutrons coming from the compound and precompound processes are shown in Fig. 25, where a symbol  $E'$  stands for the outgoing energy. The calculations reproduce the measured forward-peaked distributions. A forward peaking increases with outgoing energies, which means that the precompound mode becomes remarkable in the higher energy region.

#### 4. Evaluated Data

##### 4.1 Resonance Parameters

Resonance parameters were given in the energy range below 100 keV. The energy range was divided into the resolved resonance region below 7 keV and the unresolved resonance region from 7 keV to 100 keV.

The resolved resonance parameters for each isotope are the same as those adopted in JENDL-2, because there have been no measurements performed after the JENDL-2 evaluation.

The unresolved resonance parameters were determined so as to fit to the experimental total and capture cross sections of each isotope by using the ASREP code<sup>87)</sup>. In the fitting, the capture cross sections measured by Mizumoto et al.<sup>27)</sup> and of Macklin<sup>33)</sup> were used. As for the total cross section, the experimental data<sup>5-7)</sup> of natural silver were applied to both isotopes because the isotopic data were not available in the unresolved resonance region.

The resonance capture integrals (the cut-off energy of 0.5 eV) calculated from the present resonance parameters are compared in Table 12 with the recommended values of Mughabghab et al.<sup>34)</sup> They agree with each other for natural silver and  $^{107}\text{Ag}$ , whereas the calculated value for  $^{109}\text{Ag}$  is slightly larger than the recommended one.

Figures 26-31 show the total and capture cross sections in the resonance region.

#### 4.2 Cross Sections above Resonance Region

In the present evaluation, adopted were the theoretically calculated cross sections for the following reactions: the inelastic scattering, ( $n,2n$ ), ( $n,3n$ ), ( $n,p$ ), ( $n,\alpha$ ), ( $n,np$ ) and ( $n,n\alpha$ ). For these reactions, the cross sections of natural silver were simply constructed by a sum of the isotopic contributions, and thus the consistency is automatically kept between the natural and isotopic data.

Concerning the total and capture cross sections, the evaluation was made mainly on the basis of the experimental data, since there are a lot of measurements available for the evaluation.

The total cross section of natural silver was determined from the measurements of Foster, Jr. and Glasgow<sup>4)</sup> and of Poenitz and Whalen<sup>5)</sup> by using the least-squares method. For  $^{107}\text{Ag}$ , the experimental data of Smith et al.<sup>11)</sup> were taken in the energy range from 250 keV to 4.5 MeV, while the cross section was supplemented by that of natural silver in the ranges from 100 keV to 250 keV and from 4.5 MeV to 20 MeV where the isotopic data were not available. Then, the total cross section of  $^{109}\text{Ag}$  was obtained by subtracting that of  $^{107}\text{Ag}$  multiplied

by the isotopic abundance from that of natural silver. The 14-MeV measurements of Dukarevich et al.<sup>12)</sup> for both isotopes were successfully reproduced in the present evaluation. The evaluated results are shown in Figs. 32-34.

There are many experimental data on the capture cross sections of natural silver and its isotopes up to about 3 MeV, as mentioned in Sect. 2.2. Below 3 MeV; the capture cross sections were evaluated by using the least-squares fitting to the experimental data with keeping the consistency between the natural and isotopic data. Above 3 MeV, we adopted the theoretically calculated cross sections. The calculated cross sections were normalized to the experimental data at 3 MeV. The evaluated capture cross sections are shown in Figs. 35-37.

Finally, the elastic scattering cross section was obtained by subtracting all the other cross sections from the total cross section. Figures 38-40 show the evaluated elastic scattering cross sections.

#### 4.3 Other Quantities

##### 4.3.1 Energy and Angular Distributions of Emitted Neutrons

The angular distributions for the elastic scattering and the inelastic scattering to the discrete levels were obtained for each isotope by the theoretical calculation mentioned in Chap. 3, and those of natural silver were constructed from the isotopic data. They were stored in the form of the Legendre coefficients in the evaluated data file. The calculated elastic angular distributions are illustrated in Figs. 41-43. Isotropic angular distributions in the laboratory system were assumed for the inelastic scattering to the continuum levels and for the ( $n,2n$ ), ( $n,3n$ ), ( $n,np$ ) and ( $n,n\alpha$ ) reactions. The calculated angular distributions of continuum neutrons shown in Fig. 25 were not contained in the data file, since the ENDF-5 format was adopted for JENDL-3.

The energy distributions of the neutrons emitted from the inelastic scattering to the continuum levels and from the ( $n,2n$ ), ( $n,3n$ ), ( $n,np$ ) and ( $n,n\alpha$ ) reactions were also obtained by the theoretical calculations, and those of natural silver were constructed from the isotopic data.

##### 4.3.2 Gamma-Ray Production Cross Sections

The gamma-ray production cross sections of both isotopes were

calculated by using the TNG code. The cross sections thus obtained are for the following reactions:  $(n, n\gamma)$ ,  $(n, 2n\gamma)$ ,  $(n, 3n\gamma)$ ,  $(n, np\gamma)$ ,  $(n, n\alpha\gamma)$ ,  $(n, \gamma)$ ,  $(n, p\gamma)$  and  $(n, \alpha\gamma)$ , i.e., MT = 4, 16, 17, 22, 28, 102, 103 and 107. The calculated gamma-ray multiplicities and spectra were stored in the evaluated data file. Isotropic angular distributions were assumed for the emitted gamma-rays. The data of natural silver were consistently constructed from the isotopic data.

### 5. Concluding Remarks

The neutron nuclear data of natural silver and its isotopes were evaluated in the energy range from  $10^{-5}$  eV to 20 MeV. The present evaluation is based on the available experimental data and the theoretical calculations.

Most of the reaction cross sections were calculated with the Hauser-Feshbach theory by using the TNG code. The gamma-ray production cross section was obtained for each reaction from the TNG calculations. The neutron emission spectra were well reproduced by the calculation.

The unresolved resonance parameters were obtained by fitting the calculated values to the experimental data for the total and capture cross sections. The resolved ones were unchanged from those of JENDL-2. The experimental data were adopted for the total and capture cross sections above the resonance region with keeping the consistency between the natural and isotopic data.

On the whole, the present evaluation reproduces the experimental data more satisfactorily than the JENDL-2 and ENDF/B-V data.

### Acknowledgments

The authors would like to thank S. Igarasi, Y. Kikuchi, Y. Nakajima and T. Fukahori for their helpful discussion during the course of this work. They are indebted to S. Iijima for his advice on the level density and optical-model parameters and to M. Mizumoto for his comment on the capture cross-section measurement. One of the authors (Liu T.J.) is grateful to the Science and Technology Agency for giving him the opportunity to stay at JAERI and carry out this work. He also wishes to thank the members of the Nuclear Data Center and of the Office of International Affairs in JAERI for their hospitality during his staying in Japan.

calculated by using the TNG code. The cross sections thus obtained are for the following reactions:  $(n,n\gamma)$ ,  $(n,2n\gamma)$ ,  $(n,3n\gamma)$ ,  $(n,np\gamma)$ ,  $(n,na\gamma)$ ,  $(n,\gamma)$ ,  $(n,p\gamma)$  and  $(n,\alpha\gamma)$ , i.e., MT = 4, 16, 17, 22, 28, 102, 103 and 107. The calculated gamma-ray multiplicities and spectra were stored in the evaluated data file. Isotropic angular distributions were assumed for the emitted gamma-rays. The data of natural silver were consistently constructed from the isotopic data.

### 5. Concluding Remarks

The neutron nuclear data of natural silver and its isotopes were evaluated in the energy range from  $10^{-5}$  eV to 20 MeV. The present evaluation is based on the available experimental data and the theoretical calculations.

Most of the reaction cross sections were calculated with the Hauser-Feshbach theory by using the TNG code. The gamma-ray production cross section was obtained for each reaction from the TNG calculations. The neutron emission spectra were well reproduced by the calculation.

The unresolved resonance parameters were obtained by fitting the calculated values to the experimental data for the total and capture cross sections. The resolved ones were unchanged from those of JENDL-2. The experimental data were adopted for the total and capture cross sections above the resonance region with keeping the consistency between the natural and isotopic data.

On the whole, the present evaluation reproduces the experimental data more satisfactorily than the JENDL-2 and ENDF/B-V data.

### Acknowledgments

The authors would like to thank S. Igarasi, Y. Kikuchi, Y. Nakajima and T. Fukahori for their helpful discussion during the course of this work. They are indebted to S. Iijima for his advice on the level density and optical-model parameters and to M. Mizumoto for his comment on the capture cross-section measurement. One of the authors (Liu T.J.) is grateful to the Science and Technology Agency for giving him the opportunity to stay at JAERI and carry out this work. He also wishes to thank the members of the Nuclear Data Center and of the Office of International Affairs in JAERI for their hospitality during his staying in Japan.

calculated by using the TNG code. The cross sections thus obtained are for the following reactions:  $(n,n\gamma)$ ,  $(n,2n\gamma)$ ,  $(n,3n\gamma)$ ,  $(n,np\gamma)$ ,  $(n,na\gamma)$ ,  $(n,\gamma)$ ,  $(n,p\gamma)$  and  $(n,\alpha\gamma)$ , i.e., MT = 4, 16, 17, 22, 28, 102, 103 and 107. The calculated gamma-ray multiplicities and spectra were stored in the evaluated data file. Isotropic angular distributions were assumed for the emitted gamma-rays. The data of natural silver were consistently constructed from the isotopic data.

### 5. Concluding Remarks

The neutron nuclear data of natural silver and its isotopes were evaluated in the energy range from  $10^{-5}$  eV to 20 MeV. The present evaluation is based on the available experimental data and the theoretical calculations.

Most of the reaction cross sections were calculated with the Hauser-Feshbach theory by using the TNG code. The gamma-ray production cross section was obtained for each reaction from the TNG calculations. The neutron emission spectra were well reproduced by the calculation.

The unresolved resonance parameters were obtained by fitting the calculated values to the experimental data for the total and capture cross sections. The resolved ones were unchanged from those of JENDL-2. The experimental data were adopted for the total and capture cross sections above the resonance region with keeping the consistency between the natural and isotopic data.

On the whole, the present evaluation reproduces the experimental data more satisfactorily than the JENDL-2 and ENDF/B-V data.

### Acknowledgments

The authors would like to thank S. Igarasi, Y. Kikuchi, Y. Nakajima and T. Fukahori for their helpful discussion during the course of this work. They are indebted to S. Iijima for his advice on the level density and optical-model parameters and to M. Mizumoto for his comment on the capture cross-section measurement. One of the authors (Liu T.J.) is grateful to the Science and Technology Agency for giving him the opportunity to stay at JAERI and carry out this work. He also wishes to thank the members of the Nuclear Data Center and of the Office of International Affairs in JAERI for their hospitality during his staying in Japan.

**References**

- 1) Wapstra A.H. and Bos K.: Atomic Data Nucl. Data Tables, 19, 177 (1977).
- 2) Holden N.E., Martin R.L. and Barnes I.L.: Pure Appl. Chem., 56, 675 (1984).
- 3) Liu Ting-jin, Shibata K. and Nakagawa T.: J. Nucl. Sci. Technol., 27, 756 (1990).
- 4) Foster, Jr. D.G. and Glasgow D.W.: Phys. Rev., C3, 576 (1971).
- 5) Poenitz W.P. and Whalen J.F.: "Neutron Total Cross Section Measurements in the Energy Region from 47 keV to 20 MeV", ANL-NDM-80, (1983).
- 6) Seth K.K., Tabony R.H., Bilpuch E.G. and Newson H.W.: Phys. Lett., 16, 306 (1965).
- 7) Jain A.P., Chrien R.E., Moore J.A., and Palevsky H.: Phys. Rev., B137, 83 (1965).
- 8) Newson H.W., Gibbons J.H., Marshak H., Williamson R.M., Mobley R.C., Patterson J.R. and Nichols P.F.: Phys. Rev., 105, 198 (1957).
- 9) Selove W.: Phys. Rev., 84, 869 (1951).
- 10) Garg J.B., Rainwater J. and Havens, Jr. W.W.: Phys. Rev., B137, 547 (1965).
- 11) Smith A., Guenther P., Winkler G. and Whalen J.: Nucl. Phys., A332, 297 (1979).
- 12) Dukarevich Ju.V., Djumin A.N. and Kaminker D.M.: Nucl. Phys., A92, 433 (1967).
- 13) Moxon M.C. and Rae E.R.: "A Gamma-Ray Detector for Neutron Capture Cross Section Measurements", NP-17644, (1968).
- 14) Isakov A.I., Popov Ju.P. and Shapiro F.L.: Zh. Eksp. Teor. Fiz., 38, 989 (1960).
- 15) Diven B.C., Terrell J. and Hemmendinger A.: Phys. Rev., 120, 556 (1960).
- 16) Block R.C., Slaughter G.G., Weston L.W. and Vonderlage F.C.: Proc. NEANDC Conf. Time of Flight Methods, Saclay, 1961, p.203 (1961).
- 17) Gibbons J.H., Macklin R.L., Miller P.D. and Neiler J.H.: Phys. Rev., 122, 182 (1961).

- 18) Haddad E., Friesenhahn S. and Lopez W.M.: "Radiative Capture Cross Section Measurements", GA-3874, (1963).
- 19) Bergqvist I.: Arkiv for Fysik, 23, 425 (1963).
- 20) Kononov V.N., Stavisskij Ju.Ja., Kolesov V.E., Dovbenko A.G., Nesterenko V.S. and Soroka V.I.: Atomnaya Energiya, 19, 457 (1965).
- 21) Macklin R.L. and Gibbons J.H.: Phys. Rev., 159, 1007 (1967).
- 22) Spitz L.M., Barnard E. and Brooks F.D.: Nucl. Phys., A121, 655 (1968).
- 23) Kompe D.: Nucl. Phys., A133, 513 (1969).
- 24) Chelnokov V.B., Tolstikov V.A., Stavisskij Ju.Ja., Bergman A.A. and Samsonov A.E.: "Measurements of Radiation Capture and Fission Cross-Sections for Some Heavy Nuclei by Slowing-Down-Time Method in Plumbum", YFI-13, p.6 (1972).
- 25) Yamamuro N., Doi T., Hayase T., Fujita Y., Kobayashi K. and Block R.C.: J. Nucl. Sci. Technol., 15, 637 (1978).
- 26) Poenitz W.P.: "Fast-Neutron Capture-Cross-Section Measurements with the Argonne National Laboratory Large-Liquid-Scintillator Tank", ANL-83-4, p.239 (1982).
- 27) Mizumoto M., Sugimoto M., Nakajima Y., Ohkubo M., Furuta Y. and Kawarasaki K.: "Neutron Radiative Capture and Transmission Measurements of  $^{107}\text{Ag}$  and  $^{109}\text{Ag}$ ", Proc. Int. Conf. Nuclear Data for Science and Technology, Antwerp, 1982, p.226 (1983).
- 28) Lejpunskij A.I., Kazachkovskij O.D., Artjukhov G.Ja., Baryshnikov A.I., Belanova T.S., Galkov V.I., Stavisskij Ju.Ja., Stumbur E.A. and Sherman L.E.: Proc. Second UN Conf. The Peaceful Uses of Atomic Energy, Geneva, (1958).
- 29) Lyon W.S. and Macklin R.L.: Phys. Rev., 114, 1619 (1959).
- 30) Johnsrud A.E., Silbert M.G. and Barschall H.H.: Phys. Rev., 116, 927 (1959).
- 31) Weston L.W., Seth K.K., Bilpuch E.G. and Newson H.W.: Ann. Phys., 10, 477 (1960).
- 32) Peto G., Milligy Z. and Hunyadi I.: J. Nucl. Energy, 21, 797 (1967).
- 33) Macklin R.L.: Nucl. Sci. Eng., 82, 400 (1982).
- 34) Mughabghab S.F., Divadeenam M., Holden N.E.: "Neutron Cross Sections, Volume 1, Part A", Academic Press, (1981).

- 35) Nishimura K., Okano K. and Kikuchi S.: Nucl. Phys., 70, 421 (1965).
- 36) Augustyniak W., Herman M. and Marcinkowski A.: Nucl. Phys., A247, 231 (1975).
- 37) Wagner I. and Uhl M.: Oesterr. Akad. Wiss. Math.+ Naturw. Anzeiger, 108, 185 (1971).
- 38) Minetti B. and Pasquarelli A.: Nucl. Phys., A118, 449 (1968).
- 39) Vonach H.: Oesterr. Akad. Wiss. Math.+ Naturw. Anzeiger, 98, 116 (1961).
- 40) Reggoug A., Paic G. and Berrada M.: "Measurement of (n,2n) Reaction Cross sections by X-Ray Spectroscopy", MOH-5, p.14 (1982).
- 41) Langmann: Taken from EXFOR (1962).
- 42) Cuzzocrea P., Perillo E. and Notarrigo S.: Nuovo Cimento, B54, 53 (1968).
- 43) Forbes S.G.: Phys. Rev., 88, 1309 (1952).
- 44) Paul E.B. and Clarke R.L.: Can. J. Phys., 31, 267 (1953).
- 45) Khurana C.S. and Hans H.S.: Nucl. Phys., 28, 560 (1961).
- 46) Mukherjee S.K., Ganguly A.K. and Majumder N.K.: Proc. Phys. Soc. (London), 77, 508 (1961).
- 47) Yasumi S.: J. Phys. Soc. Jpn., 12, 443 (1957).
- 48) Liskien H.: Nucl. Phys., A118, 379 (1968).
- 49) Bayhurst B.P., Gilmore J.S., Prestwood R.J., Wilhelmy, J.B., Jarmie, N., Erkkila, B.H., Harderkopf, R.A.: Phys. Rev., C12, 451 (1975).
- 50) Dzantijev B.G., Levkovskij V.N. and Malijevskij A.D.: Doklady Akademii Nauk SSSR, 113, 537 (1956).
- 51) Coleman R.F., Hawker B.E., O'connor L.P., Perkin J.L.: Proc. Phys. Soc. (London), 73, 215 (1959).
- 52) Bayhurst B.P. and Prestwood R.J.: J. Inorg. Nucl. Chem., 23, 173 (1961).
- 53) Levkovskij V.N.: Zh. Eksp. Teor. Fiz., 45, 305 (1963).
- 54) Levkovskij V.N., Vinitskaja G.P., Kovel'skaja G.E. and Stepanov V.M.: Nucl. Phys., 10, 44 (1969).
- 55) Ryves T.B., Kolkowski P. and Lewis V.E.: J. Phys., G14, 77 (1988).

- 56) Fu C.Y.: "A Consistent Nuclear Model for Compound and Precompound Reactions with Conservation of Angular Momentum", ORNL/TM-7042, (1980).
- 57) Shibata K. and Fu C.Y.: "Recent Improvements of the TNG Statistical Model Code", ORNL/TM-10093, (1986).
- 58) Igarasi S.: J. Nucl. Sci. Technol., 12, 67 (1975).
- 59) Smith A.B., Guenther P.T., Whalen J.F.: Nucl. Phys., A415, 1 (1984).
- 60) Beyster J.R., Henkel R.L., Nobles R.A., Kister J.M.: Phys. Rev., 98, 1216 (1955).
- 61) Beyster J.R., Walt M. and Salmi E.W.: Phys. Rev., 104, 1319 (1956).
- 62) Graves E.R. and Davis R.W.: Phys. Rev., 97, 1205 (1955).
- 63) Taylor H.L., Lonsjo O. and Bonner T.W.: Phys. Rev., 100, 174 (1955).
- 64) Bonner T.W. and Slattery J.H.: Phys. Rev., 113, 1088 (1959).
- 65) Jasicek H.A.: Taken from EXFOR (1973).
- 66) Perey F.G.: Phys. Rev., 131, 745 (1963).
- 67) Arthur E.D. and Young P.G.: "Evaluated Neutron-Induced Cross Sections for  $^{54,56}\text{Fe}$  to 40 MeV", LA-8626-MS, (1980).
- 68) Lemos O.F.: "Diffusion Elastique de Particules Alpha de 21 à 29.6 MeV sur des Noyaux de la Région Ti-Zn", Orsay Report, Series A, No. 136 (1972).
- 69) De Frenne D., Jacobs E. and Verboven M.: Nucl. Data Sheets, 45, 363 (1985).
- 70) Blachot J., Husson J.P., Oms J. and Berrier G.: Nucl. Data Sheets, 41, 325 (1984).
- 71) De Frenne D., Jacobs E., Verboven M. and De Gelder P.: Nucl. Data Sheets, 47, 261 (1986).
- 72) Harmatz B.: Nucl. Data Sheets, 30, 305 (1980).
- 73) Haramtz B.: Nucl. Data Sheets, 34, 643 (1981).
- 74) Haese R.L., Bertrand F.E., Harmatz B. and Martin M.J.: Nucl. Data Sheets, 37, 289 (1982).
- 75) Blachot J.: Nucl. Data Sheets, 41, 111 (1984).
- 76) De Gelder P., Jacobs E. and De Frenne D.: Nucl. Data Sheets, 38, 545 (1983).

- 77) Gilbert A. and Cameron A.G.W.: Can. J. Phys., 43, 1446 (1965).
- 78) Facchini U. and Saetta-Menichella E.: Energ. Nucl., 15, 54 (1968).
- 79) Iijima S., Yoshida T., Aoki T., Watanabe T. and Sasaki M.: J. Nucl. Sci. Technol., 21, 10 (1984).
- 80) Iijima S.: Private communication (1987).
- 81) Fuller E.G. and Hayward E.: "Nuclear Reactions", Vol.2, edited by Endt P.M. and Smith, P.B., North-Holland Publishing Co., P.113 (1962).
- 82) Bormann M., Schmidt W., Shroeder V., Scobel W. and Seebeck U.: Nucl. Phys., A186, 65 (1972).
- 83) Kneff D.W., Oliver B.M., Farrar IV H. and Greenwood L.R.: Nucl. Sci. Eng., 92, 491 (1986).
- 84) Irie Y., Hyakutake M., Matoba M., Kumabe I. and Sonoda M.: "Precompound Processes in Inelastic Scattering of 14.1 MeV Neutrons by Cu, As, Nb and Ag", Memoirs of the Faculty of Engineering, Kyushu University, 37, 19 (1977).
- 85) Vonach H., Chalupka A., Wenninger F. and Staffel G.: "Measurement of the Angle-Integrated Secondary Neutron Spectra from Interaction of 14 MeV Neutrons with Medium and Heavy Nuclei", Proc. Symp. Neutron Cross-Sections from 10 to 50 MeV, BNL, 1980, p.343 (1980).
- 86) Dickens J.K., Love T.A. and Morgan G.L.: "Gamma-Ray Production due to Neutron Interactions with Silver for Incident Neutron Energies between 0.3 and 20 MeV", ORNL/TM-5081, (1975).
- 87) Kikuchi, Y.: Private communication (1987).

Table 1 Isotopic abundances and reaction  
Q-values of  $^{107}\text{Ag}$  and  $^{109}\text{Ag}$

	$^{107}\text{Ag}$	$^{109}\text{Ag}$
a) Abundance(%)		
	51.839	48.161
b) Q-values(MeV)		
(n,2n)	-9.5467	-9.1917
(n,3n)	-17.4724	-16.4614
(n,p)	0.7495	-0.3335
(n, $\alpha$ )	4.1947	3.2967
(n,np)	-5.7802	-6.4882
(n,n $\alpha$ )	-2.8049	-3.2919
(n, $\gamma$ )	7.2697	6.8057

Table 2 Status of presently evaluated quantities

Natural silver

Quantities	Energy range(eV)*		Comments
	min.	max.	
<b>a) Resonance parameters</b>			
Resolved resonance	1.0 -5	7.0 +3	Figs. 26,29
Unresolved resonance	7.0 +3	1.0 +5	Figs. 26,29
<b>b) Cross sections</b>			
Total	1.0 -5	2.0 +7	Figs. 26,32
Elastic scattering	1.0 -5	2.0 +7	Fig. 38
Inelastic scattering	8.88+4	2.0 +7	
Capture	1.0 -5	2.0 +7	Figs. 29,35
(n,2n)	9.28+6	2.0 +7	Fig. 5
(n,3n)	1.66+7	2.0 +7	Fig. 8
(n,nα)	2.83+6	2.0 +7	Fig. 17
(n,np)	5.83+6	2.0 +7	Fig. 20
(n,p)	1.0 -5	2.0 +7	Fig. 11
(n,α)	1.0 -5	2.0 +7	Fig. 14
<b>c) Angular distributions of secondary neutrons</b>			
Elastic scattering	1.0 -5	2.0 +7	Fig. 41
Inelastic scattering	8.88+4	2.0 +7	Fig. 25
<b>b) Energy distributions of secondary neutrons</b>			Fig. 23
Inelastic scattering to continuum	1.19+6	2.0 +7	
(n,2n)	9.28+6	2.0 +7	
(n,3n)	1.66+7	2.0 +7	
(n,nα)	2.83+6	2.0 +7	
(n,np)	5.83+6	2.0 +7	
<b>c) Photon production cross sections</b>			Fig. 24
Inelastic scattering	8.88+4	2.0 +7	
Capture	1.0 -5	2.0 +7	
(n,2n)	9.28+6	2.0 +7	
(n,3n)	1.66+7	2.0 +7	
(n,nα)	2.83+6	2.0 +7	
(n,np)	5.83+6	2.0 +7	
(n,p)	1.0 -5	2.0 +7	
(n,α)	1.0 -5	2.0 +7	

\*  $2.0+7$  denotes  $2.0 \times 10^7$ .

Table 2 (continued)

 $^{107}\text{Ag}$ 

Quantities	Energy range(eV) <sup>*</sup>		Comments
	min.	max.	
<b>a) Resonance parameters</b>			
Resolved resonance	1.0 -5	7.0 +3	Figs. 27,30
Unresolved resonance	7.0 +3	1.0 +5	Figs. 27,30
<b>b) Cross sections</b>			
Total	1.0 -5	2.0 +7	Figs. 27,33
Elastic scattering	1.0 -5	2.0 +7	Fig. 39
Inelastic scattering	9.39+4	2.0 +7	Fig. 3
Capture	1.0 -5	2.0 +7	Figs. 30,36
(n,2n)	9.64+6	2.0 +7	Fig. 6
(n,3n)	1.76+7	2.0 +7	Fig. 9
(n,n $\alpha$ )	2.83+6	2.0 +7	Fig. 18
(n,np)	5.83+6	2.0 +7	Fig. 21
(n,p)	1.0 -5	2.0 +7	Fig. 12
(n, $\alpha$ )	1.0 -5	2.0 +7	Fig. 15
<b>c) Angular distributions of secondary neutrons</b>			
Elastic scattering	1.0 -5	2.0 +7	Fig. 42
Inelastic scattering	9.39+4	2.0 +7	
<b>b) Energy distributions of secondary neutrons</b>			
Inelastic scattering to continuum	1.43+6	2.0 +7	
(n,2n)	9.64+6	2.0 +7	
(n,3n)	1.76+7	2.0 +7	
(n,n $\alpha$ )	2.83+6	2.0 +7	
(n,np)	5.83+6	2.0 +7	
<b>c) Photon production cross sections</b>			
Inelastic scattering	9.39+4	2.0 +7	
Capture	1.0 -5	2.0 +7	
(n,2n)	9.64+6	2.0 +7	
(n,3n)	1.76+7	2.0 +7	
(n,n $\alpha$ )	2.83+6	2.0 +7	
(n,np)	5.83+6	2.0 +7	
(n,p)	1.0 -5	2.0 +7	
(n, $\alpha$ )	1.0 -5	2.0 +7	

\*  $2.0+7$  denotes  $2.0 \times 10^7$ .

Table 2 (continued)

 $^{109}\text{Ag}$ 

Quantities	Energy range(eV)*		Comments
	min.	max.	
<b>a) Resonance parameters</b>			
Resolved resonance	1.0 -5	7.0 +3	Figs. 28,31
Unresolved resonance	7.0 +3	1.0 +5	Figs. 28,31
<b>b) Cross sections</b>			
Total	1.0 -5	2.0 +7	Figs. 28,34
Elastic scattering	1.0 -5	2.0 +7	Fig. 40
Inelastic scattering	8.88+4	2.0 +7	Fig. 4
Capture	1.0 -5	2.0 +7	Figs. 31,37
(n,2n)	9.28+6	2.0 +7	Fig. 7
(n,3n)	1.66+7	2.0 +7	Fig. 10
(n,n $\alpha$ )	3.32+6	2.0 +7	Fig. 19
(n,np)	6.54+6	2.0 +7	Fig. 22
(n,p)	3.37+5	2.0 +7	Fig. 13
(n, $\alpha$ )	1.0 -5	2.0 +7	Fig. 16
<b>c) Angular distributions of secondary neutrons</b>			
Elastic scattering	1.0 -5	2.0 +7	Fig. 43
Inelastic scattering	8.88+4	2.0 +7	
<b>b) Energy distributions of secondary neutrons</b>			
Inelastic scattering to continuum	1.19+6	2.0 +7	
(n,2n)	9.28+6	2.0 +7	
(n,3n)	1.66+7	2.0 +7	
(n,n $\alpha$ )	3.32+6	2.0 +7	
(n,np)	6.54+6	2.0 +7	
<b>c) Photon production cross sections</b>			
Inelastic scattering	8.88+4	2.0 +7	
Capture	1.0 -5	2.0 +7	
(n,2n)	9.28+6	2.0 +7	
(n,3n)	1.66+7	2.0 +7	
(n,n $\alpha$ )	3.32+6	2.0 +7	
(n,np)	6.54+6	2.0 +7	
(n,p)	3.37+5	2.0 +7	
(n, $\alpha$ )	1.0 -5	2.0 +7	

\*  $2.0 \times 10^7$  denotes  $2.0 \times 10^7$ .

Table 3 Optical-model potential parameters  
used in the present calculations

	Depth (MeV)	Radius(fm)	Diffuseness(fm)
<b>a) Neutron</b>			
	$V = 48.25 - 0.3 \times E_n$	$r_0 = 1.249$	$a_0 = 0.603$
	$W_s = 8.501 - 0.15 \times E_n$	$r_s = 1.270$	$a_s = 0.575$
	$W_v = 0.0$		
	$V_{so} = 6.0$	$r_{so} = 1.249$	$a_{so} = 0.603$
<b>b) Proton</b>			
	$V = 66.06 - 0.55 \times E_n$	$r_0 = 1.150$	$a_0 = 0.650$
	$W_s = 12.50 - 0.10 \times E_n$	$r_s = 1.250$	$a_s = 0.470$
	$W_v = 0.0$	$r_c = 1.150$	
	$V_{so} = 0.0$		
<b>c) <math>\alpha</math>-particle</b>			
	$V = 193.0 - 0.15 \times E_n$	$r_0 = 1.370$	$a_0 = 0.560$
	$W_v = 21.0 + 0.25 \times E_n$	$r_v = 1.370$	$a_v = 0.560$
	$W_s = 0.0$	$r_c = 1.370$	
	$V_{so} = 0.0$		

Table 4 Discrete levels of  $^{105}\text{Ag}$  and  $^{106}\text{Ag}$ 

N	$^{105}\text{Ag}$		$^{106}\text{Ag}$	
	E (MeV)	J $\pi$	E (MeV)	J $\pi$
1	0.0	1/2 $^-$	0.0	1 $^+$
2	0.0255	7/2 $^+$	0.0896	6 $^+$
3	0.0531	9/2 $^+$	0.1107	2 $^+$
4	0.3469	3/2 $^-$	0.2059	3 $^+$
5	0.4332	5/2 $^-$	0.2347	2 $^+$
6	0.6687	11/2 $^+$	0.2770	2 $^-$
7	0.8778	3/2 $^-$	0.2389	5 $^+$
8	0.9173	13/2 $^+$	0.3326	7 $^-$
9	0.9873	5/2 $^+$	0.3644	3 $^-$
10	1.0237	7/2 $^-$	0.3892	3 $^+$
11	1.0427	3/2 $^-$		
12	1.0972	9/2 $^+$		
13	1.1663	7/2 $^-$		

Table 5 Discrete levels of  $^{107}\text{Ag}$  and  $^{108}\text{Ag}$ 

N	$^{107}\text{Ag}$		$^{108}\text{Ag}$	
	E (MeV)	$J^\pi$	E (MeV)	$J^\pi$
1	0.0	$1/2^-$	0.0	$1^+$
2	0.0931	$7/2^+$	0.0791	$2^-$
3	0.1256	$9/2^+$	0.1095	$6^+$
4	0.3248	$3/2^-$	0.1559	$6^+$
5	0.4232	$5/2^-$	0.1931	$1^+$
6	0.7733	$11/2^+$	0.2066	$2^+$
7	0.7866	$3/2^-$	0.2154	$3^+$
8	0.9221	$5/2^+$	0.2946	$2^+$
9	0.9497	$5/2^-$	0.3245	$3^+$
10	0.9733	$7/2^-$		
11	0.9910	$13/2^+$		
12	1.0610	$1/2^-$		
13	1.1420	$1/2^+$		
14	1.1469	$7/2^-$		
15	1.2230	$5/2^+$		
16	1.2589	$3/2^+$		
17	1.3258	$3/2^+$		

Table 6 Discrete levels of  $^{109}\text{Ag}$  and  $^{110}\text{Ag}$ 

N	$^{109}\text{Ag}$		$^{110}\text{Ag}$	
	E (MeV)	J $\pi$	E (MeV)	J $\pi$
1	0.0	$1/2^-$	0.0	$1^+$
2	0.0880	$7/2^+$	0.0011	$2^-$
3	0.1327	$9/2^+$	0.1176	$6^+$
4	0.3114	$3/2^-$	0.1187	$3^+$
5	0.4152	$5/2^-$	0.1916	$3^+$
6	0.7019	$3/2^-$	0.1987	$2^+$
7	0.7070	$3/2^+$	0.2369	$2^-$
8	0.7244	$3/2^+$	0.2371	$0^-$
9	0.7359	$5/2^+$	0.2672	$2^+$
10	0.8628	$5/2^-$	0.2694	$1^-$
11	0.8695	$5/2^+$	0.2714	$3^+$
12	0.9110	$7/2^+$	0.3045	$2^+$
13	0.9121	$7/2^-$		
14	1.0910	$9/2^-$		
15	1.0985	$5/2^+$		

Table 7 Discrete levels of  $^{106}\text{Pd}$  and  $^{107}\text{Pd}$ 

N	$^{106}\text{Pd}$		$^{107}\text{Pd}$	
	E (MeV)	$J^\pi$	E (MeV)	$J^\pi$
1	0.0	$0^+$	0.0	$5/2^+$
2	0.5119	$2^+$	0.1157	$1/2^+$
3	1.1280	$2^+$	0.2149	$11/2^-$
4	1.1337	$0^+$	0.3028	$5/2^+$
5	1.2292	$4^+$	0.3128	$7/2^+$
6	1.5577	$3^+$	0.3482	$1/2^+$
7	1.5622	$2^+$	0.3668	$1/2^+$
8	1.7065	$0^+$	0.3818	$3/2^+$
9	1.9094	$2^+$	0.4712	$3/2^+$
10	1.9323	$4^+$	0.5677	$5/2^+$
11	2.0015	$0^+$	0.6701	$5/2^+$
12	2.0774	$4^+$	0.6881	$15/2^-$
13	2.0843	$3^-$	0.6962	$1/2^+$
14	2.2424	$2^+$		
15	2.2782	$0^+$		
16	2.2830	$4^+$		
17	2.3060	$4^-$		
18	2.3088	$2^+$		
19	2.3508	$4^+$		
20	2.3660	$4^+$		

Table 8 Discrete levels of  $^{108}\text{Pd}$  and  $^{109}\text{Pd}$ 

N	$^{108}\text{Pd}$		$^{109}\text{Pd}$	
	E (MeV)	$J^\pi$	E (MeV)	$J^\pi$
1	0.0	$0^+$	0.0	$5/2^+$
2	0.4339	$2^+$	0.1134	$1/2^+$
3	0.9312	$2^+$	0.1890	$11/2^-$
4	1.0482	$4^+$	0.2451	$7/2^-$
5	1.0528	$0^+$	0.2663	$1/2^+$
6	1.3142	$0^+$	0.2763	$7/2^+$
7	1.3352	$3^+$	0.2873	$9/2^-$
8	1.4412	$2^+$	0.2914	$3/2^+$
9	1.5400	$1^+$	0.3253	$3/2^+$
10	1.6251	$4^+$	0.3269	$5/2^+$
11	1.7712	$6^+$	0.3395	$5/2^-$

Table 9 Discrete levels of  $^{103}\text{Rh}$  and  $^{104}\text{Rh}$ 

N	$^{103}\text{Rh}$		$^{104}\text{Rh}$	
	E (MeV)	$J^\pi$	E (MeV)	$J^\pi$
1	0.0	$1/2^-$	0.0	$1^+$
2	0.0398	$7/2^+$	0.0514	$2^-$
3	0.0930	$9/2^+$	0.0971	$2^+$
4	0.2950	$3/2^-$	0.1290	$5^-$
5	0.3574	$5/2^-$	0.1808	$1^-$
6	0.5368	$5/2^+$	0.1860	$1^-$
7	0.6075	$7/2^+$	0.1979	$3^+$
8	0.6501	$5/2^+$	0.2131	$1^+$
9	0.6518	$3/2^+$	0.2208	$1^-$
10	0.6577	$11/2^+$	0.2244	$2^+$
11	0.7805	$9/2^+$		
12	0.8031	$1/2^-$		
13	0.8215	$13/2^+$		
14	0.8476	$7/2^+$		
15	0.8805	$5/2^-$		
16	0.9201	$9/2^-$		

Table 10 Discrete levels of  $^{105}\text{Rh}$  and  $^{106}\text{Rh}$ 

N	$^{105}\text{Rh}$		$^{106}\text{Rh}$	
	E (MeV)	$J^\pi$	E (MeV)	$J^\pi$
1	0.0	$7/2^+$	0.0	$1^+$
2	0.1298	$1/2^-$	0.1400	$6^+$
3	0.1492	$9/2^+$		
4	0.3927	$3/2^-$		
5	0.4556	$5/2^-$		
6	0.4694	$3/2^+$		
7	0.4993	$5/2^+$		
8	0.6387	$7/2^+$		
9	0.7243	$5/2^+$		
10	0.7621	$3/2^-$		

Table 11 Level density parameters

Residual Nuclei	$E_c$ (MeV)	$E_x$ (MeV)	$E_0$ (MeV)	T (MeV)	$a$ (MeV $^{-1}$ )	c	$\Delta$ (MeV)
$^{103}\text{Rh}$	0.990	5.409	-0.612	0.655	15.50	49.73	0.94
$^{104}\text{Rh}$	0.230	4.351	-1.476	0.650	15.43	49.82	0.00
$^{105}\text{Rh}$	0.770	5.700	-0.582	0.630	16.80	54.59	1.24
$^{106}\text{Rh}$	0.150	3.869	-1.193	0.575	17.50	57.23	0.00
$^{106}\text{Pd}$	2.380	8.004	0.326	0.666	17.17	56.15	2.59
$^{107}\text{Pd}$	0.700	7.693	-1.290	0.769	14.98	49.29	1.35
$^{108}\text{Pd}$	1.900	7.957	0.362	0.646	17.90	59.27	2.60
$^{109}\text{Pd}$	0.360	7.380	-1.288	0.687	17.50	58.30	1.35
$^{105}\text{Ag}$	1.230	5.830	-1.052	0.609	18.57	60.34	0.94
$^{106}\text{Ag}$	0.400	3.549	-1.277	0.563	17.16	56.11	0.00
$^{107}\text{Ag}$	1.420	5.918	-0.356	0.693	14.55	47.88	1.24
$^{108}\text{Ag}$	0.270	3.014	-0.715	0.576	15.04	49.80	0.00
$^{109}\text{Ag}$	1.180	6.112	-0.445	0.705	14.50	48.31	1.25
$^{110}\text{Ag}$	0.320	3.150	-0.060	0.454	17.01	57.02	0.00

The meaning of the symbols used is given in Ref.(77) and in the text.

Table 12 Capture resonance integrals with cut-off energy of 0.5 eV

(barns)

	Calculated	Mughabghab et al. <sup>34)</sup>
Natural	762	756±20
$^{107}\text{Ag}$	103	100± 5
$^{109}\text{Ag}$	1472	1400±48

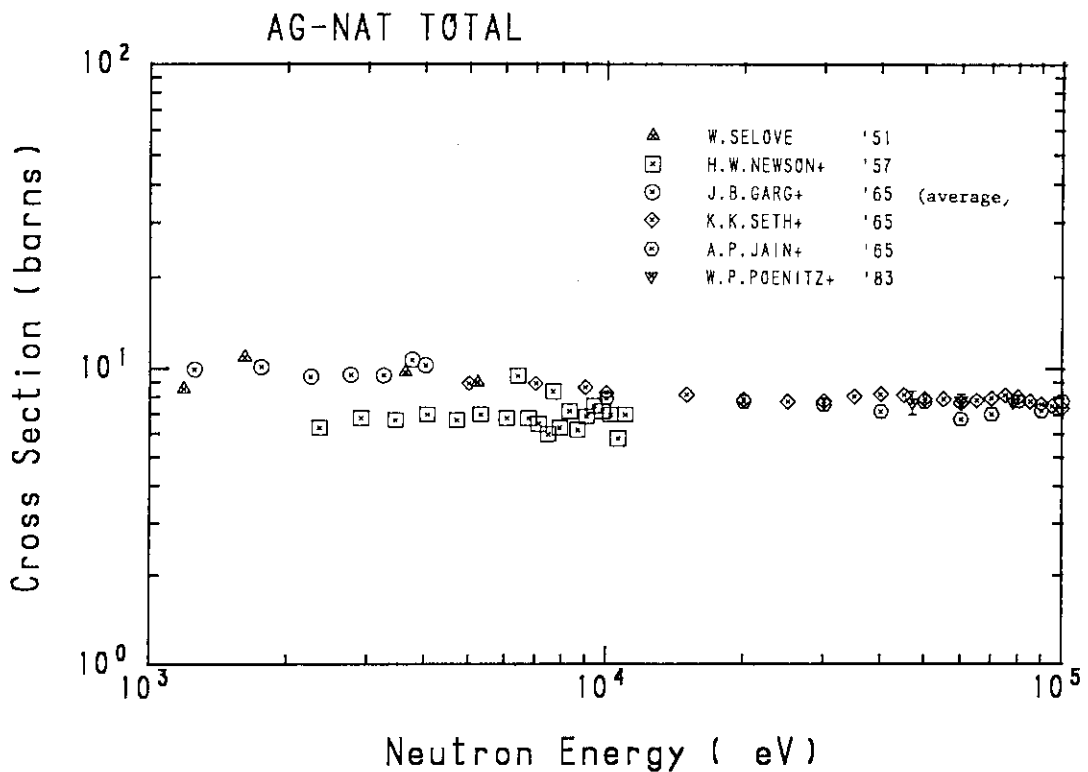


Fig. 1 Measured total cross section of natural silver in the energy region from 1 keV to 100 keV.

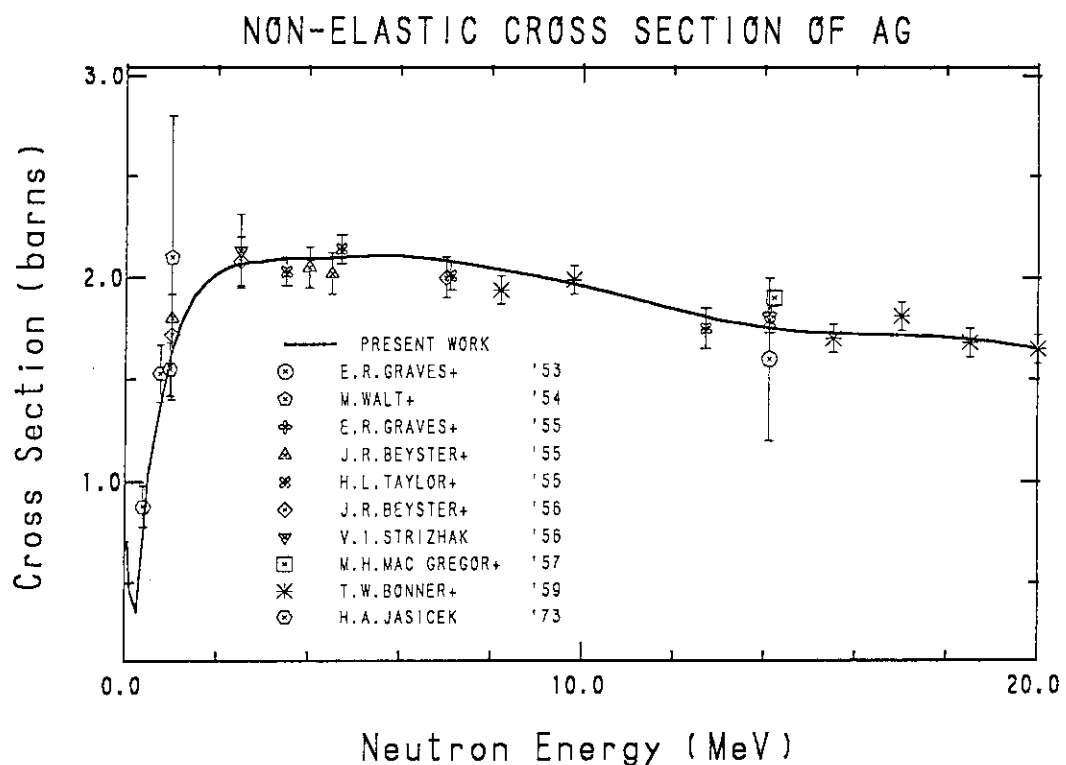


Fig. 2 Non-elastic scattering cross section of natural silver.

The solid line is the optical-model calculation.

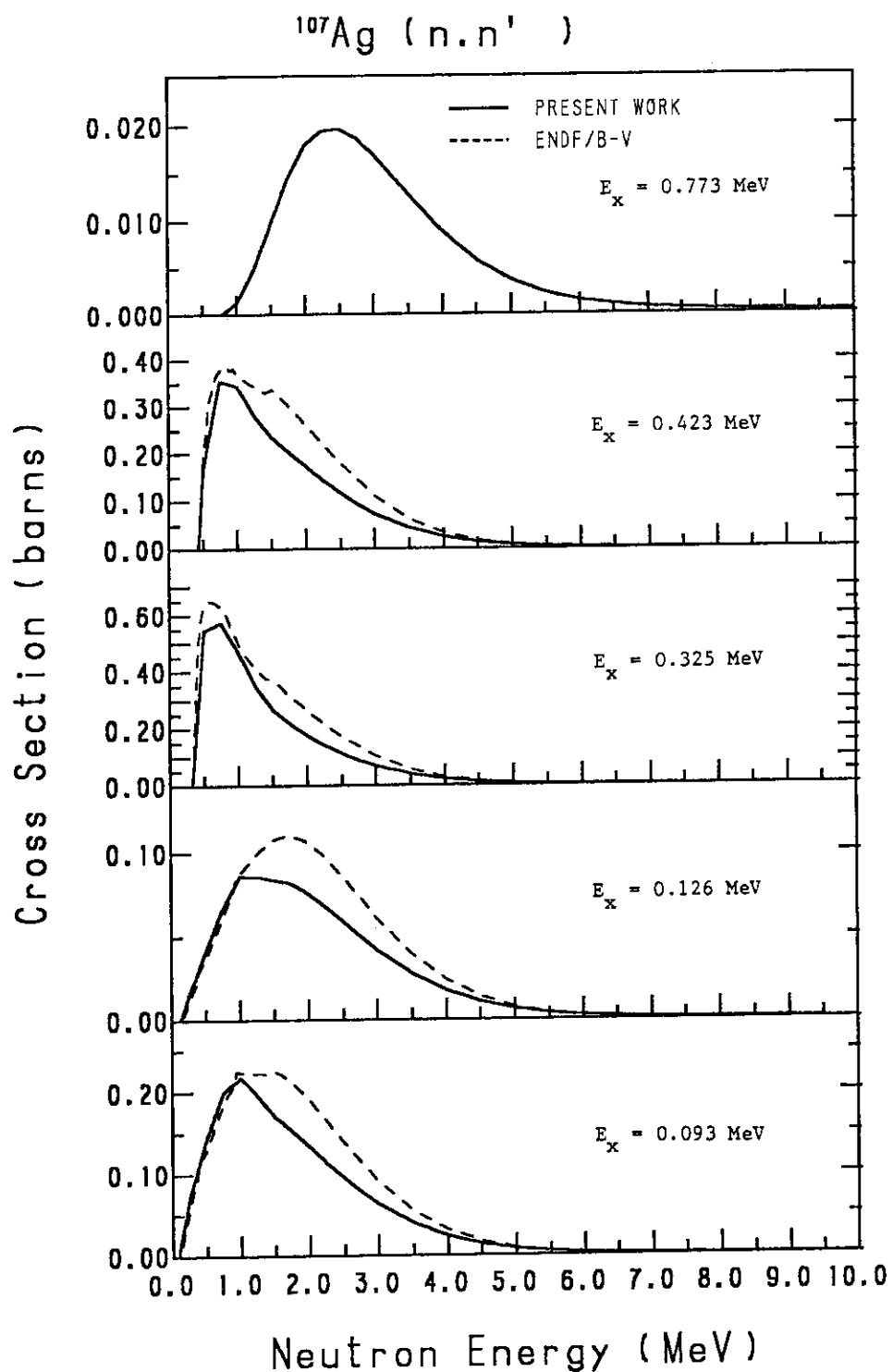


Fig. 3(a) Inelastic scattering cross sections of  $^{107}\text{Ag}$  up to an excitation energy of 0.773 MeV.

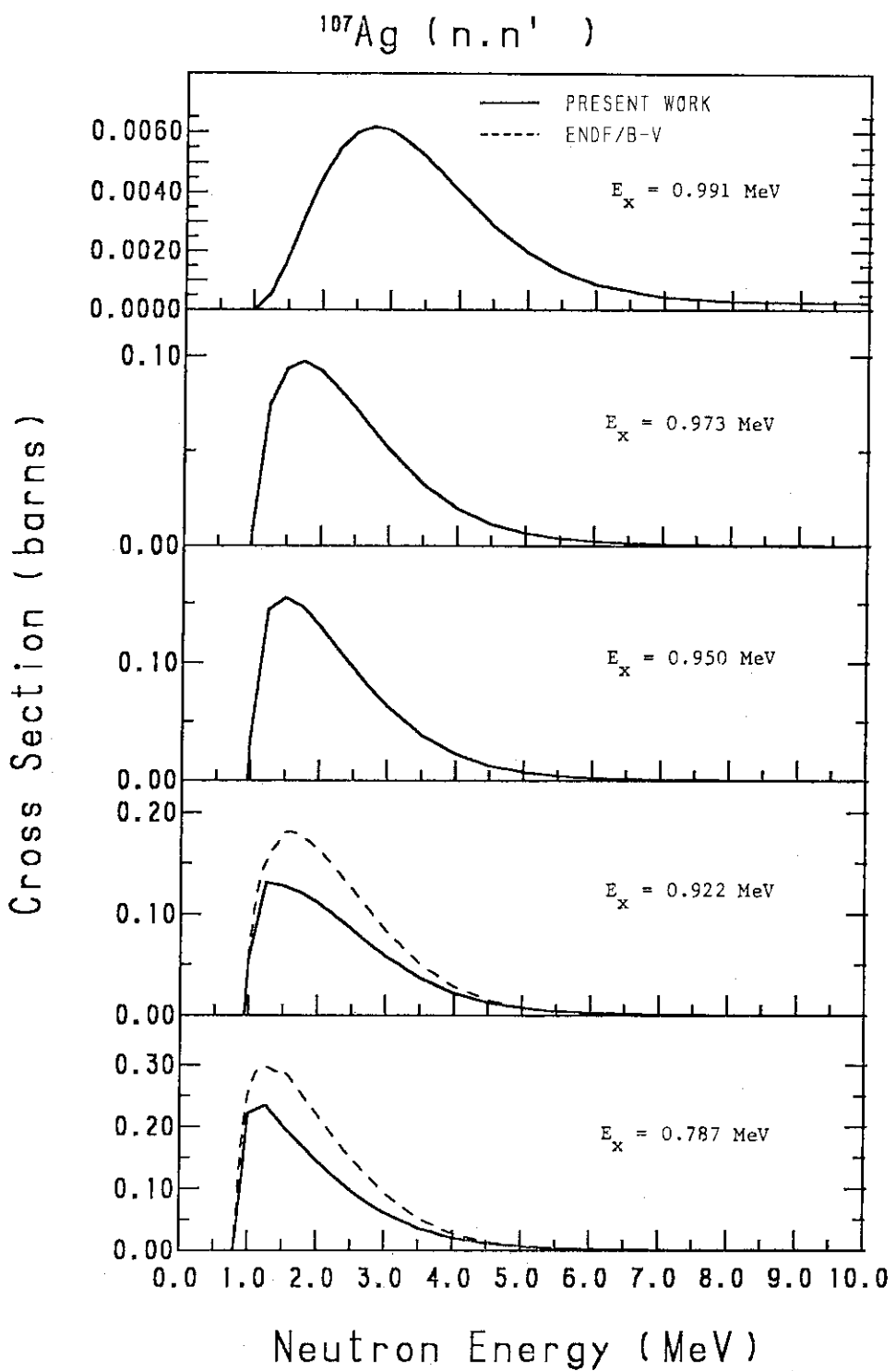


Fig. 3(b) Inelastic scattering cross sections of  $^{107}\text{Ag}$  up to an excitation energy of 0.991 MeV.

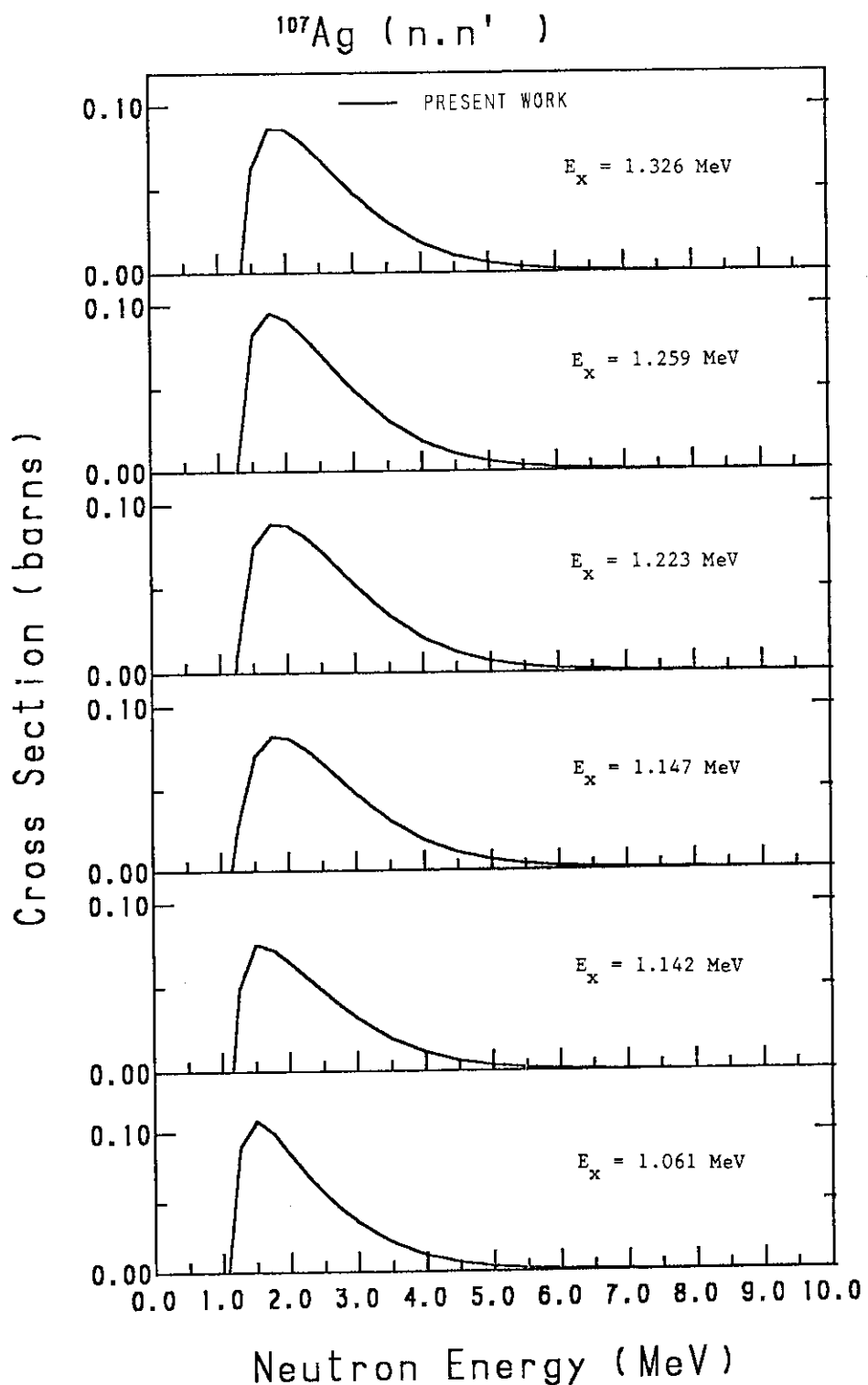


Fig. 3(c) Inelastic scattering cross sections of  $^{107}\text{Ag}$  up to an excitation energy of 1.326 MeV.

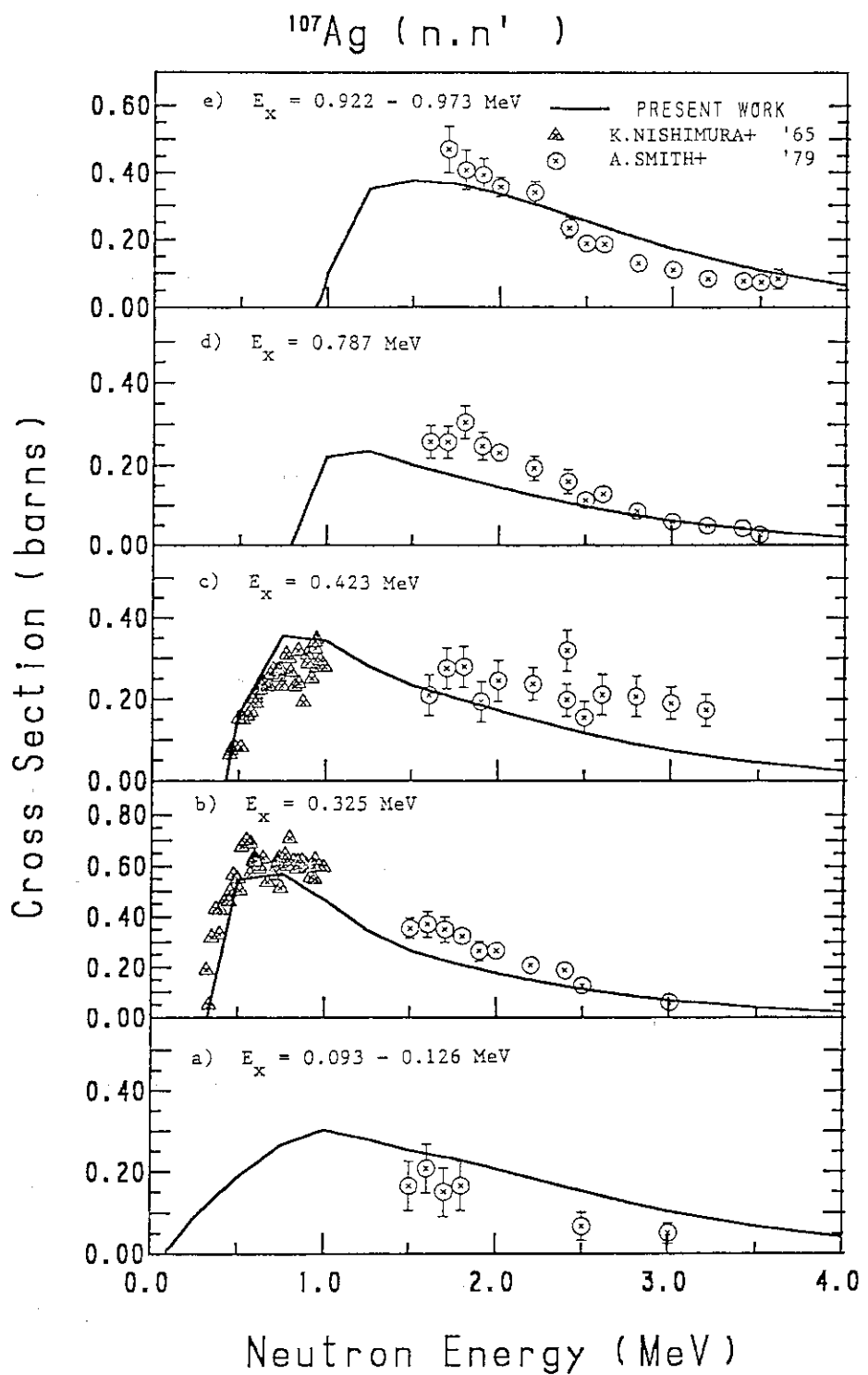


Fig. 3(d) Inelastic scattering cross sections of  $^{107}\text{Ag}$ .

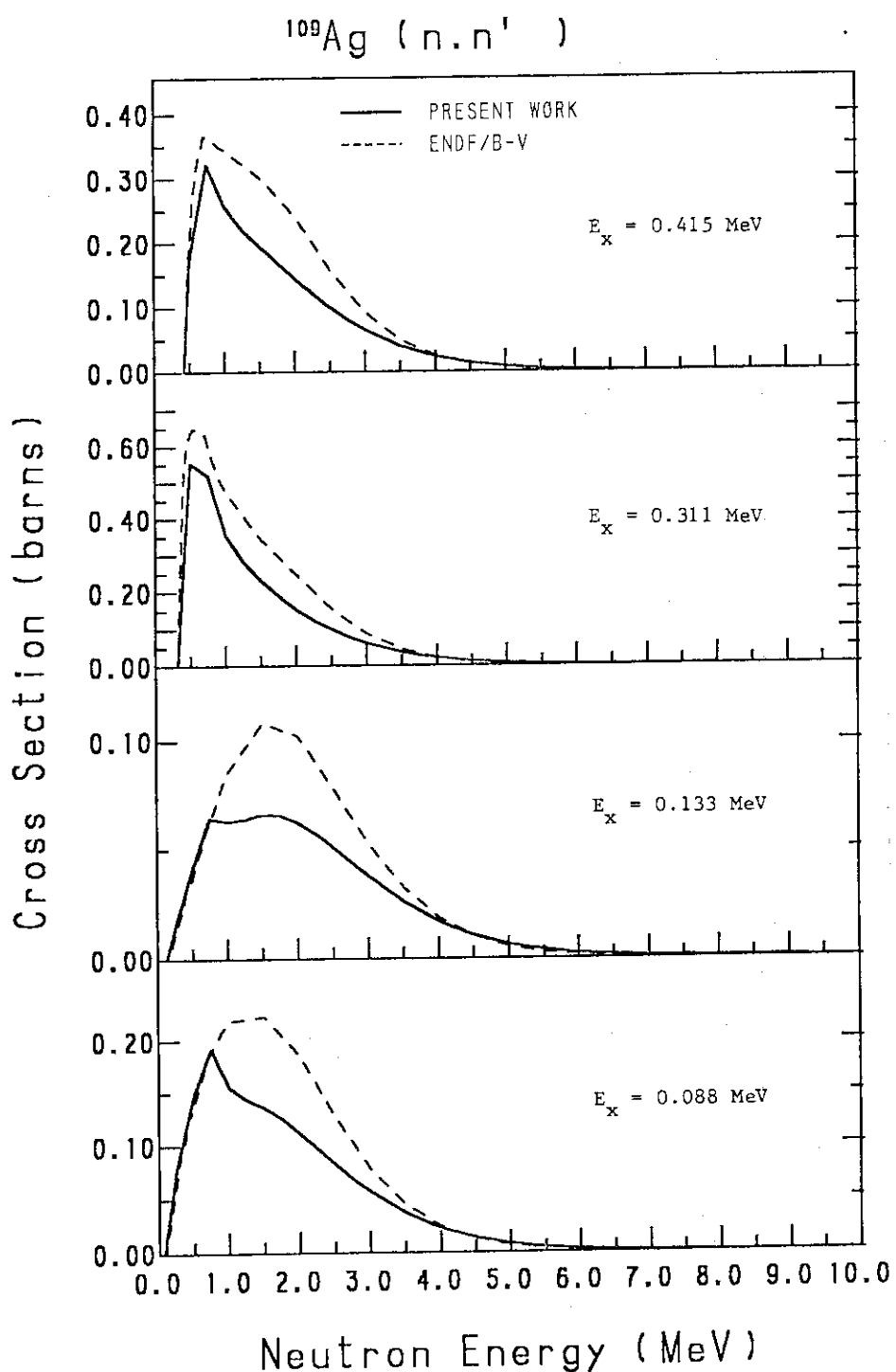


Fig. 4(a) Inelastic scattering cross sections of  $^{109}\text{Ag}$  up to an excitation energy of 0.415 MeV.

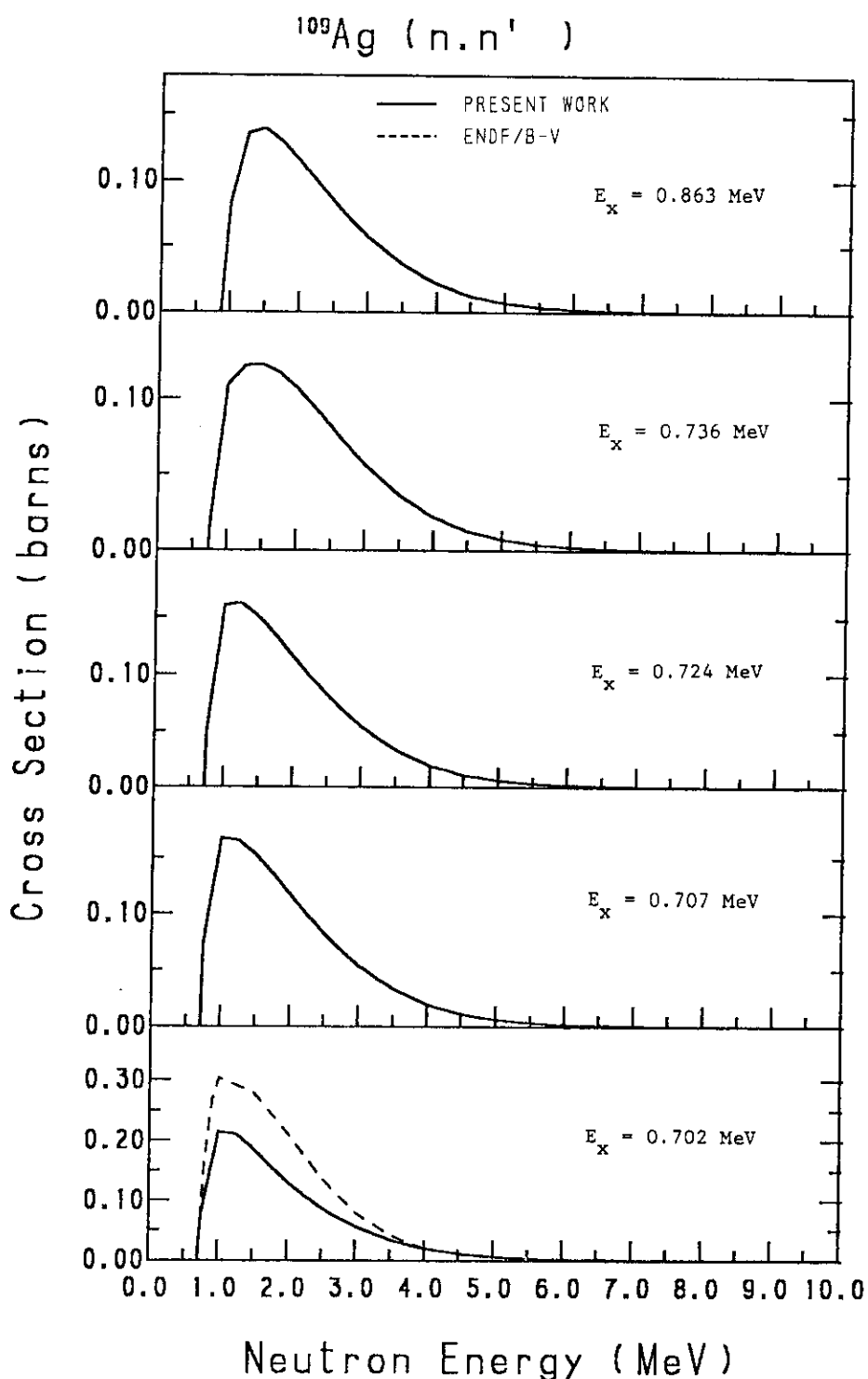


Fig. 4(b) Inelastic scattering cross sections of  $^{109}\text{Ag}$  up to an excitation energy of 0.863 MeV.

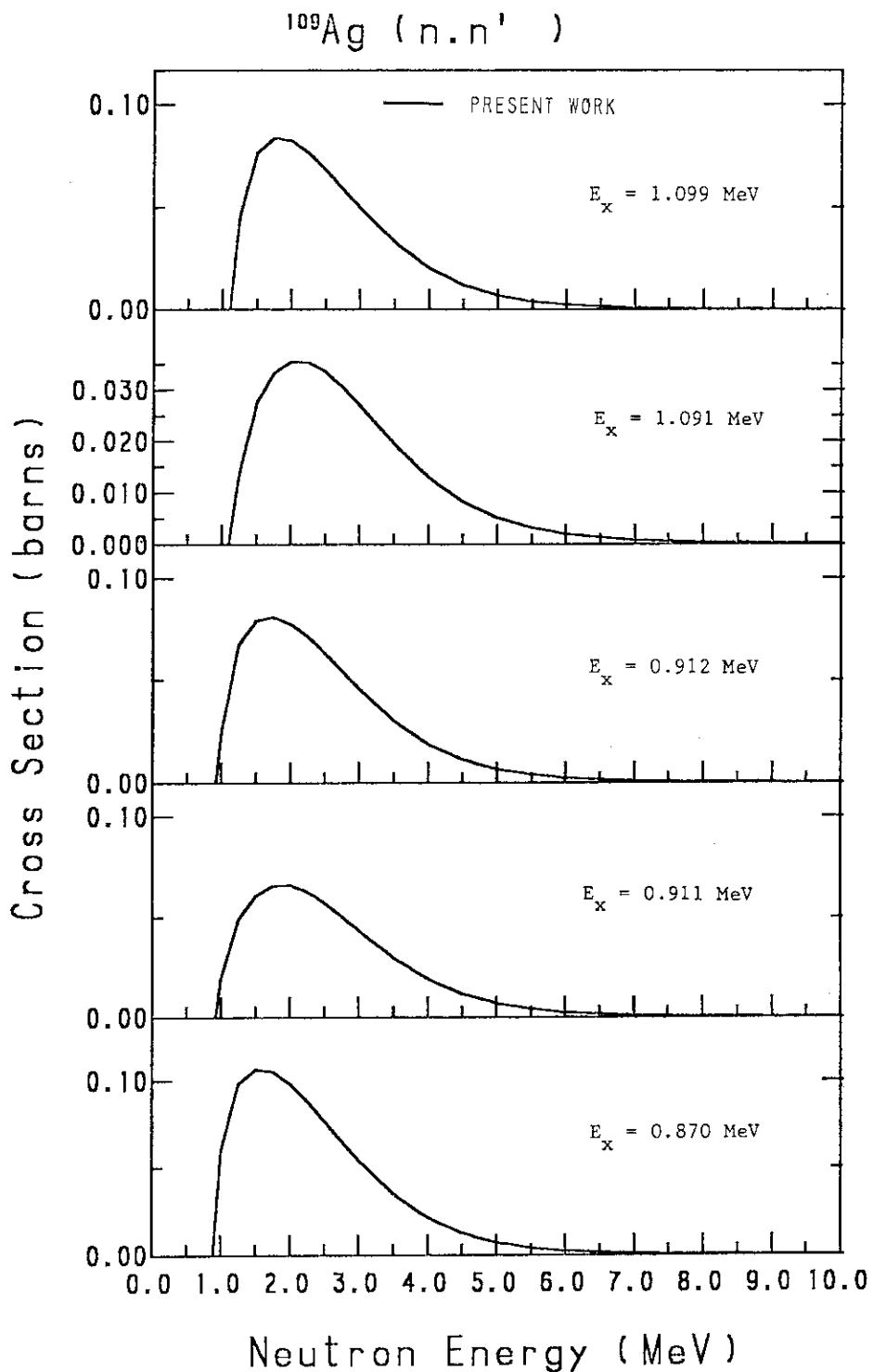
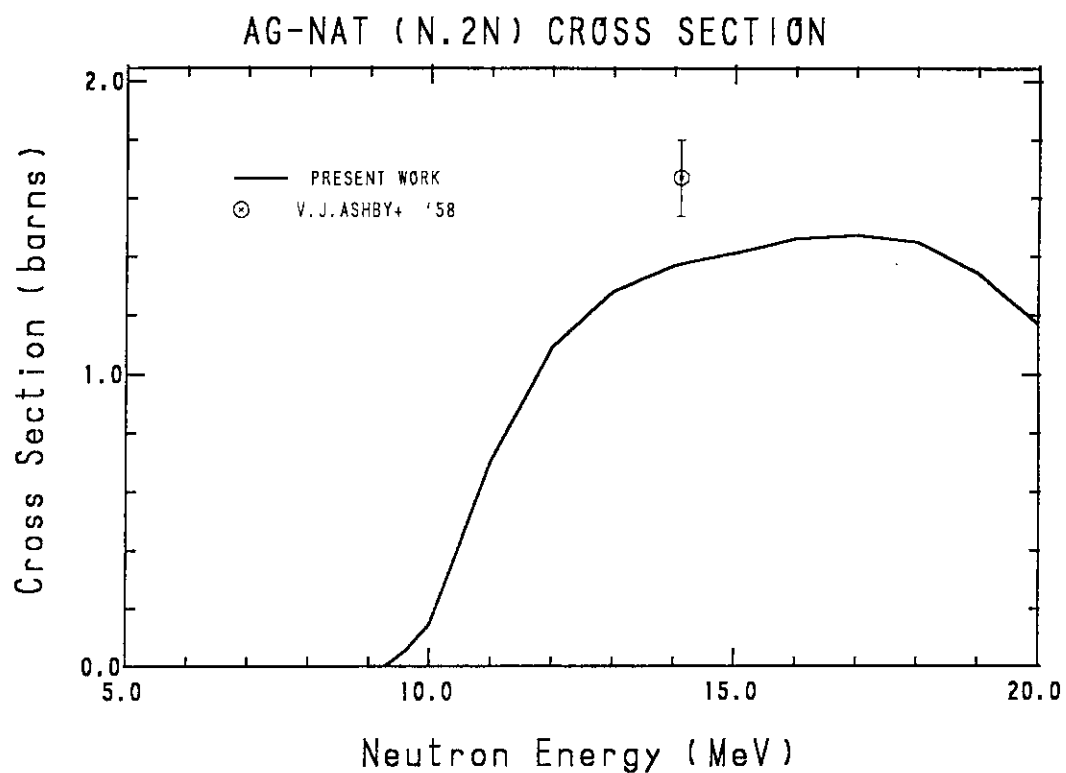
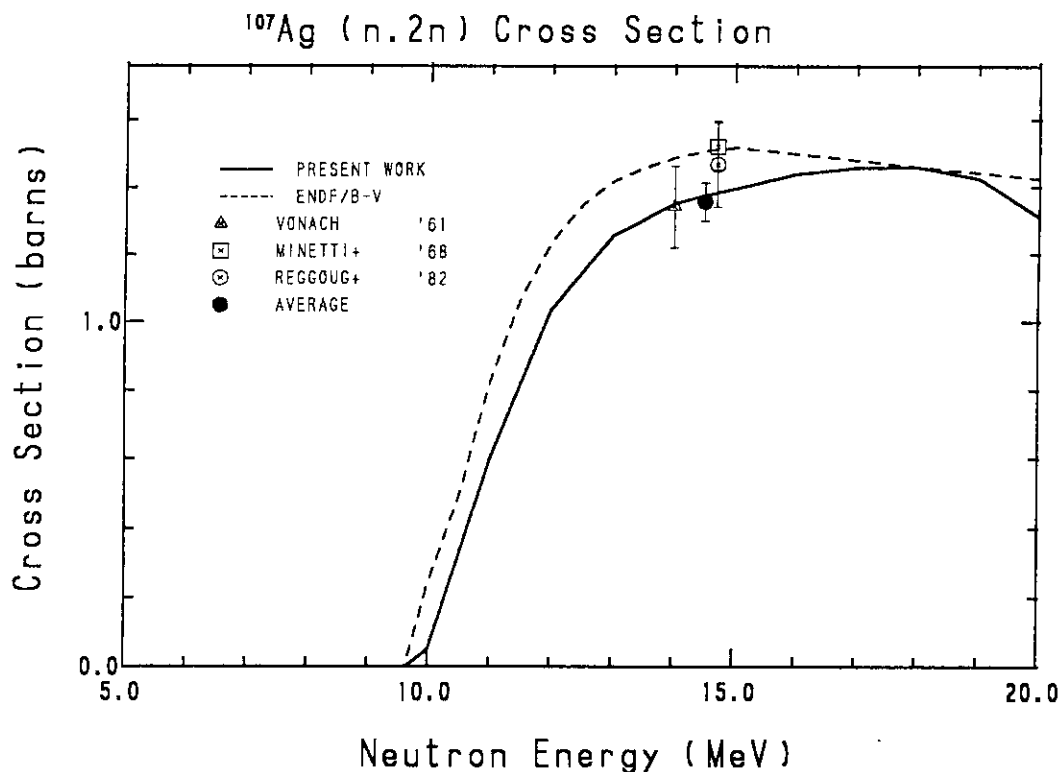
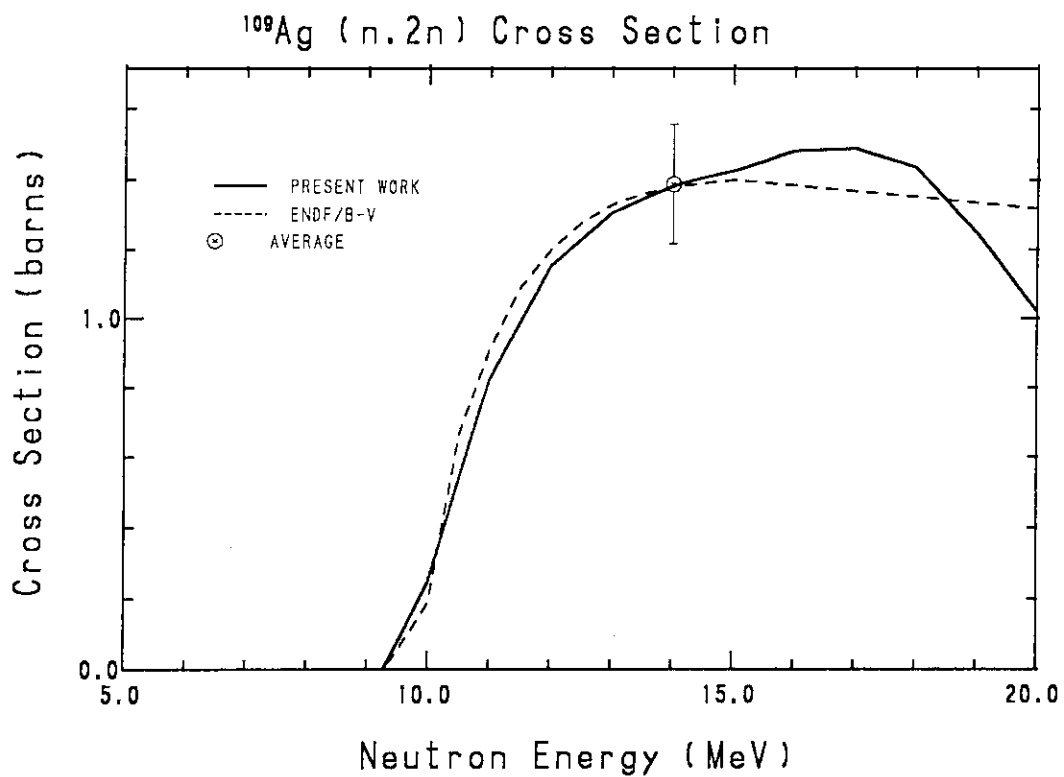
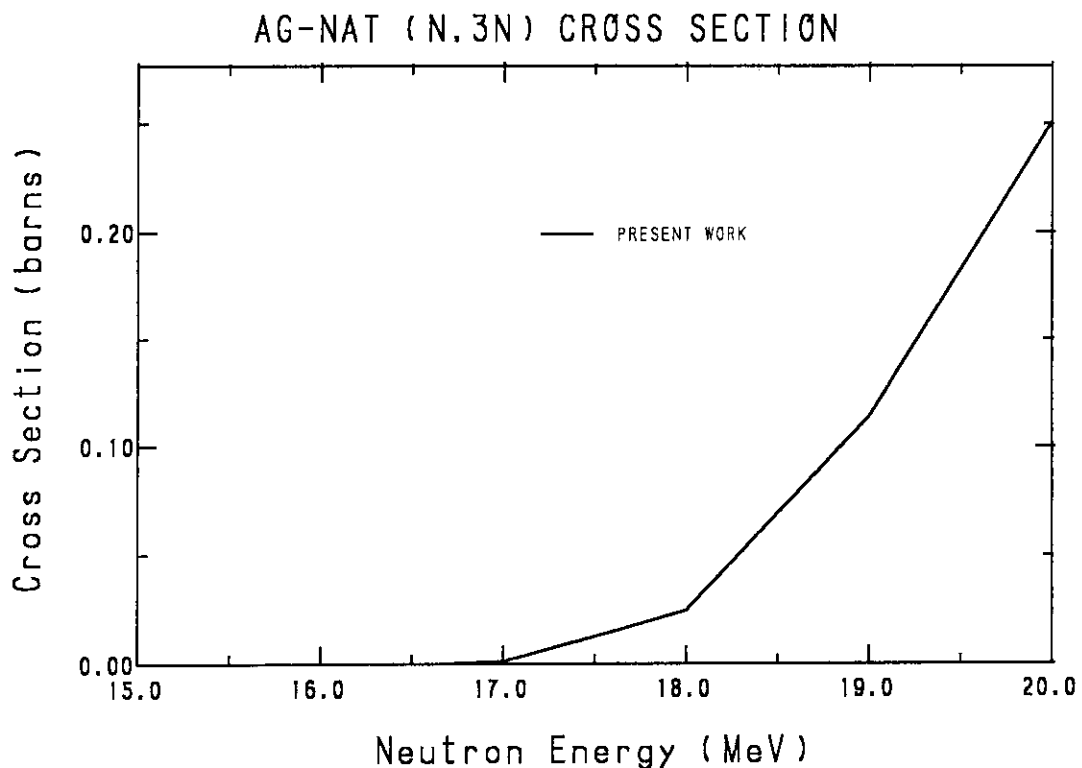
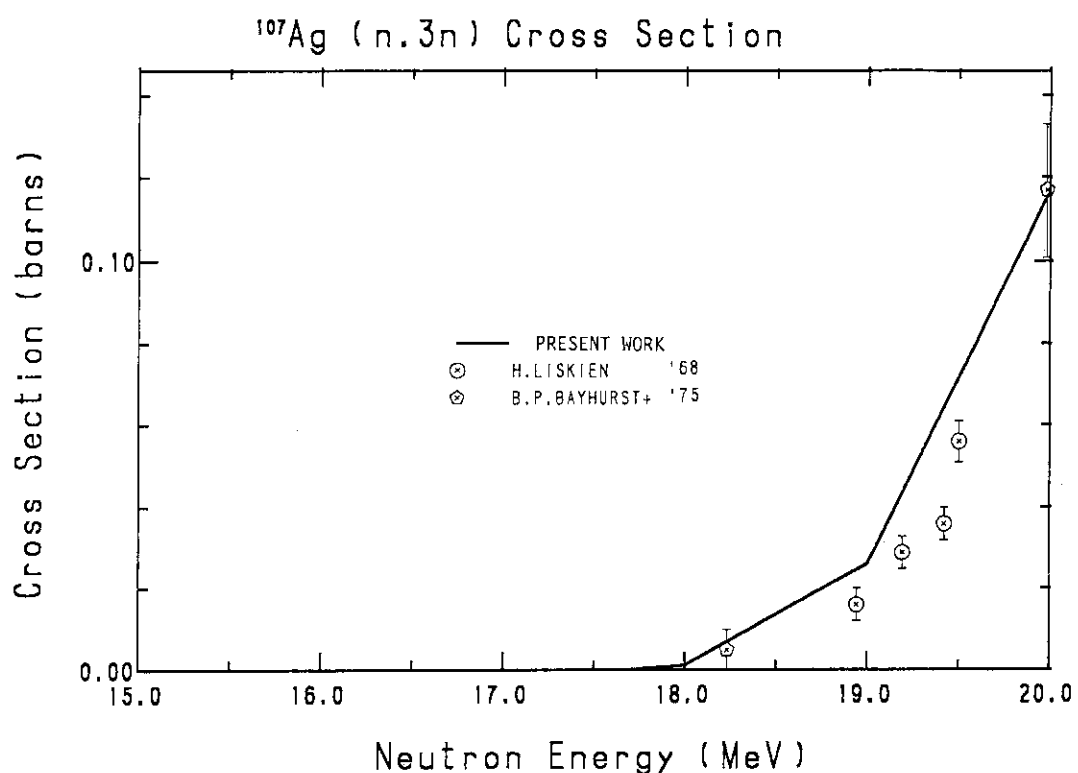
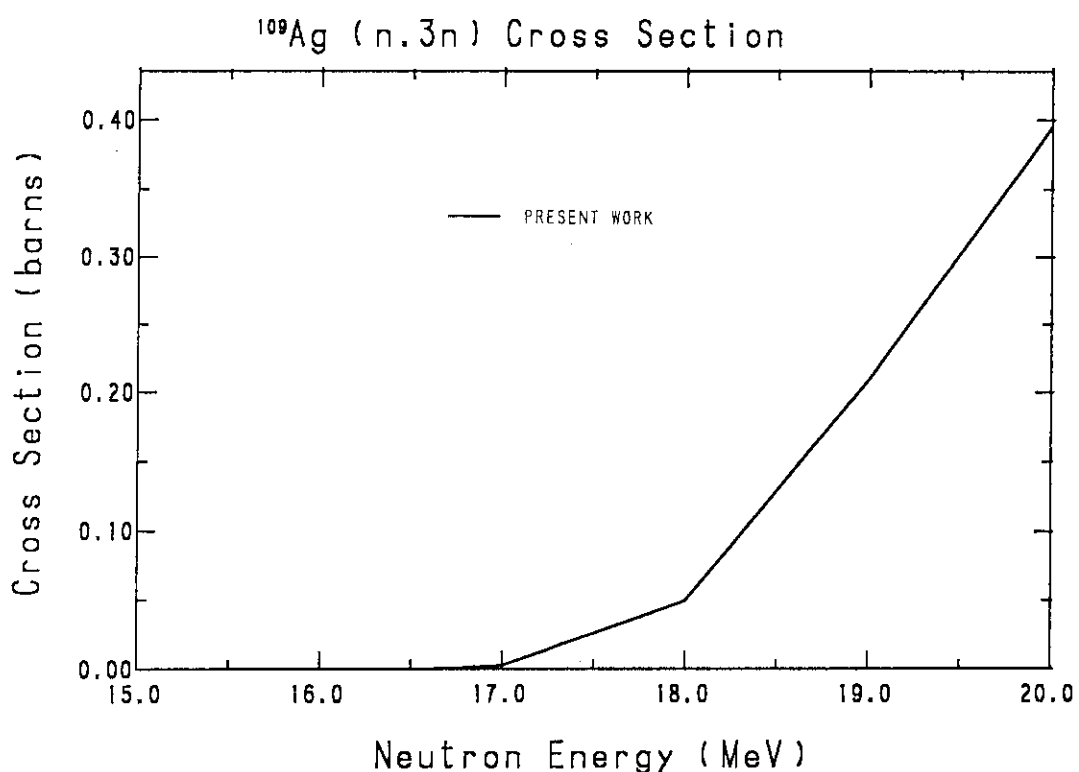
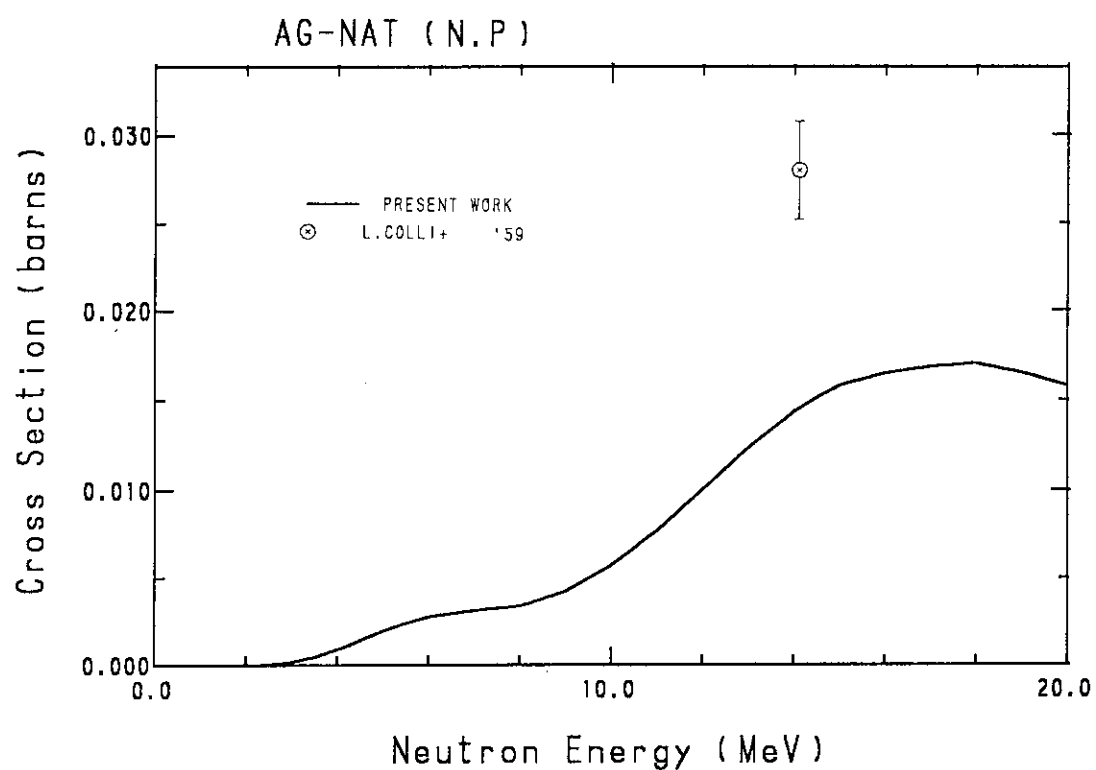
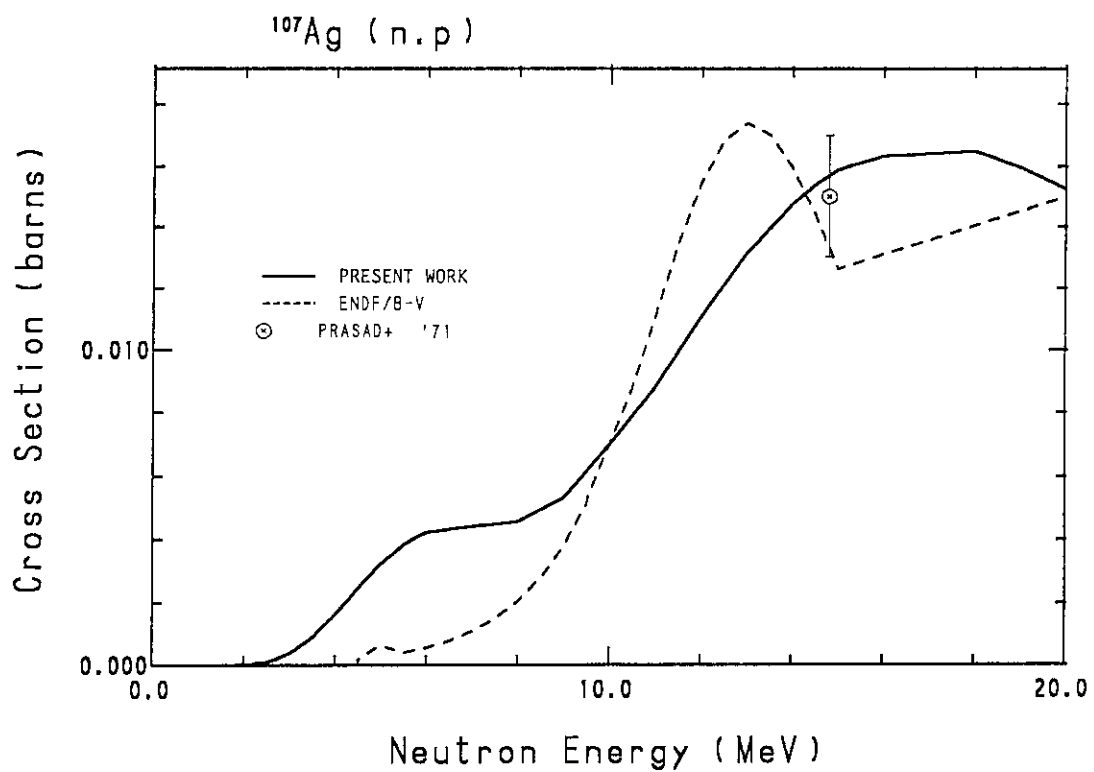


Fig. 4(c) Inelastic scattering cross sections of  $^{109}\text{Ag}$  up to an excitation energy of 1.099 MeV.

Fig. 5 ( $n, 2n$ ) reaction cross section of natural silver.Fig. 6 ( $n, 2n$ ) reaction cross section of  $^{107}\text{Ag}$ .

Fig. 7 ( $n,2n$ ) reaction cross section of  $^{109}\text{Ag}$ .Fig. 8 ( $n,3n$ ) reaction cross section of natural silver.

Fig. 9 ( $n,3n$ ) reaction cross section of  $^{107}\text{Ag}$ .Fig. 10 ( $n,3n$ ) reaction cross section of  $^{109}\text{Ag}$ .

Fig. 11 ( $n,p$ ) reaction cross section of natural silver.Fig. 12 ( $n,p$ ) reaction cross section of  $^{107}\text{Ag}$ .

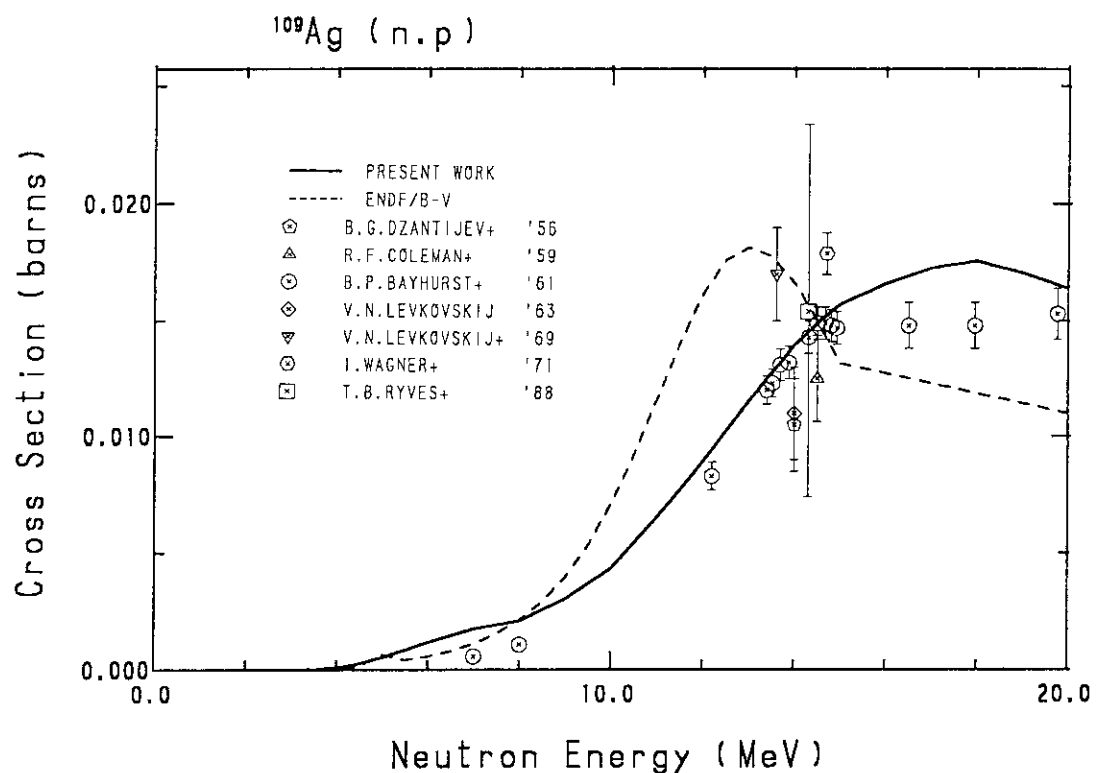
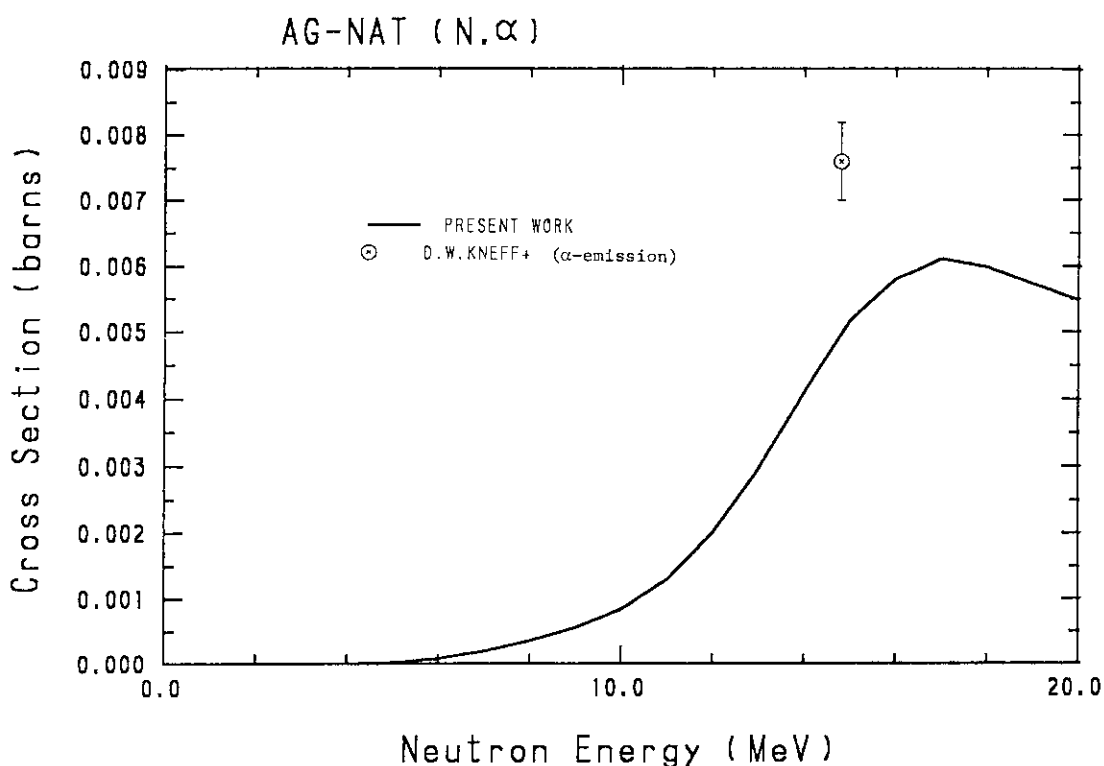
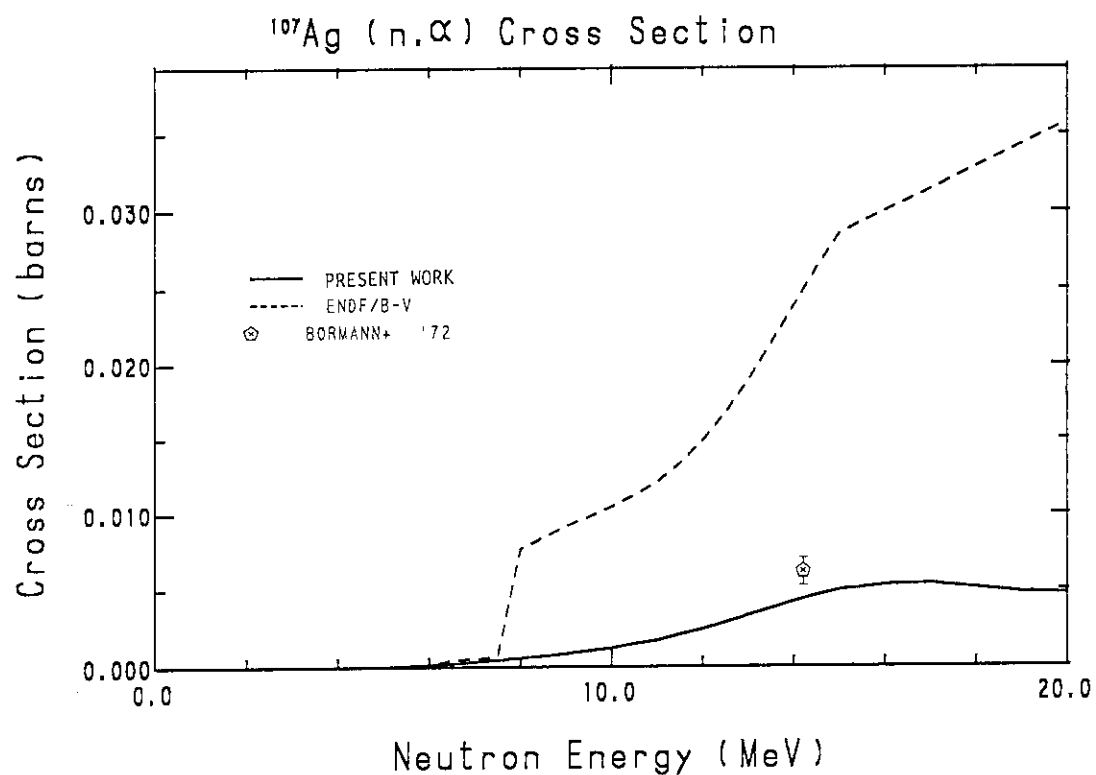
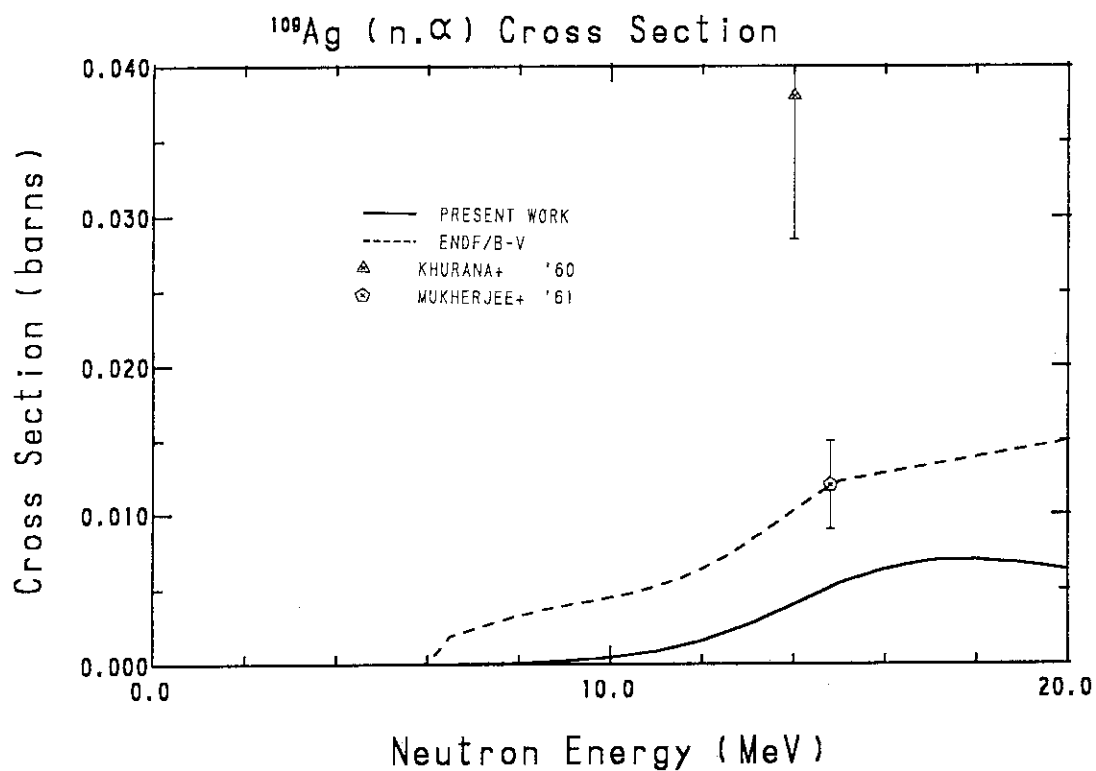
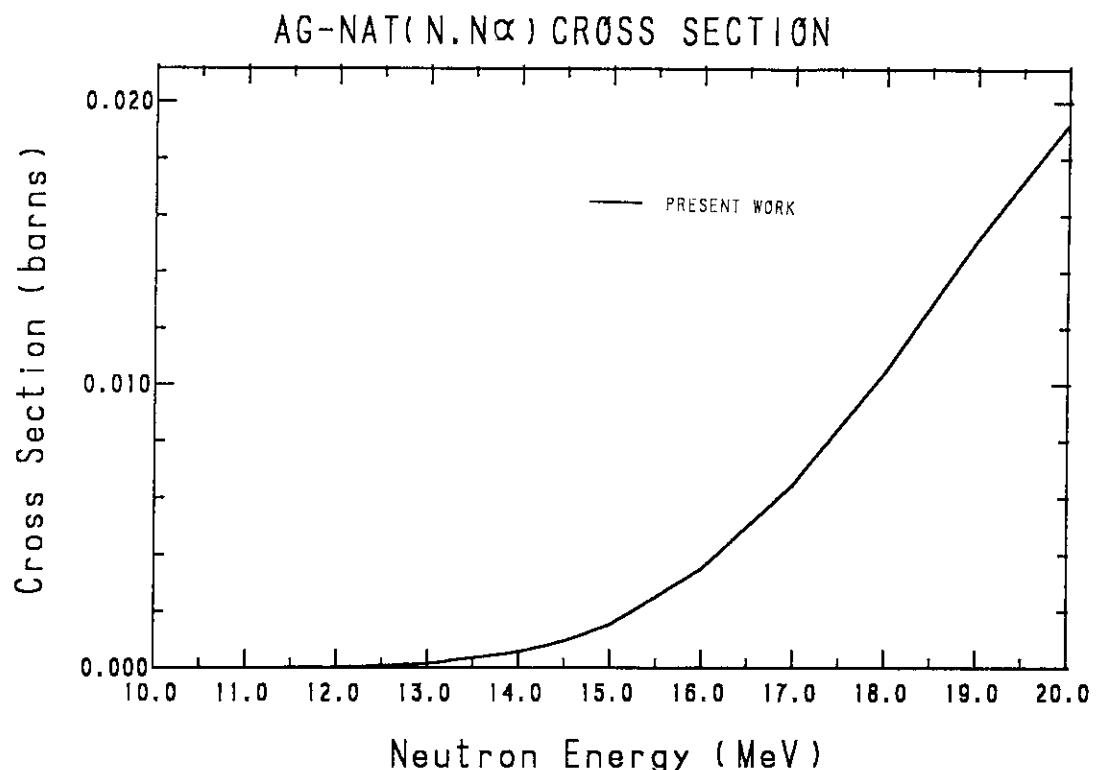
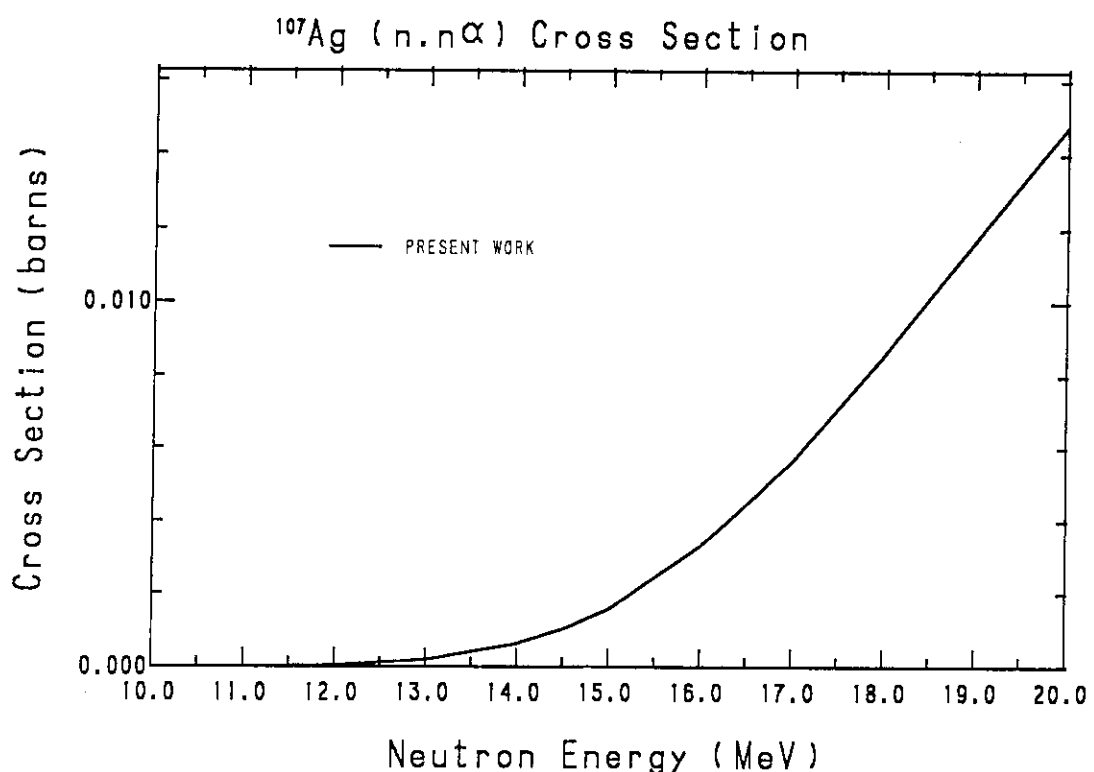
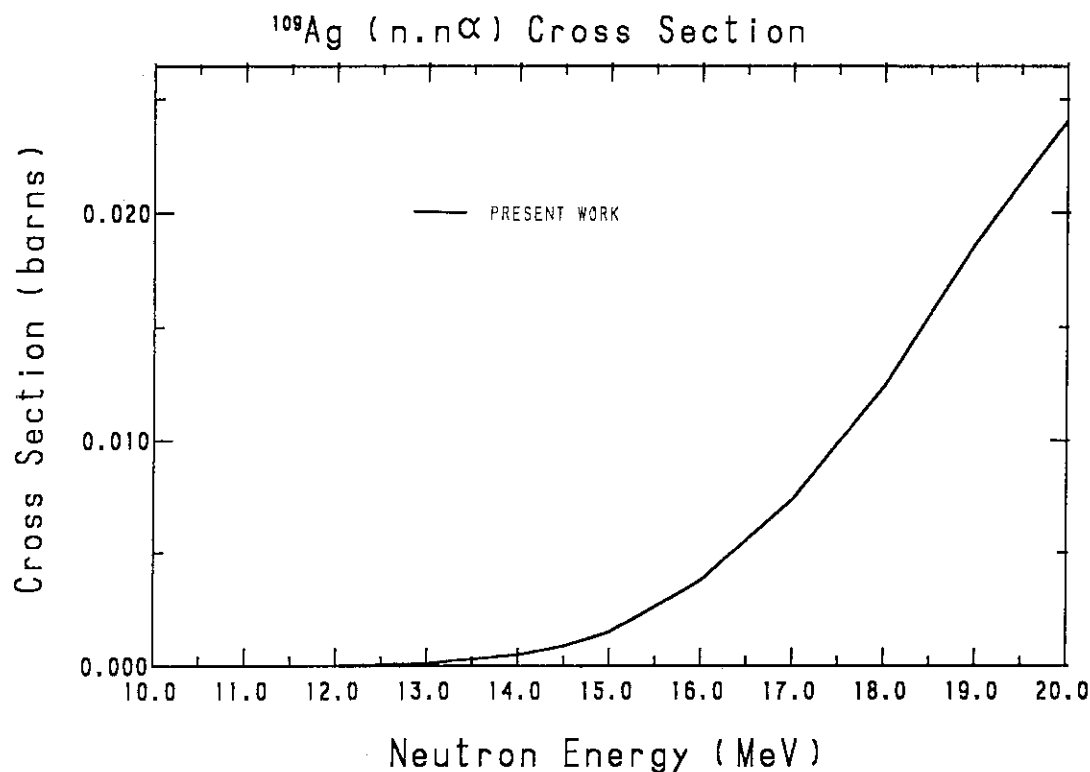
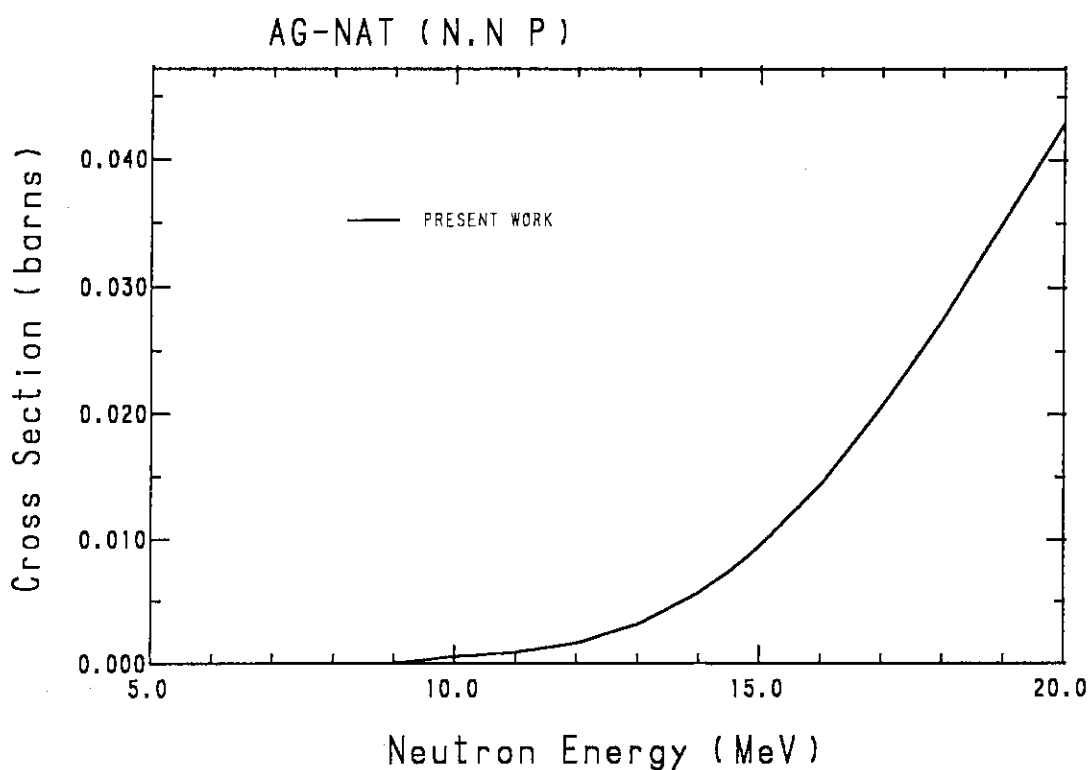
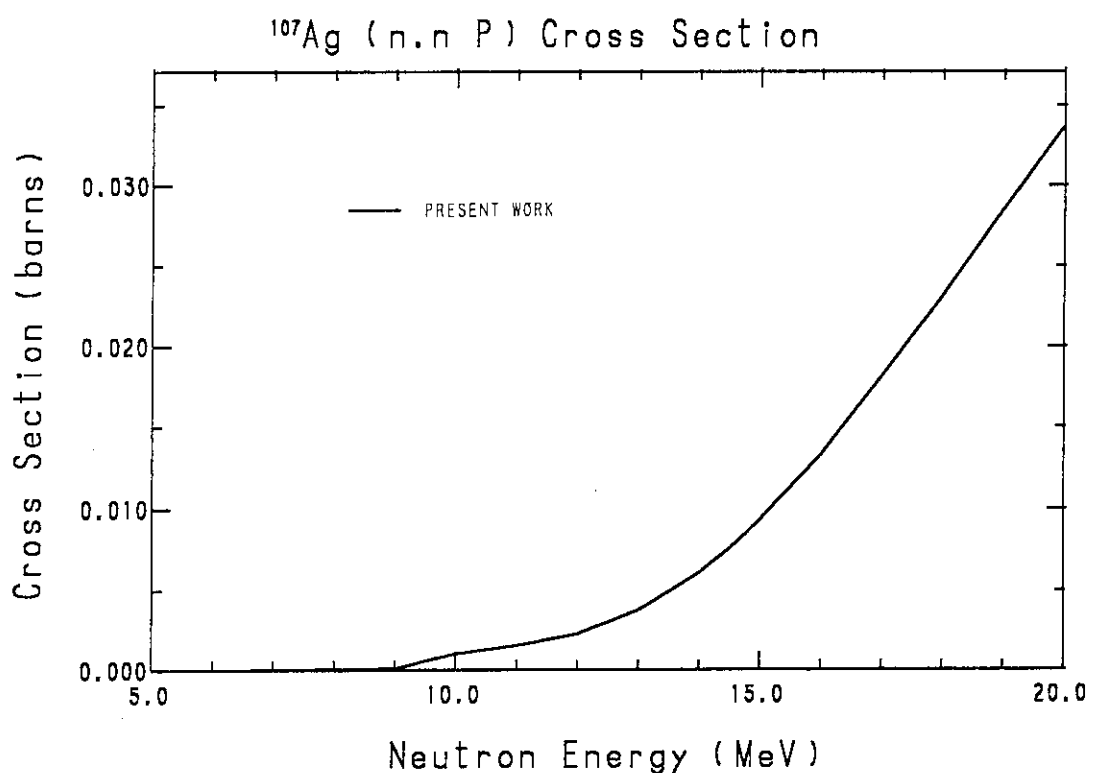
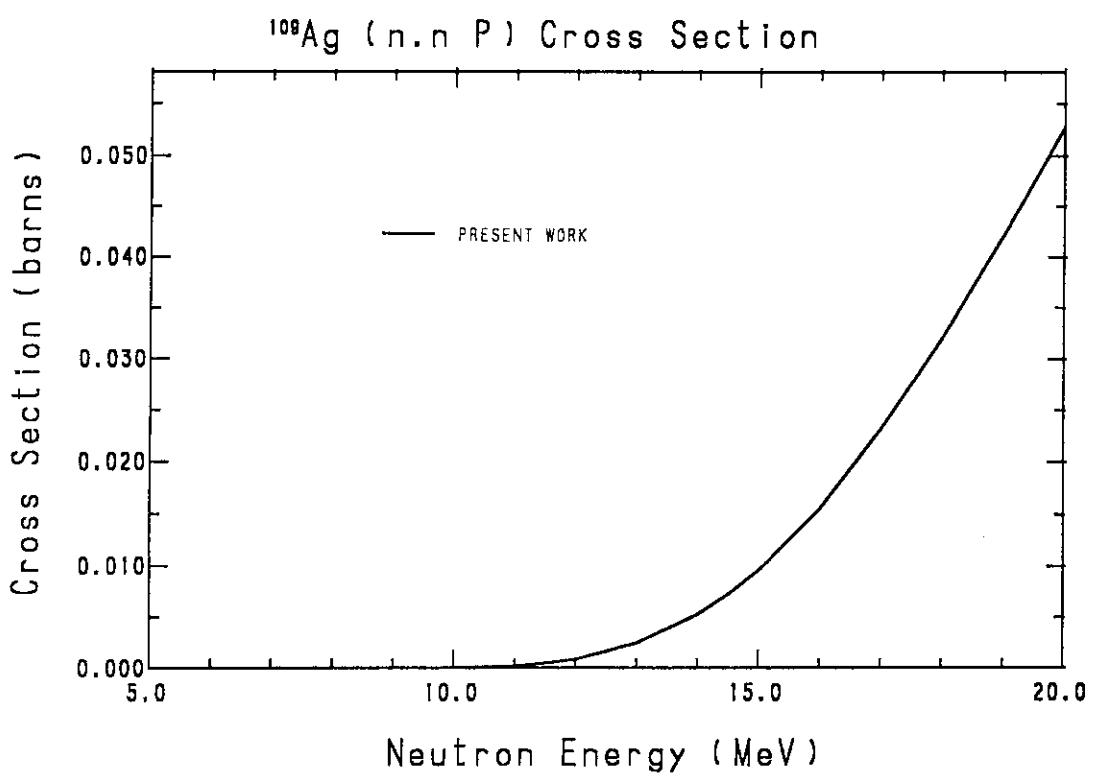
Fig. 13 (n,p) reaction cross section of  $^{109}\text{Ag}$ .

Fig. 14 (n,α) reaction cross section of natural silver.

Fig. 15 ( $n,\alpha$ ) reaction cross section of  $^{107}\text{Ag}$ .Fig. 16 ( $n,\alpha$ ) reaction cross section of  $^{109}\text{Ag}$ .

Fig. 17 ( $n, n\alpha$ ) reaction cross section of natural silver.Fig. 18 ( $n, n\alpha$ ) reaction cross section of  $^{107}\text{Ag}$ .

Fig. 19 ( $n, n\alpha$ ) reaction cross section of  $^{109}\text{Ag}$ .Fig. 20 ( $n, np$ ) reaction cross section of natural silver.

Fig. 21 (n,np) reaction cross section of  $^{107}\text{Ag}$ .Fig. 22 (n,np) reaction cross section of  $^{109}\text{Ag}$ .

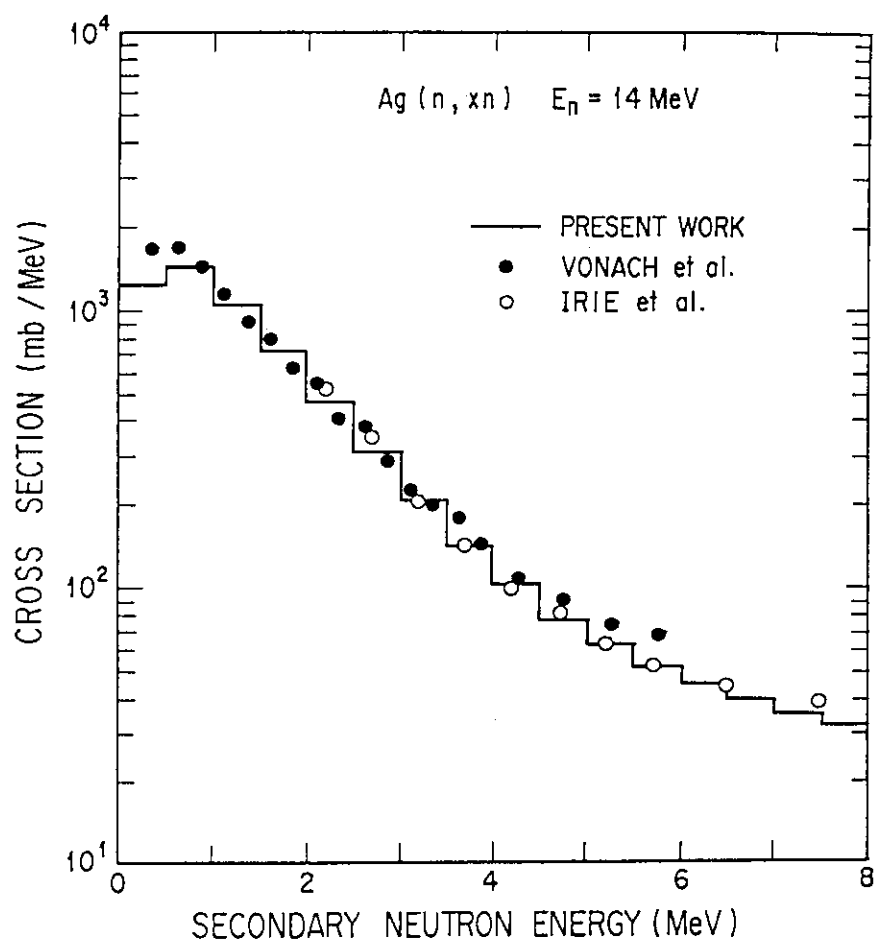


Fig. 23 Neutron emission spectra for natural silver at 14 MeV.

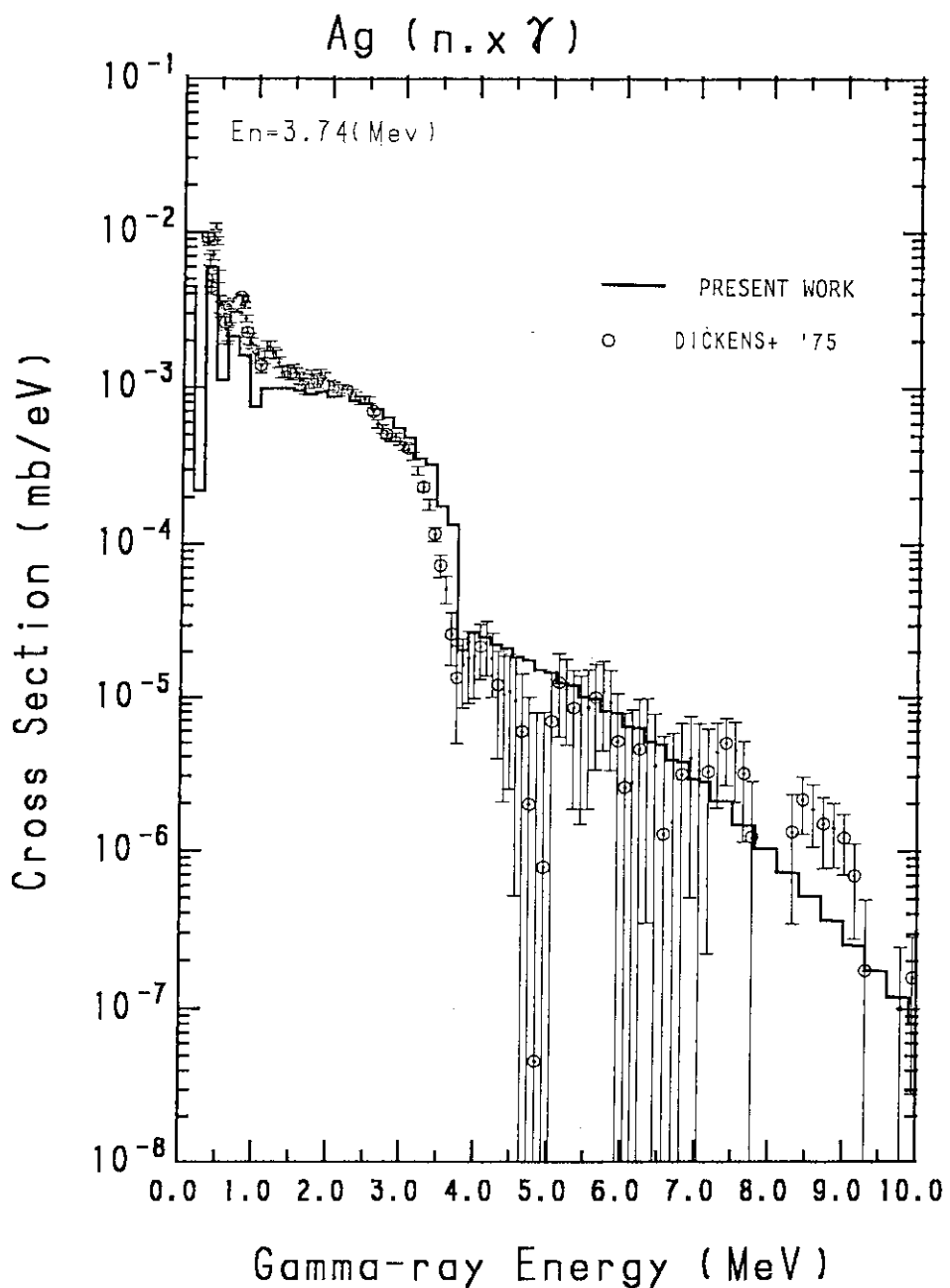


Fig. 24(a) Gamma-ray emission spectra for natural silver at 3.74 MeV.

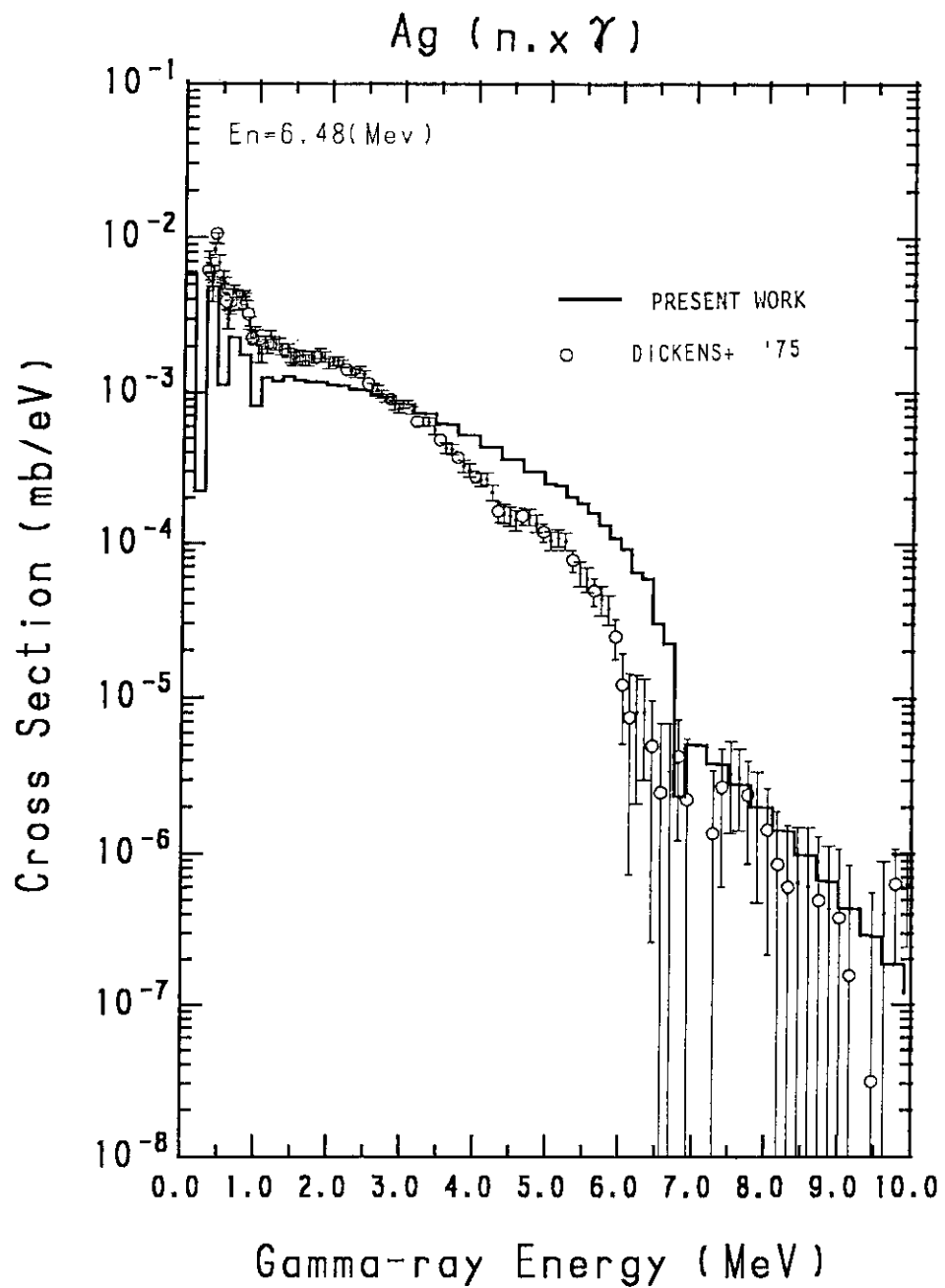


Fig. 24(b) Gamma-ray emission spectra for natural silver at 6.48 MeV.

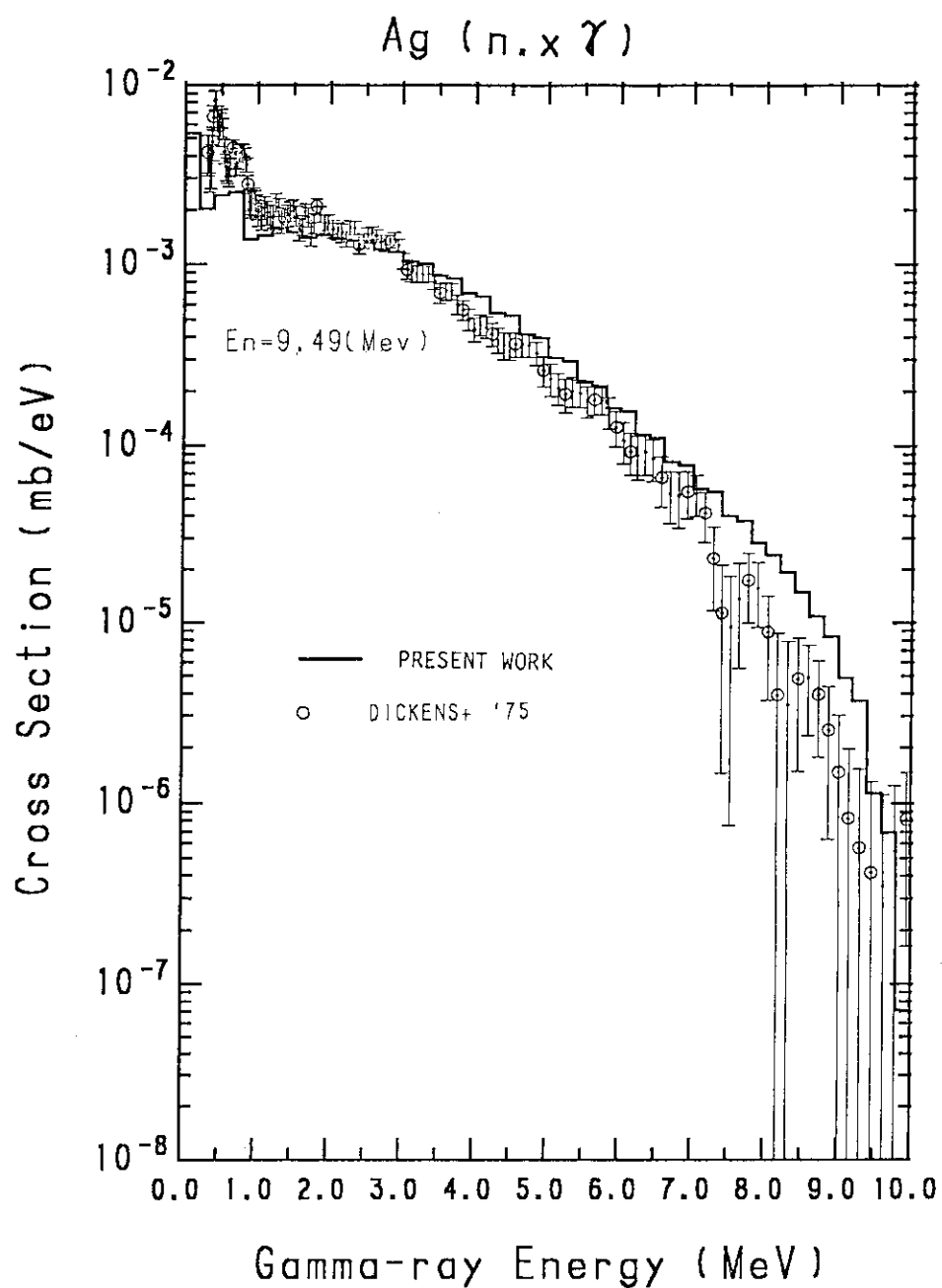


Fig. 24(c) Gamma-ray emission spectra for natural silver at 9.49 MeV.

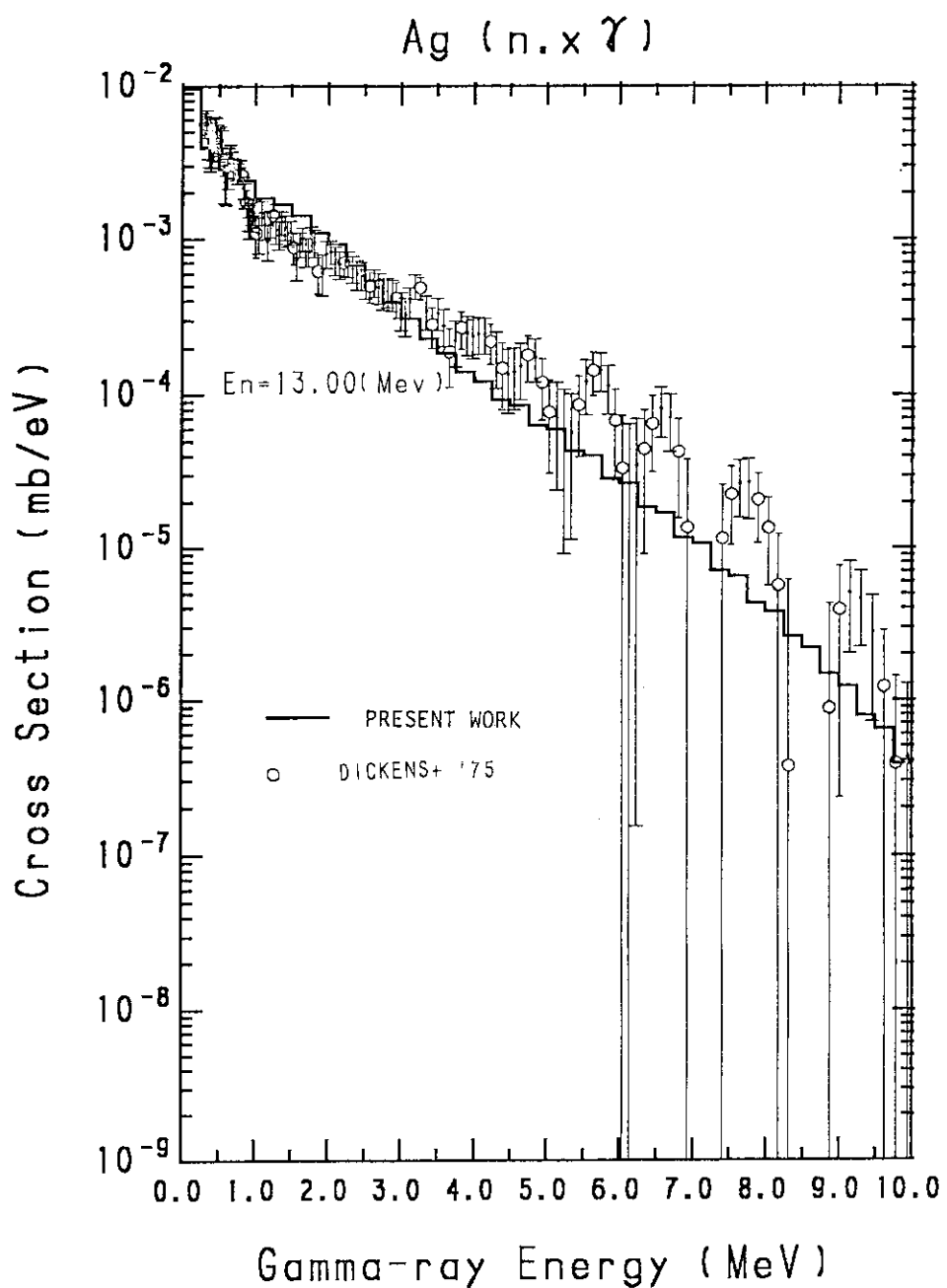


Fig. 24(d) Gamma-ray emission spectra for natural silver at 13.0 MeV.

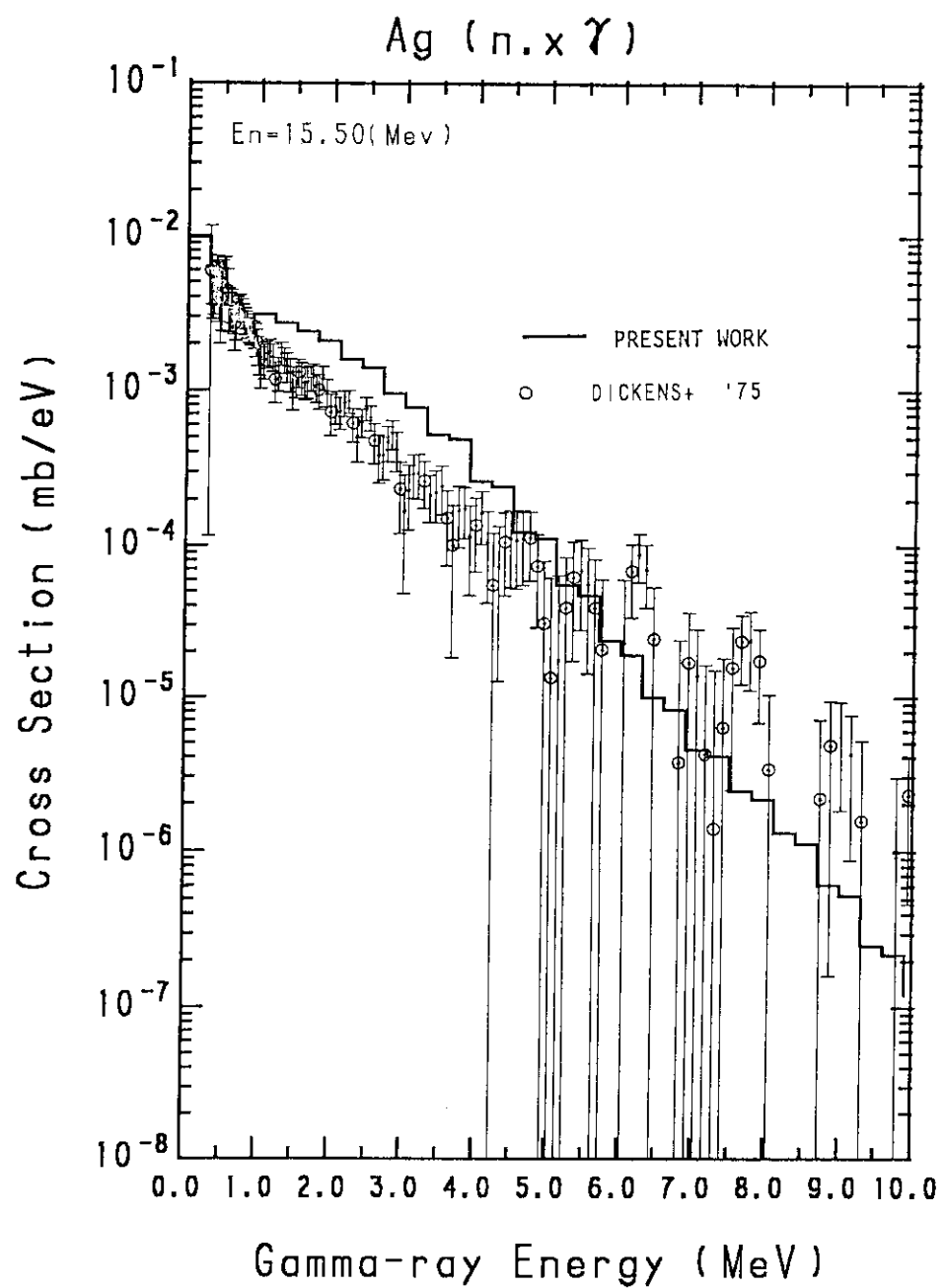


Fig. 24(e) Gamma-ray emission spectra for natural silver at 15.5 MeV.

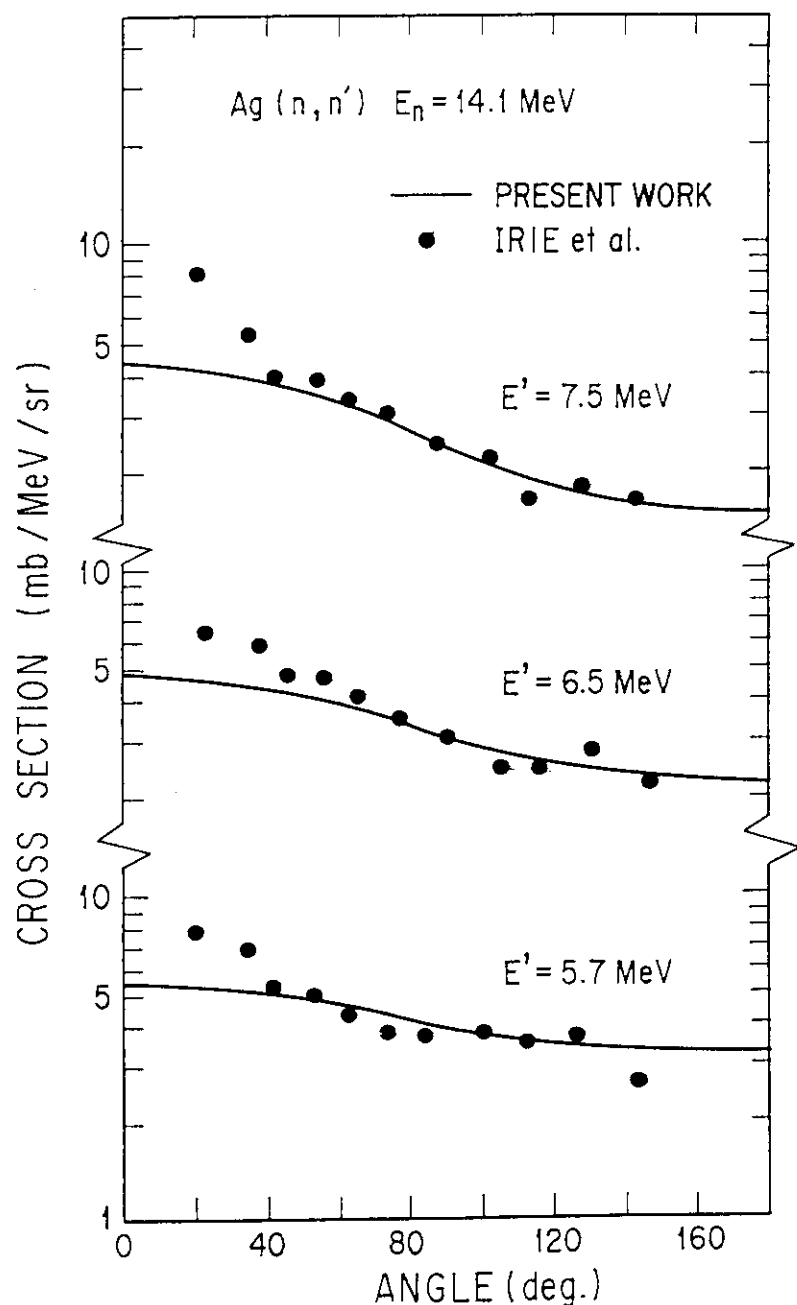


Fig. 25 Angular distributions of neutrons inelastically scattered to continuum levels of natural silver at 14.1 MeV.  
The symbol  $E'$  stands for an outgoing-neutron energy.

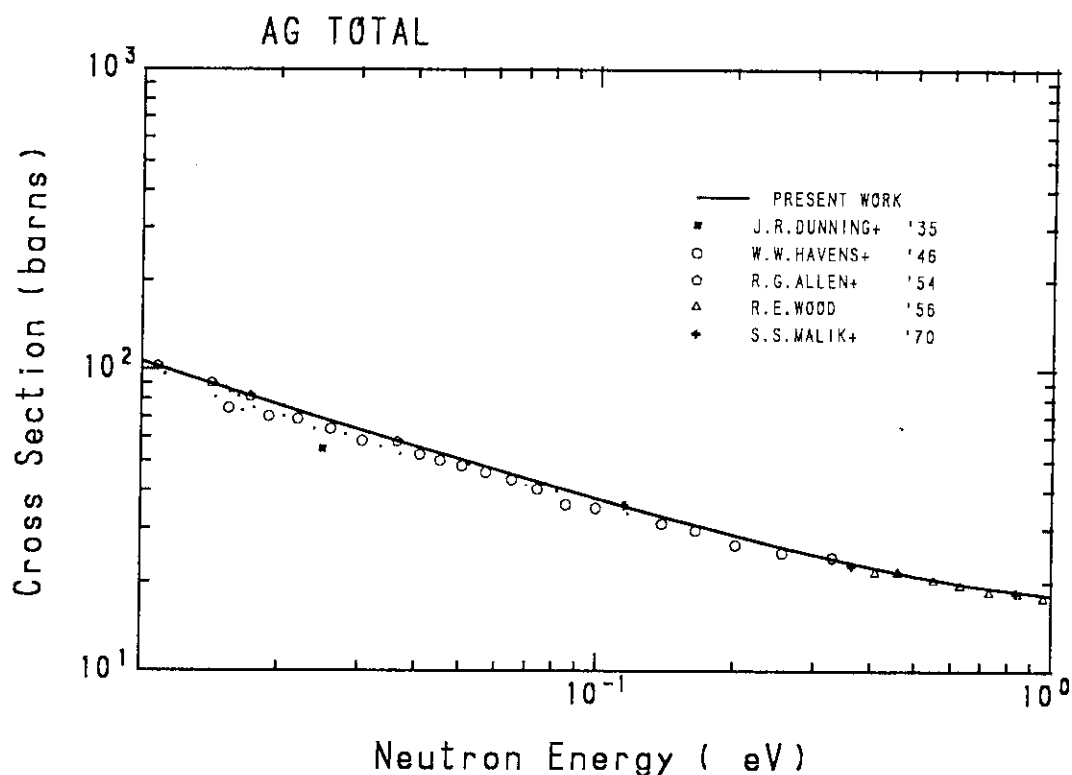


Fig. 26(a) Total cross section of natural silver in the energy region from  $10^{-2}$  eV to 1 eV.

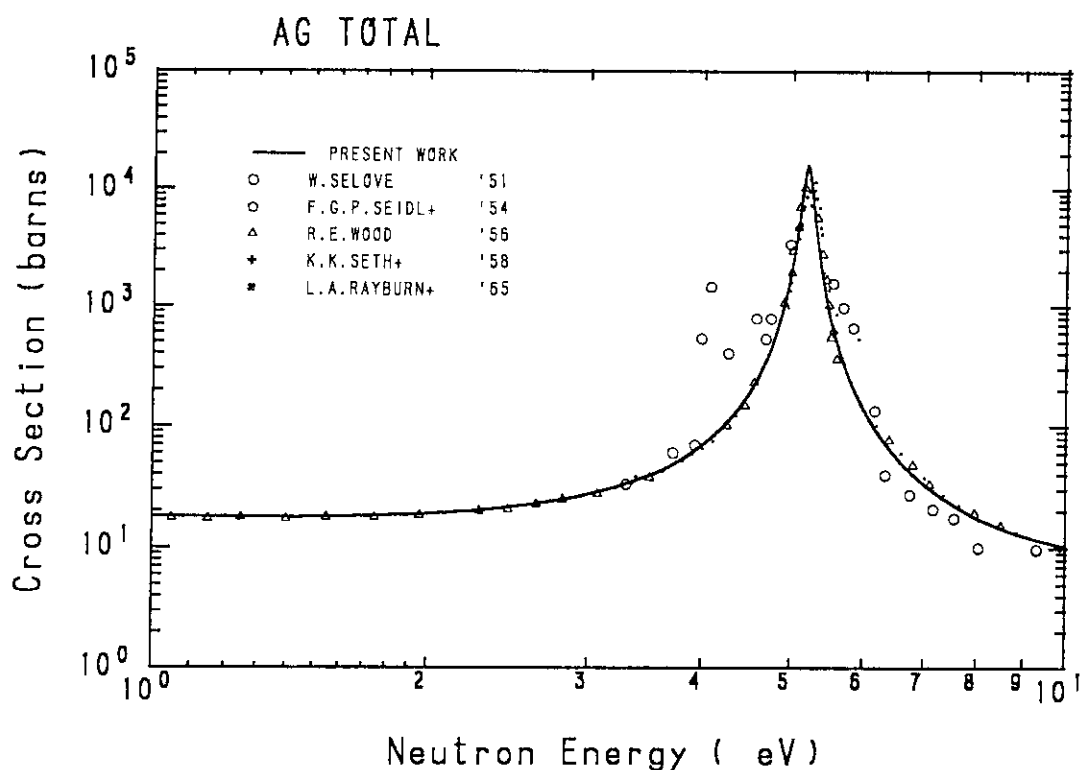


Fig. 26(b) Total cross section of natural silver in the energy region from 1 eV to 10 eV.

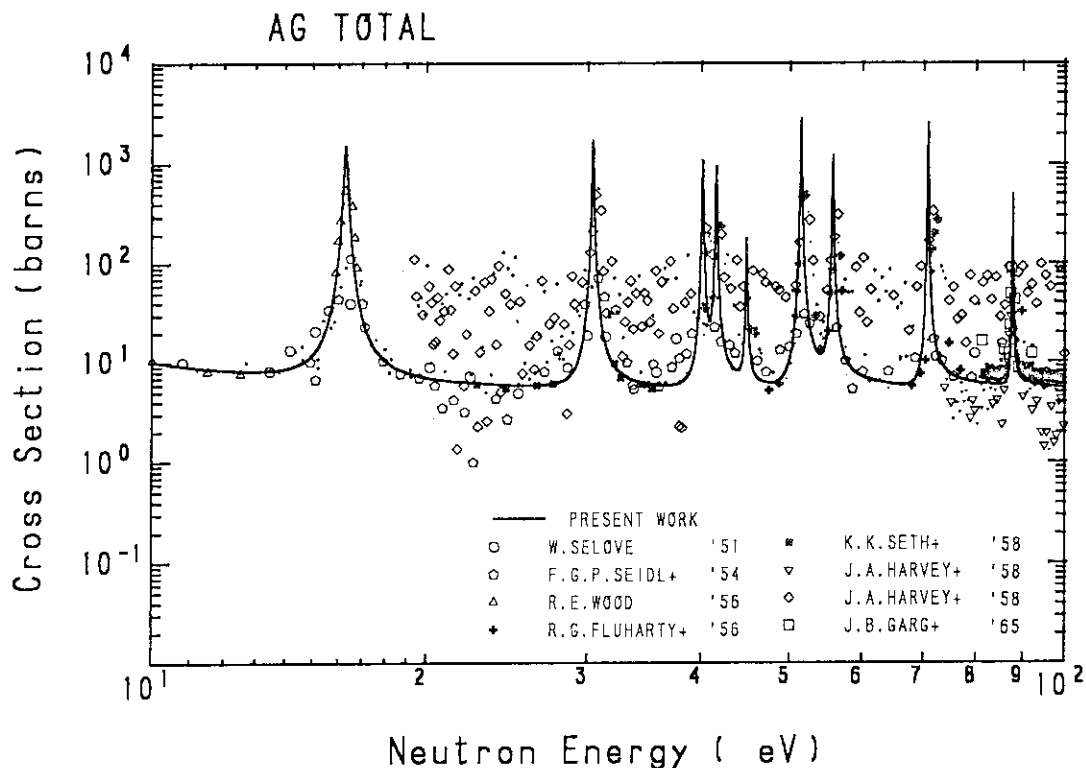


Fig. 26(c) Total cross section of natural silver in the energy region from 10 eV to 100 eV.

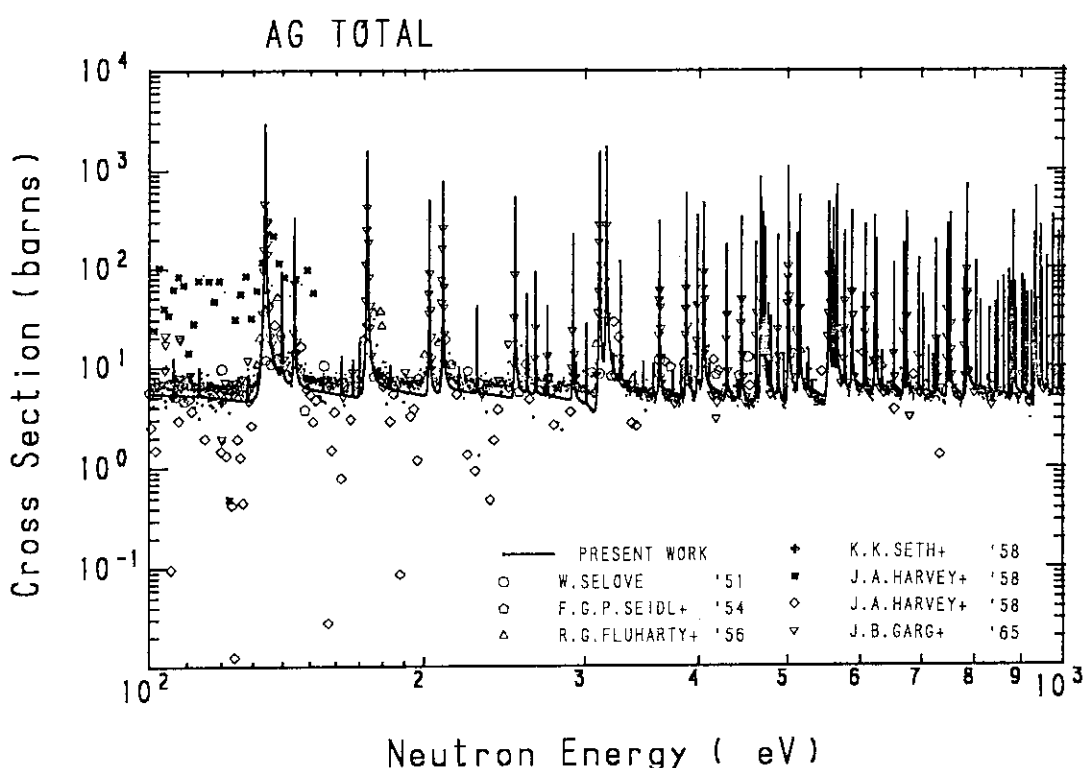


Fig. 26(d) Total cross section of natural silver in the energy region from 100 eV to 1 keV.

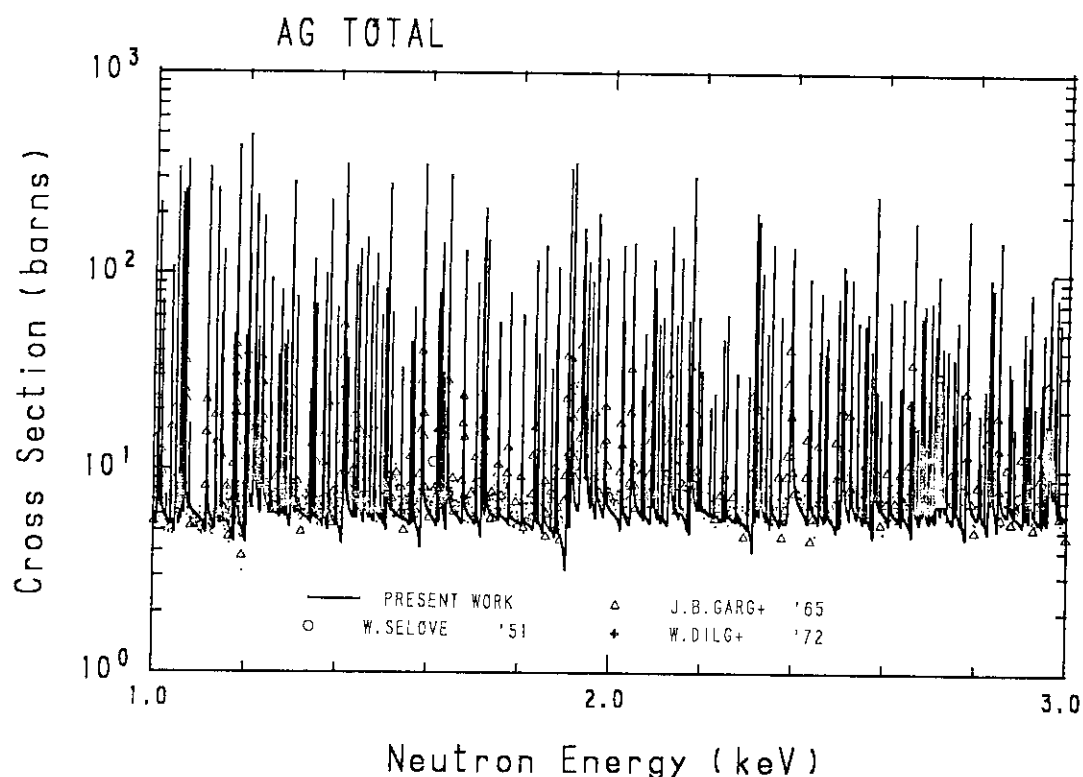


Fig. 26(e) Total cross section of natural silver in the energy region from 1 keV to 3 keV.

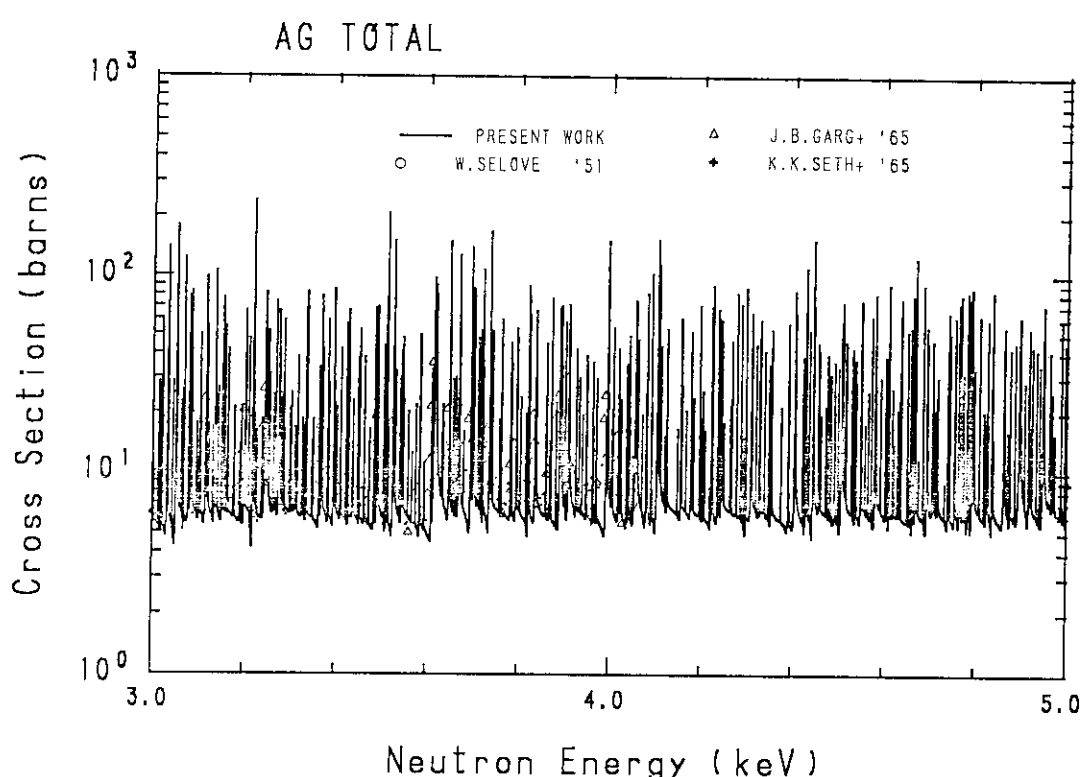


Fig. 26(f) Total cross section of natural silver in the energy region from 3 keV to 5 keV.

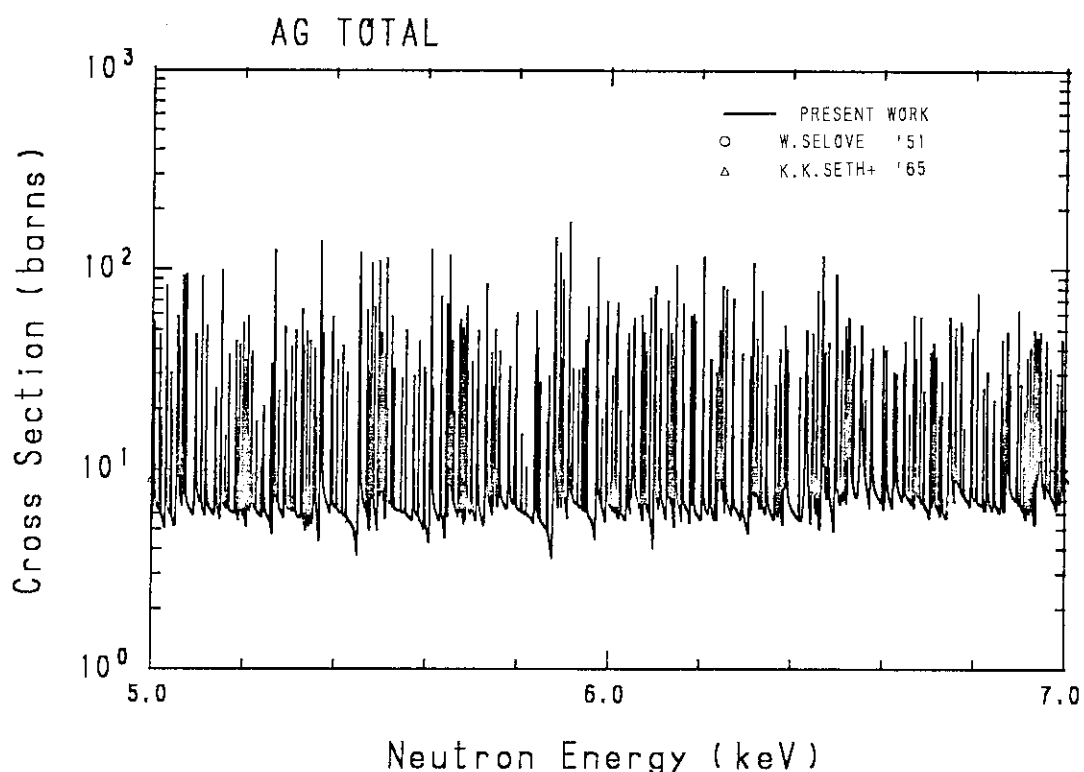


Fig. 26(g) Total cross section of natural silver in the energy region from 5 keV to 7 keV.

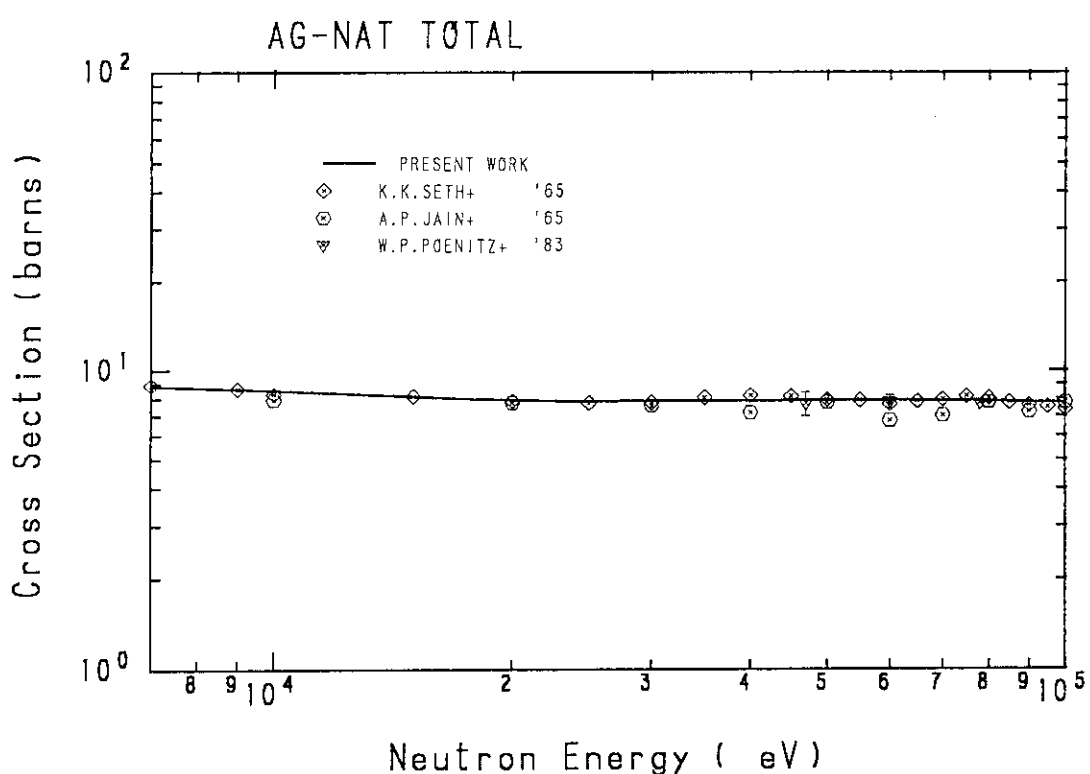


Fig. 26(h) Total cross section of natural silver in the energy region from 7 keV to 100 keV.

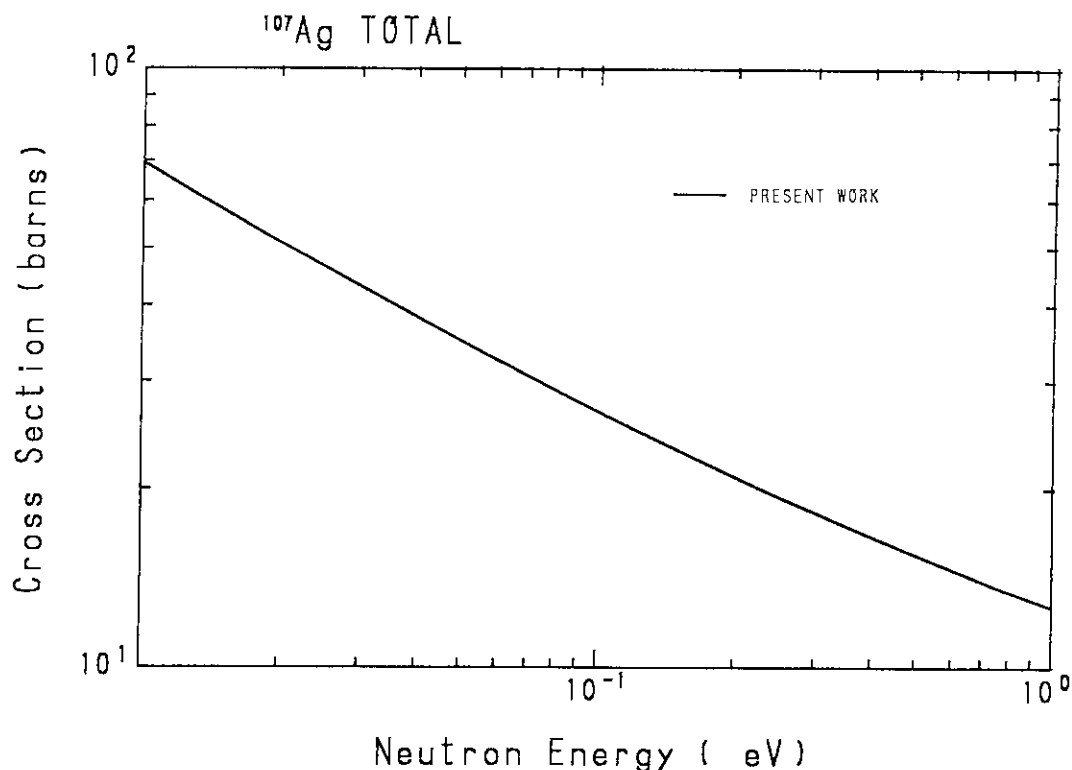


Fig. 27(a) Total cross section of  $^{107}\text{Ag}$  in the energy region from  $10^{-2}$  eV to 1 eV.

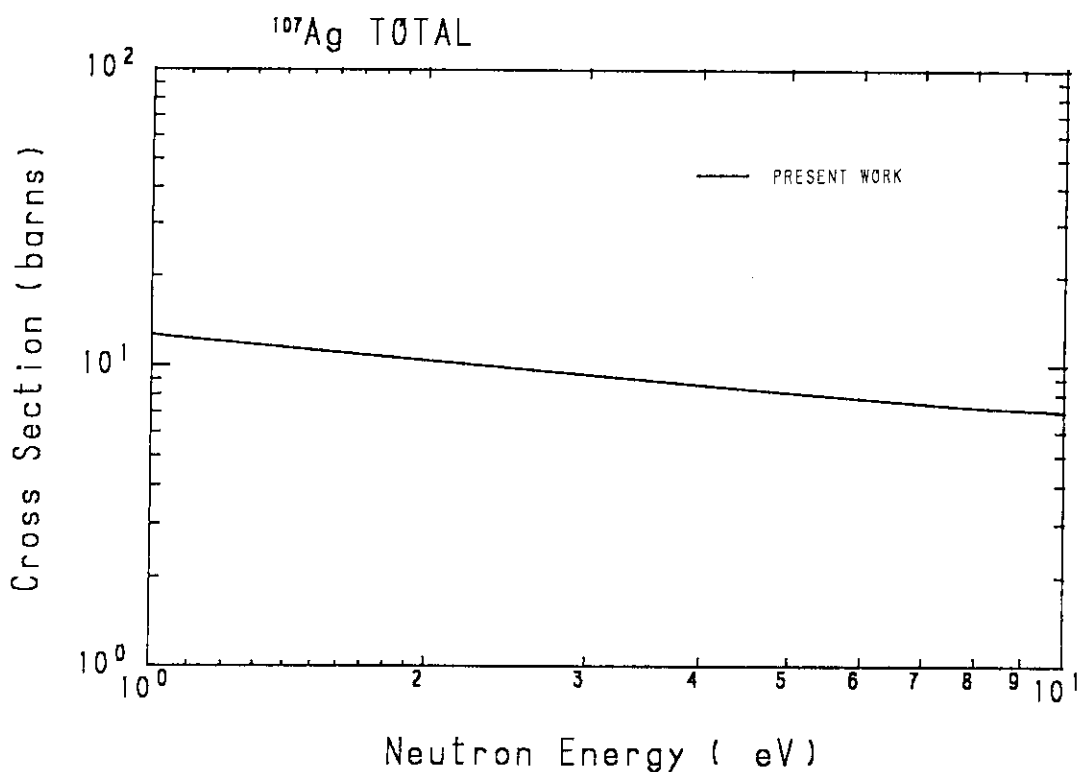


Fig. 27(b) Total cross section of  $^{107}\text{Ag}$  in the energy region from 1 eV to 10 eV.

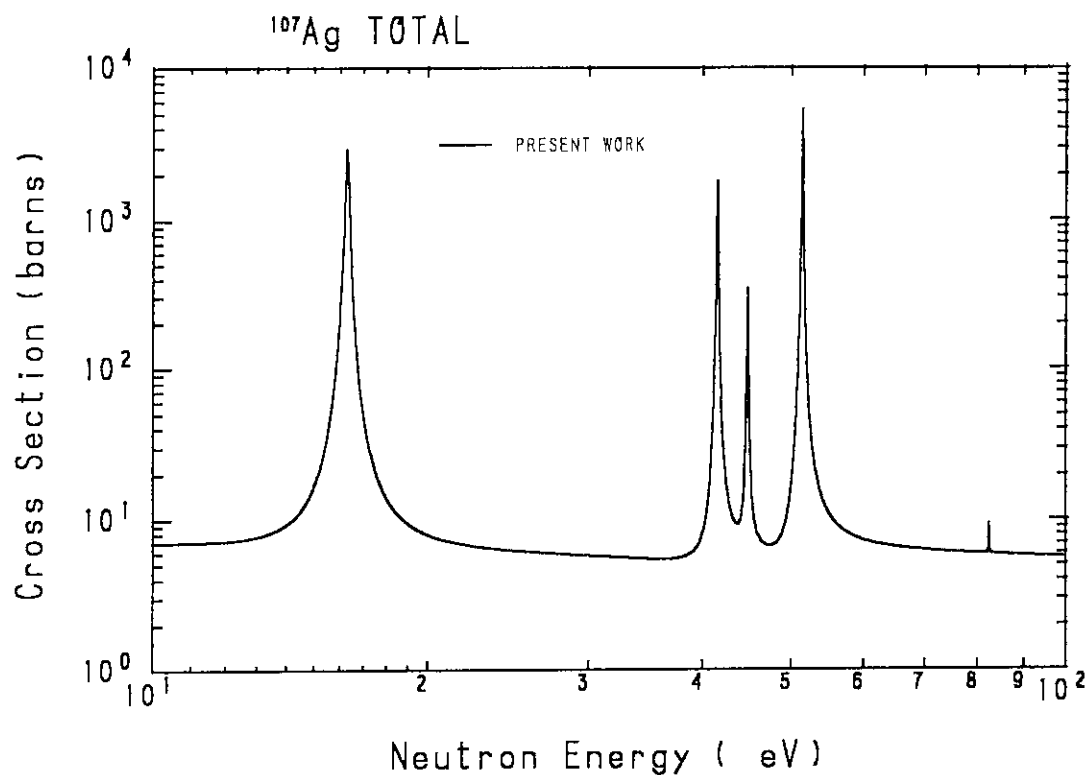


Fig. 27(c) Total cross section of  $^{107}\text{Ag}$  in the energy region from 10 eV to 100 eV.

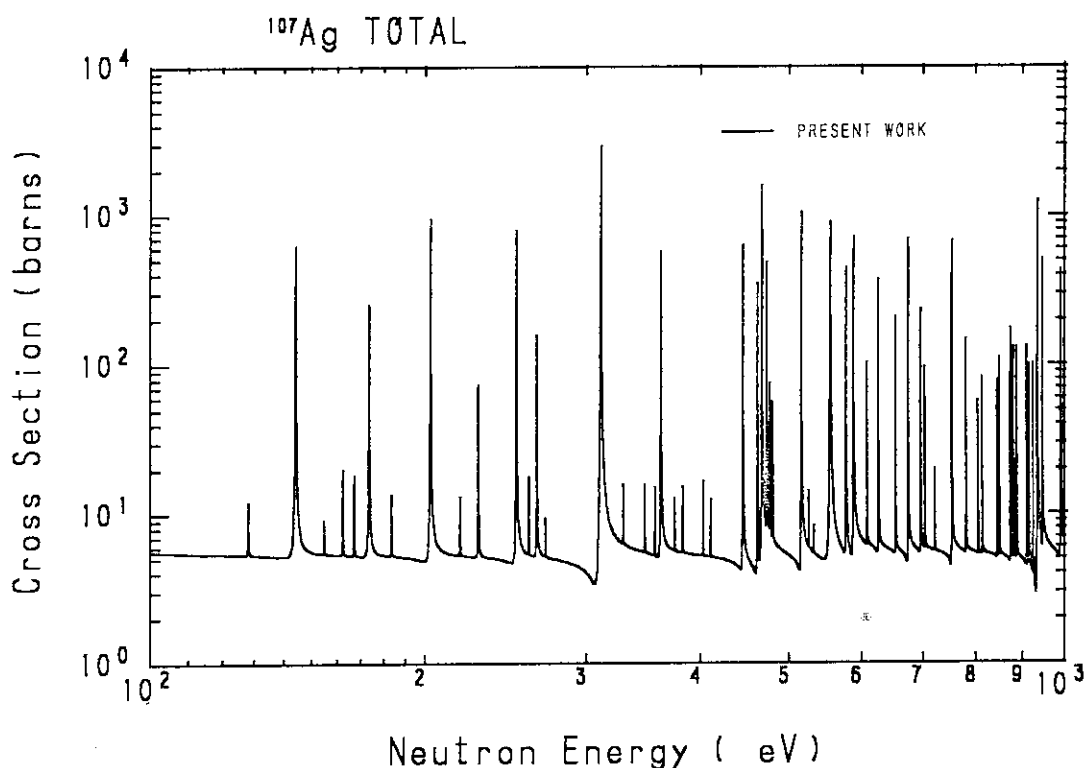


Fig. 27(d) Total cross section of  $^{107}\text{Ag}$  in the energy region from 100 eV to 1 keV.

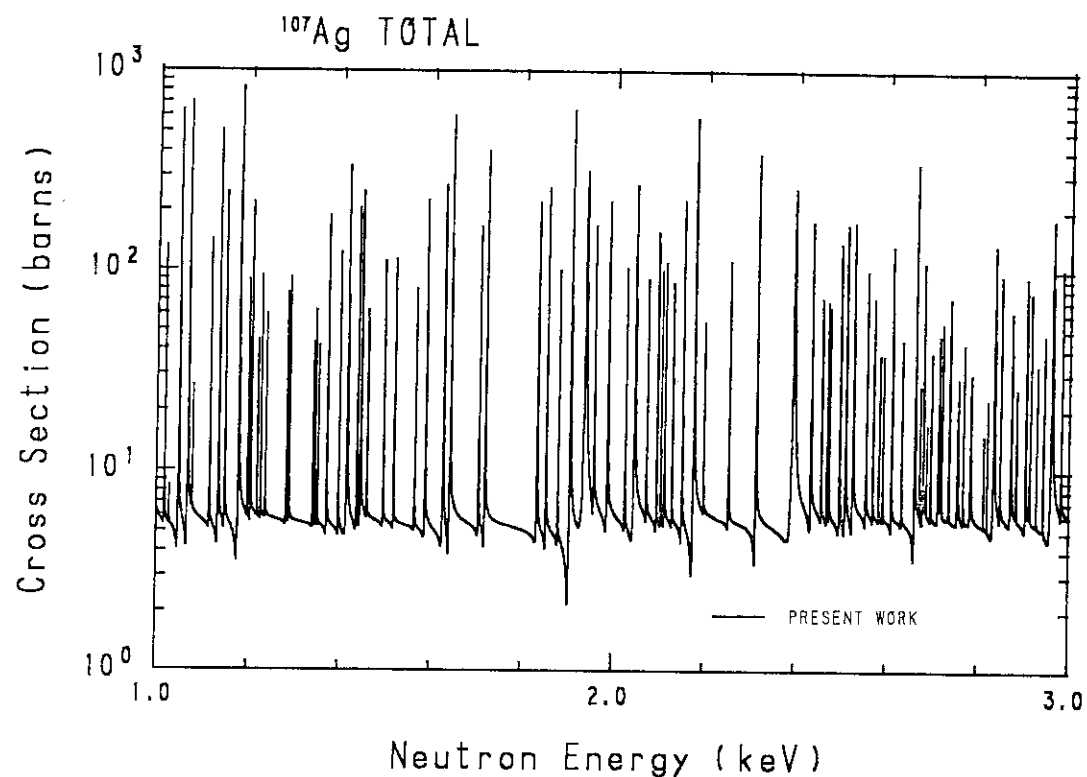


Fig. 27(e) Total cross section of  $^{107}\text{Ag}$  in the energy region from 1 keV to 3 keV.

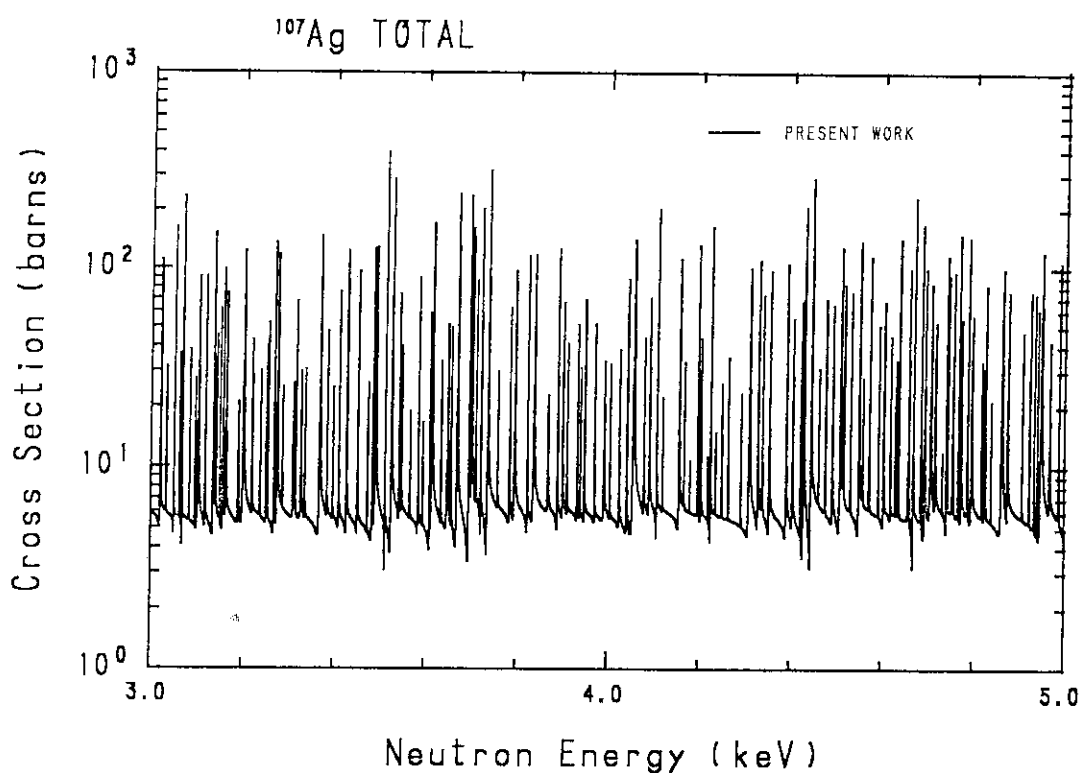


Fig. 27(f) Total cross section of  $^{107}\text{Ag}$  in the energy region from 3 keV to 5 keV.

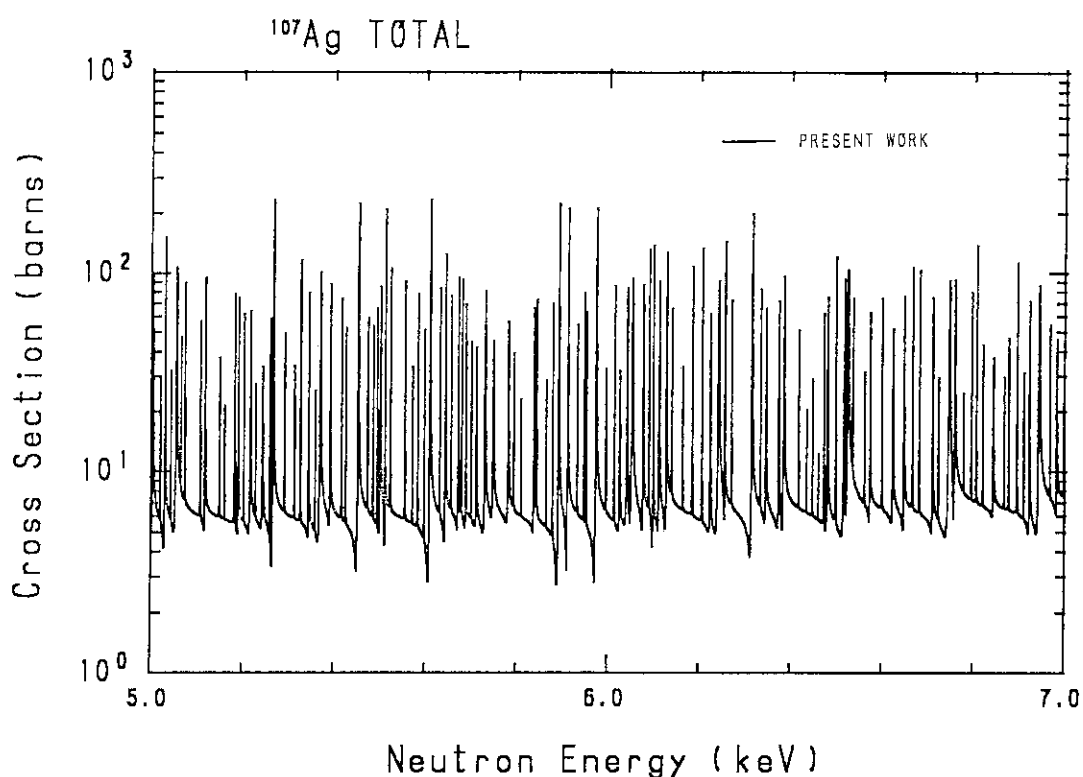


Fig. 27(g) Total cross section of  $^{107}\text{Ag}$  in the energy region from 5 keV to 7 keV.

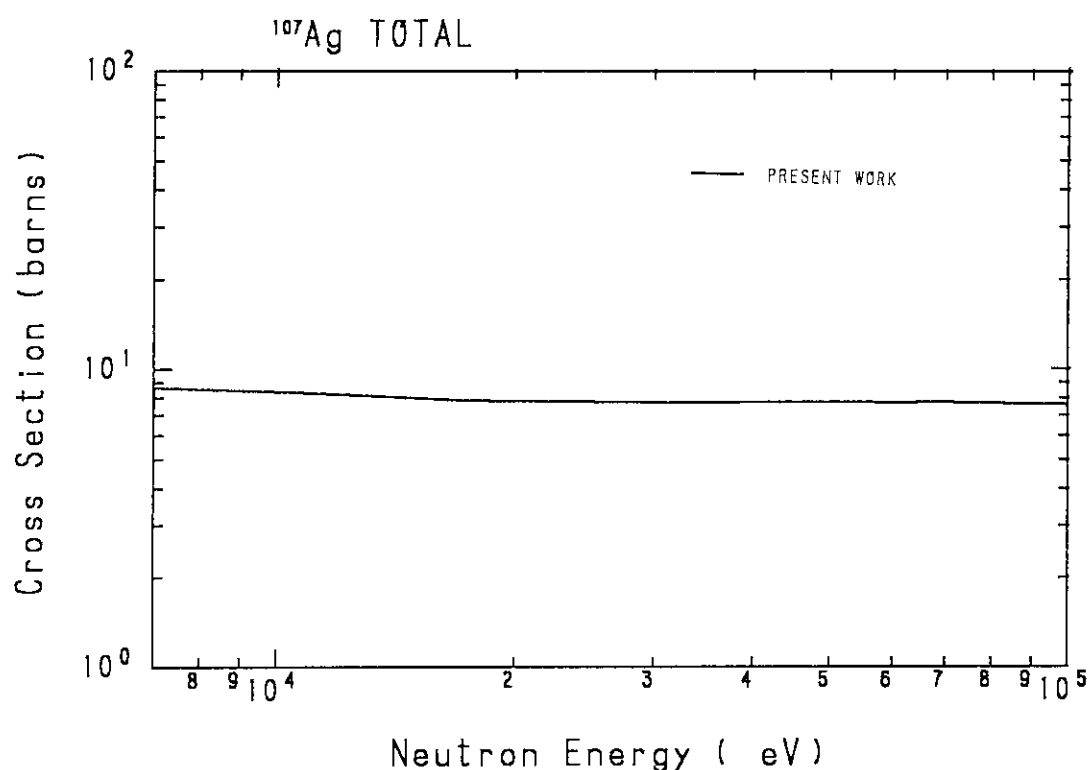


Fig. 27(h) Total cross section of  $^{107}\text{Ag}$  in the energy region from 7 keV to 100 keV.

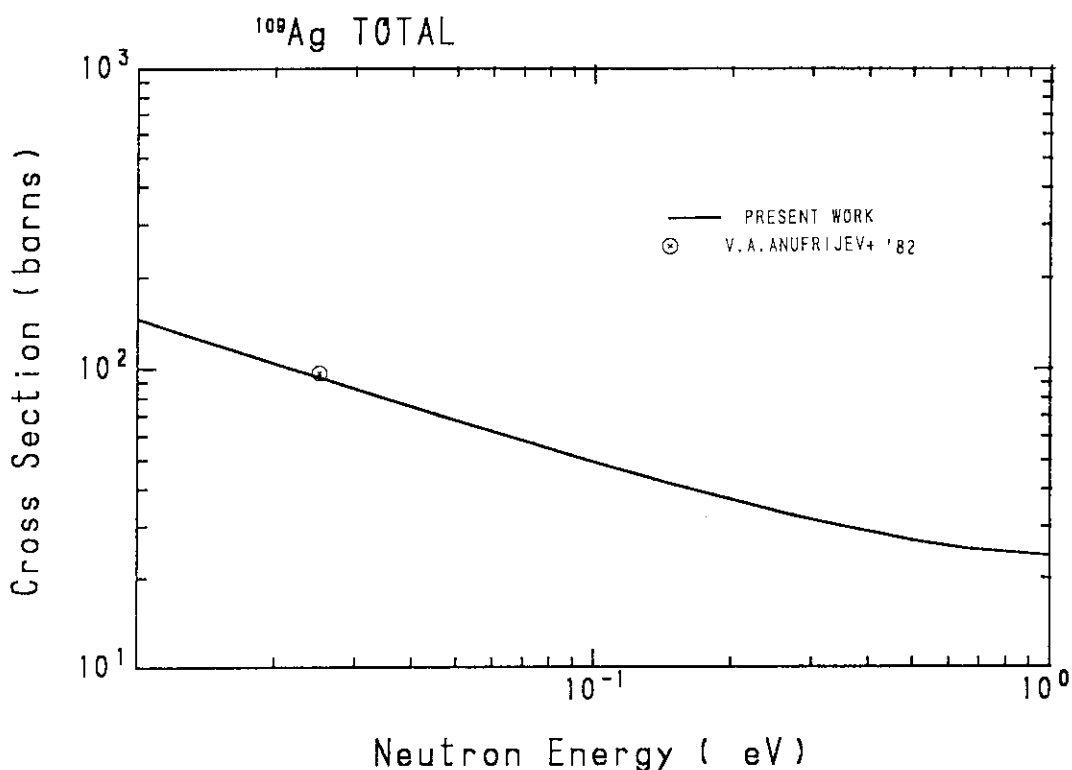


Fig. 28(a) Total cross section of  $^{109}\text{Ag}$  in the energy region from  $10^{-2}$  eV to 1 eV.

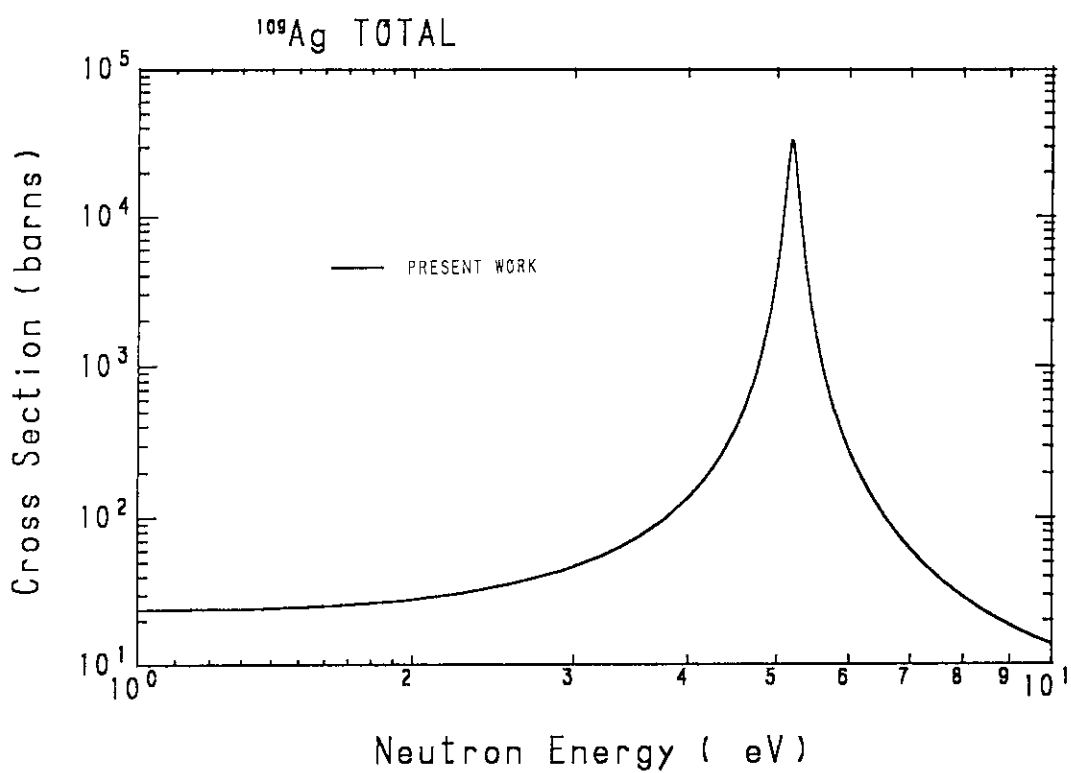


Fig. 28(b) Total cross section of  $^{109}\text{Ag}$  in the energy region from 1 eV to 10 eV.

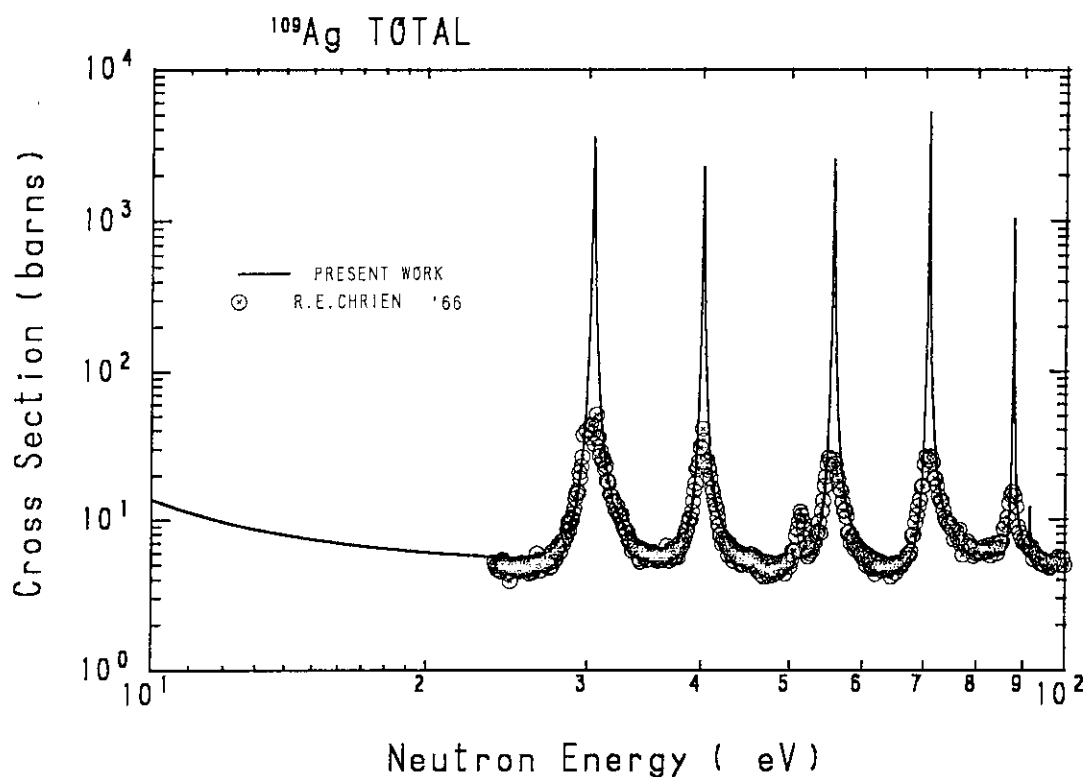


Fig. 28(c) Total cross section of  $^{109}\text{Ag}$  in the energy region from 10 eV to 100 eV.

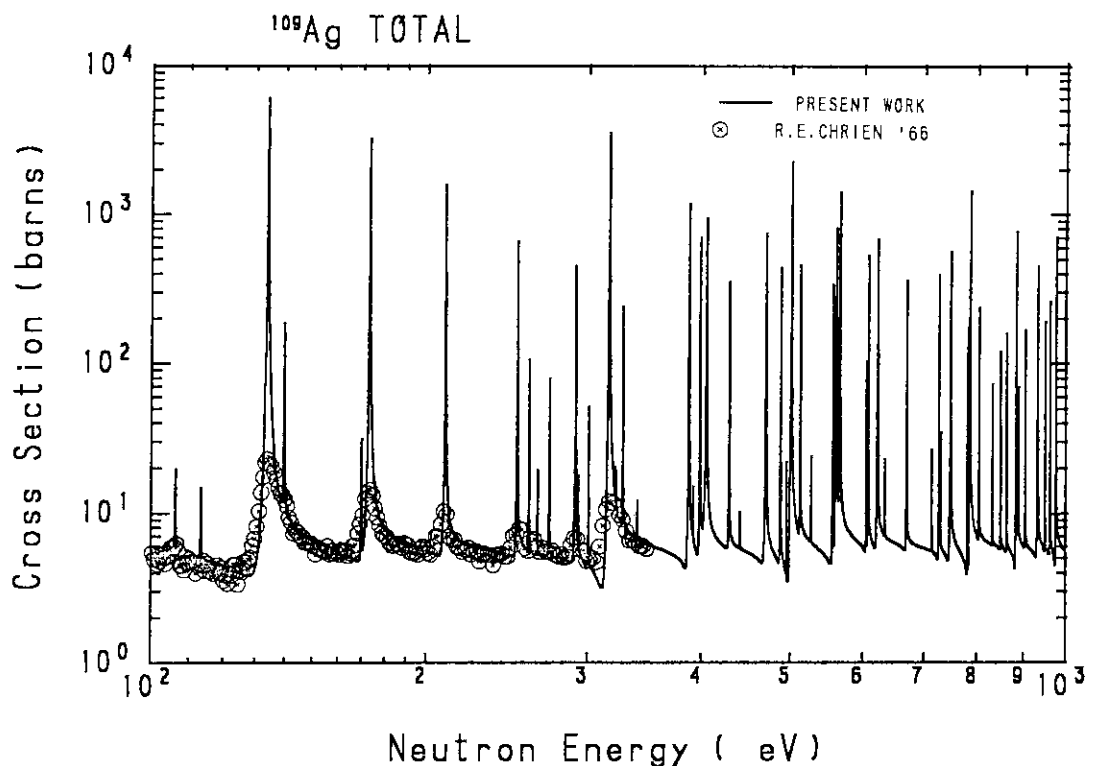


Fig. 28(d) Total cross section of  $^{109}\text{Ag}$  in the energy region from 100 eV to 1 keV.

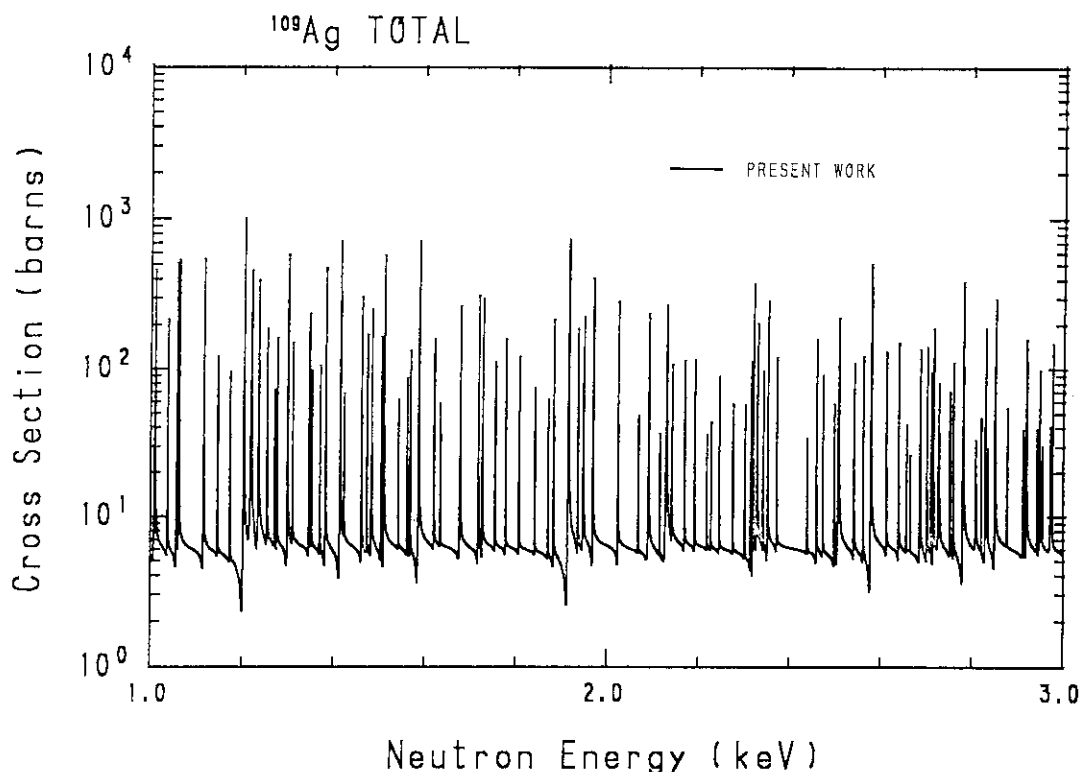


Fig. 28(e) Total cross section of  $^{109}\text{Ag}$  in the energy region from 1 keV to 3 keV.

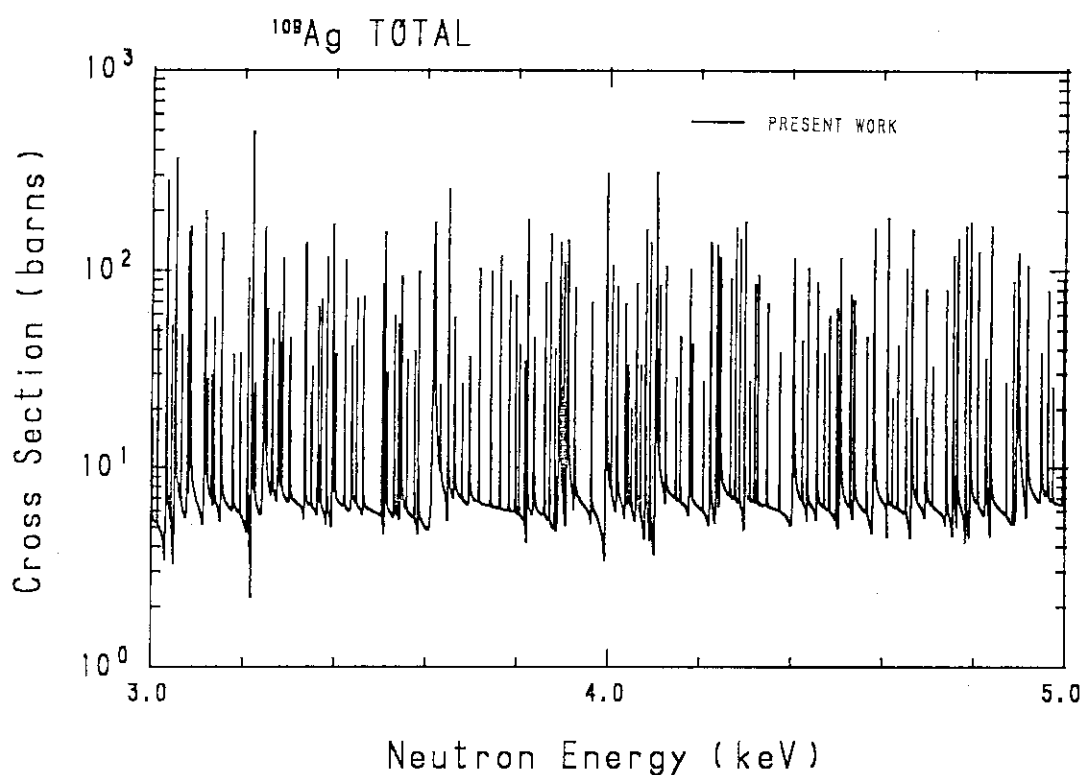


Fig. 28(f) Total cross section of  $^{109}\text{Ag}$  in the energy region from 3 keV to 5 keV.

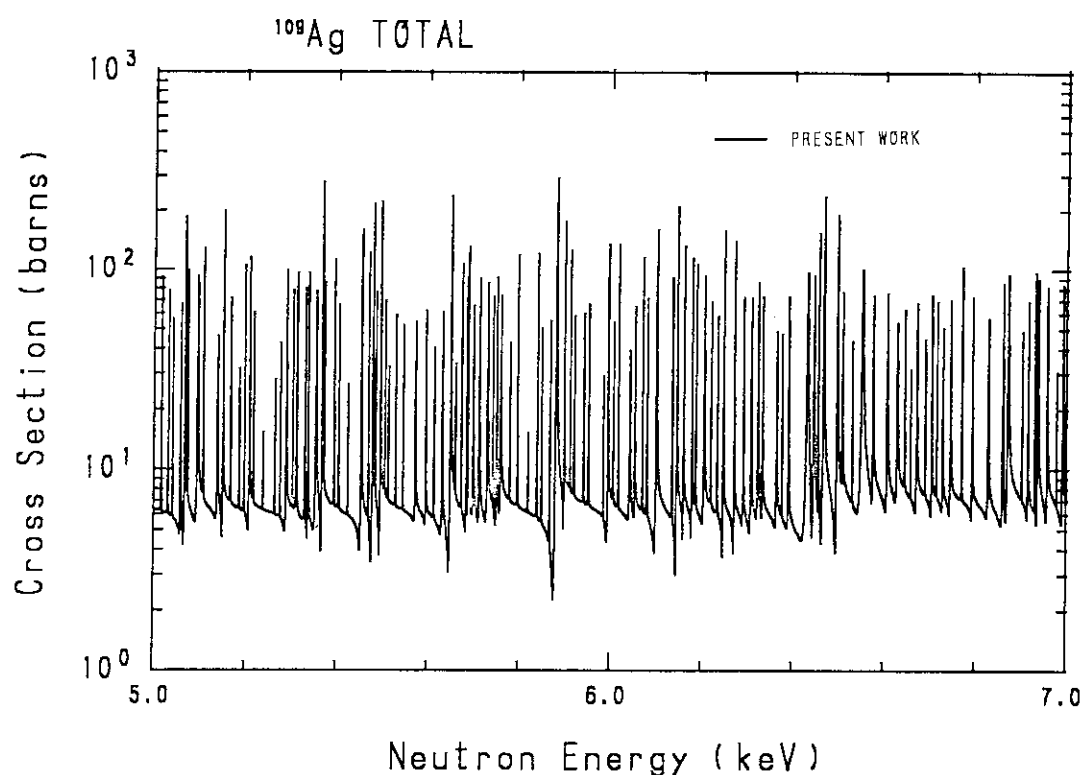


Fig. 28(g) Total cross section of  $^{109}\text{Ag}$  in the energy region from 5 keV to 7 keV.

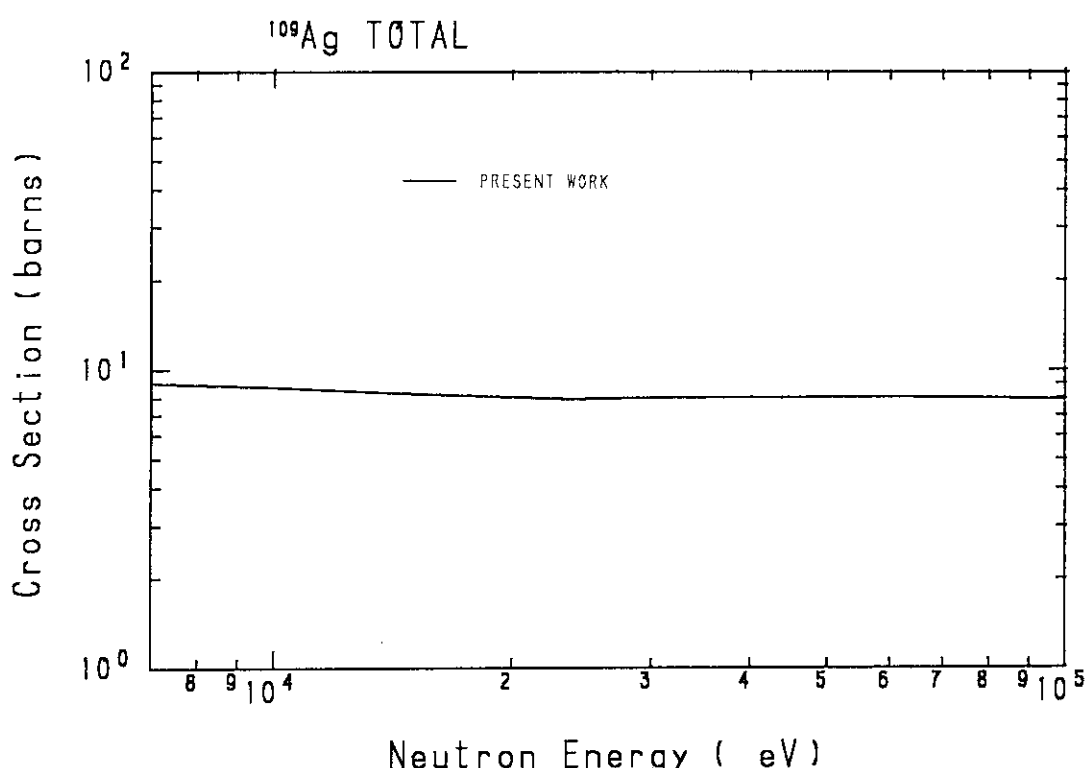
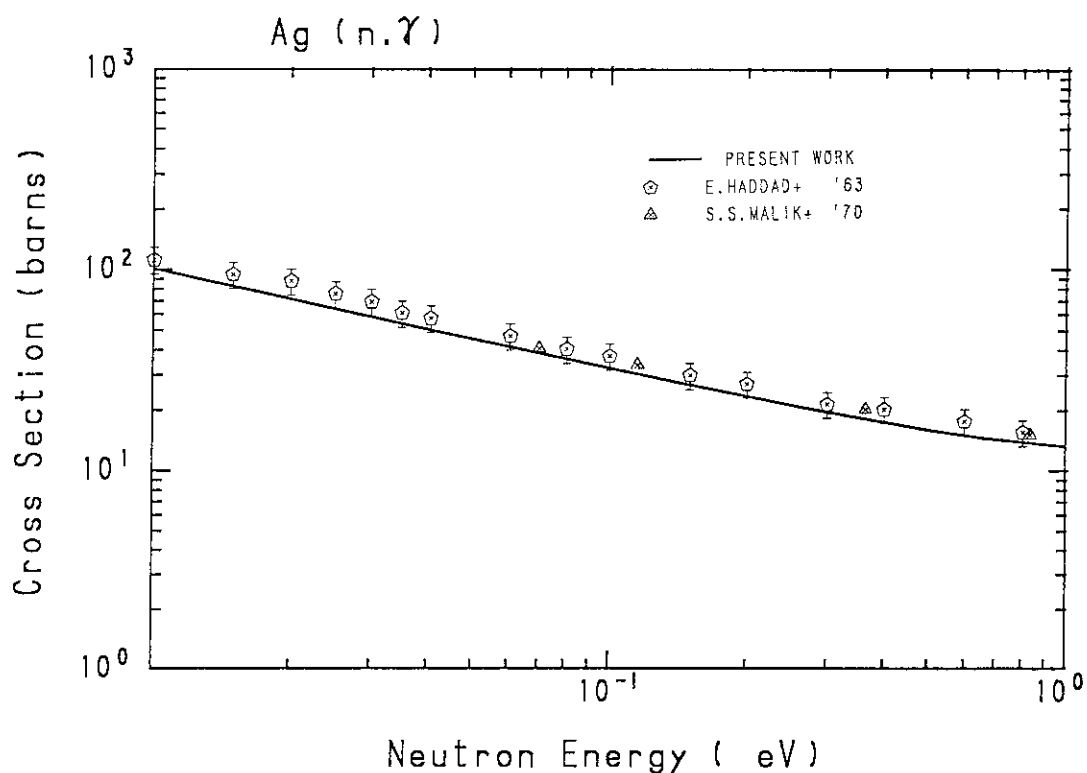
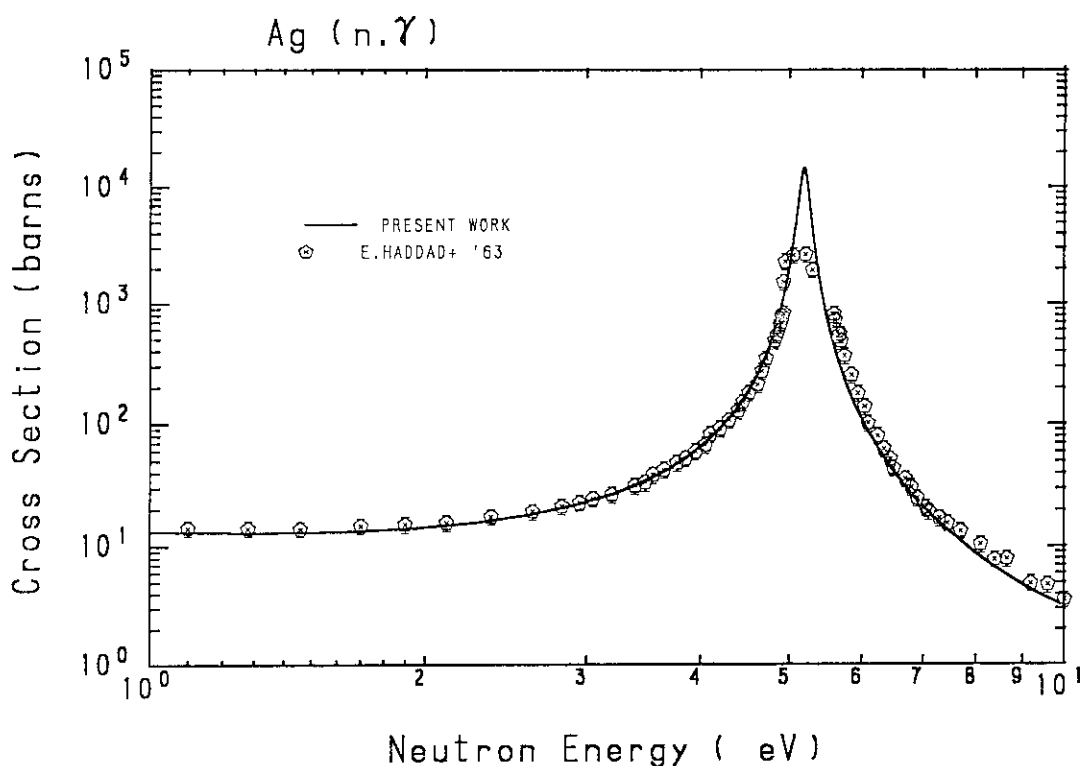


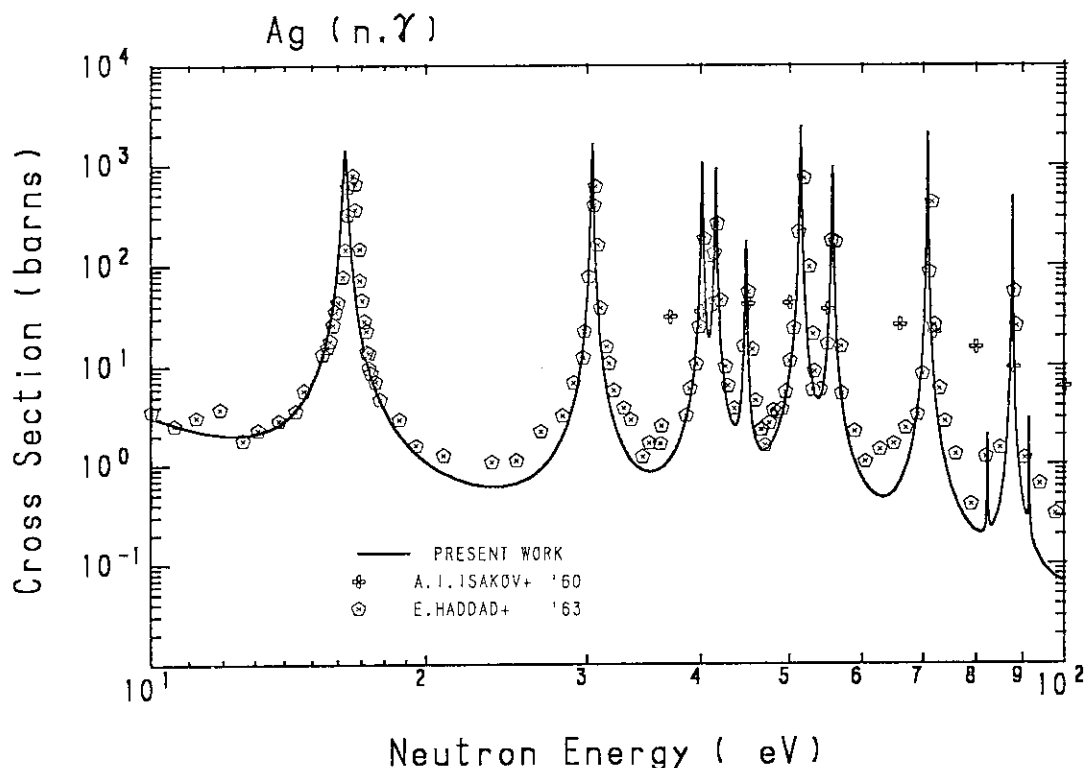
Fig. 28(h) Total cross section of  $^{109}\text{Ag}$  in the energy region from 7 keV to 100 keV.



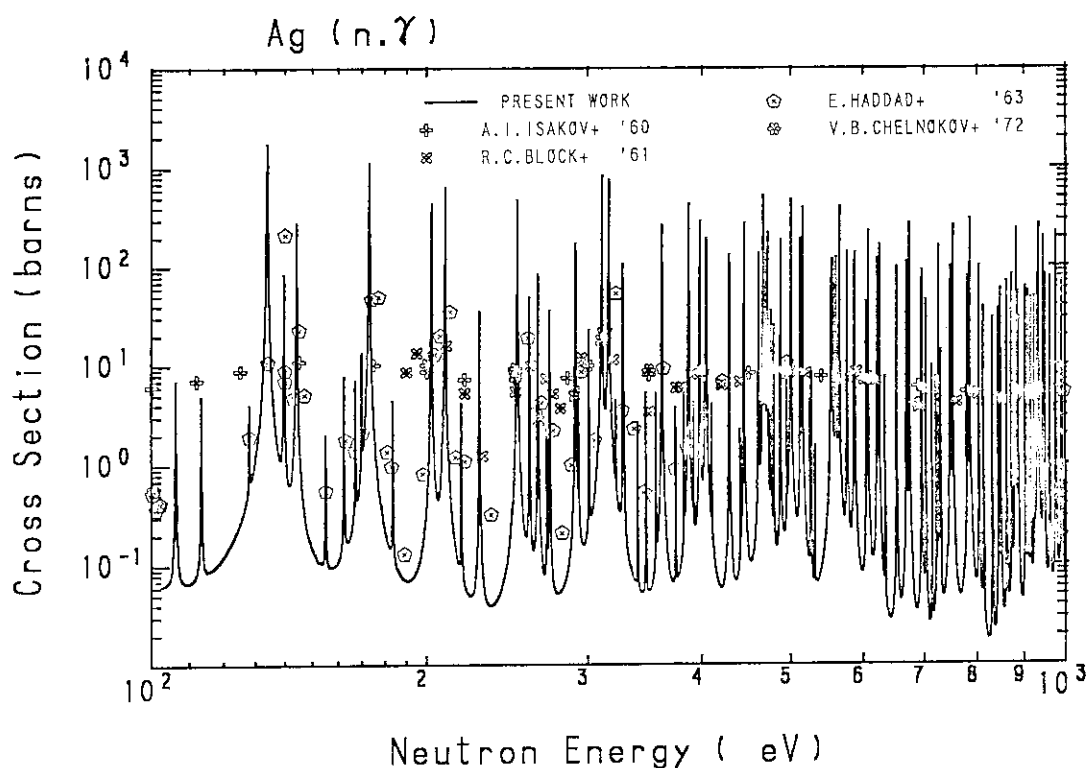
Fog. 29(a) Capture cross section of natural silver in the energy region from  $10^{-2}$  eV to 1 eV.



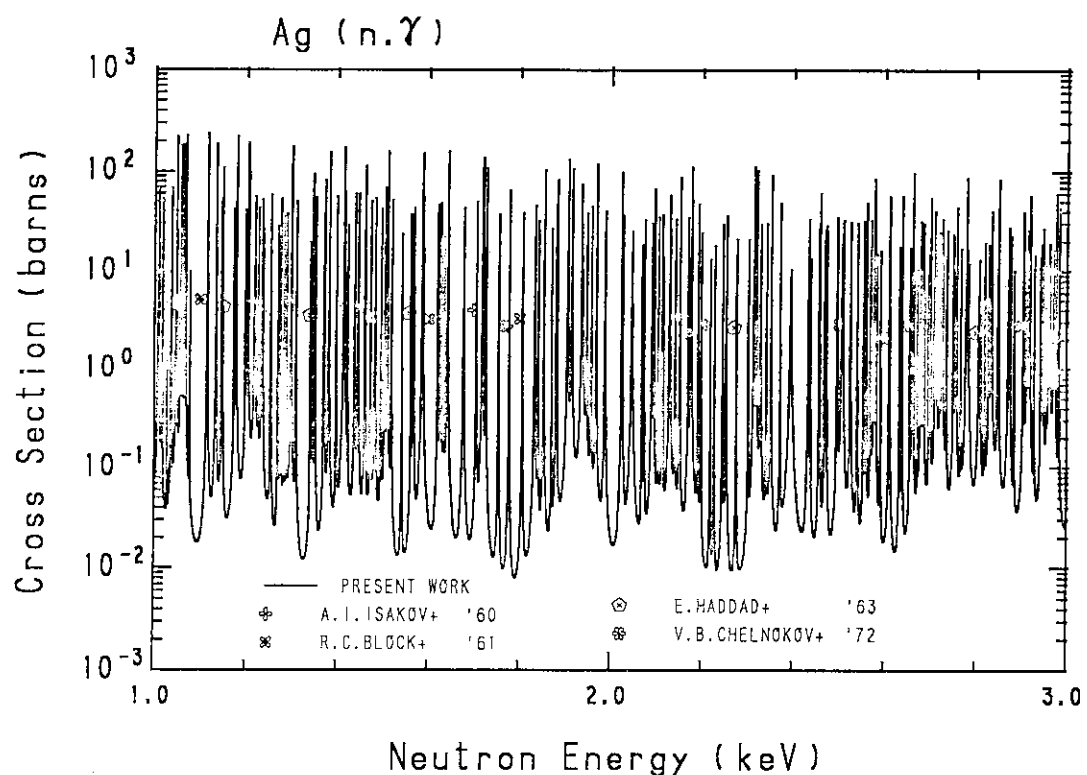
Fog. 29(b) Capture cross section of natural silver in the energy region from 1 eV to 10 eV.



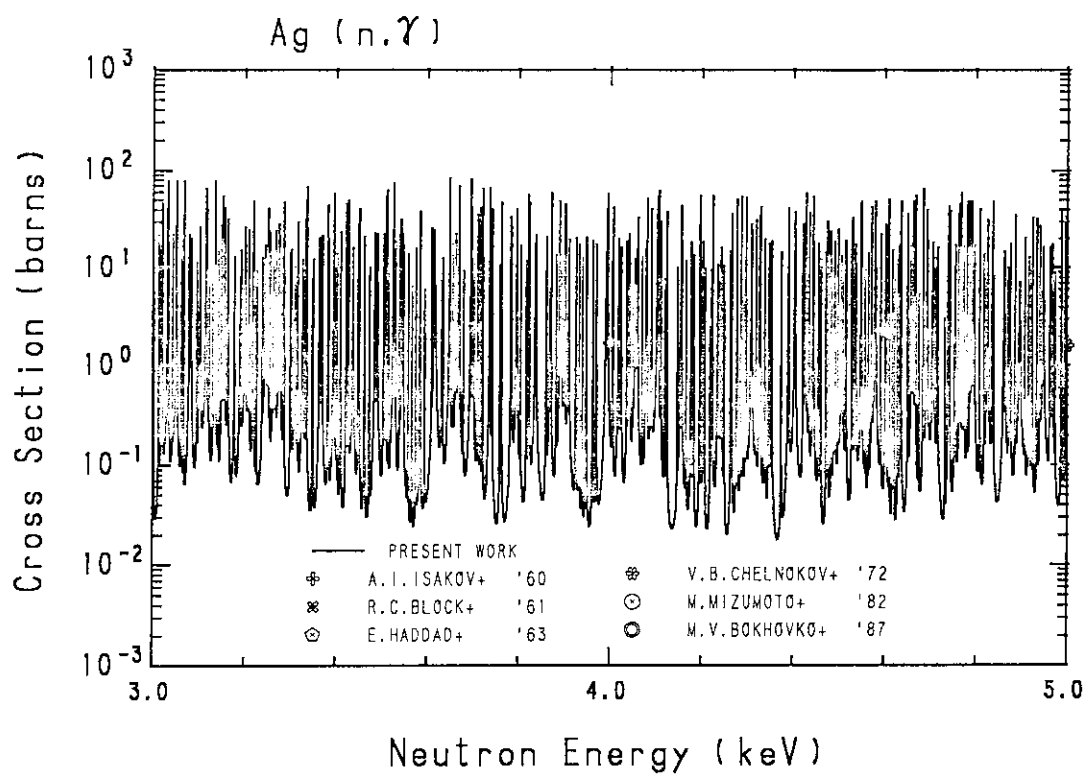
Fog. 29(c) Capture cross section of natural silver in the energy region from 10 eV to 100 eV.



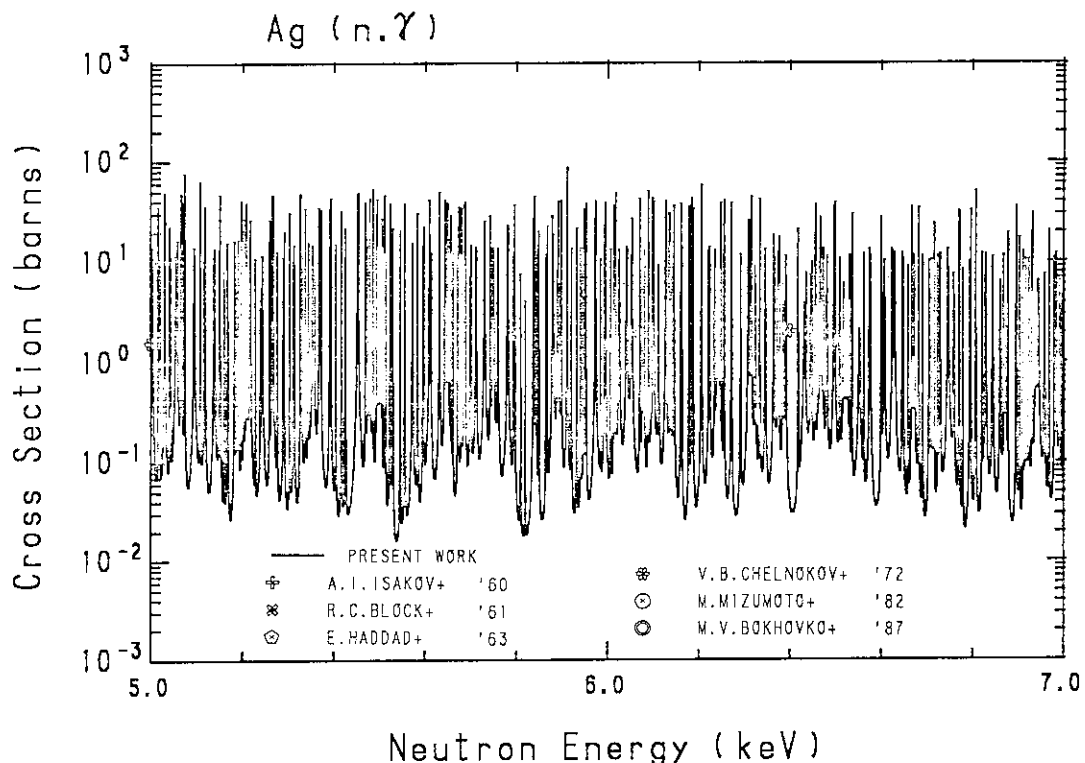
Fog. 29(d) Capture cross section of natural silver in the energy region from 100 eV to 1 keV.



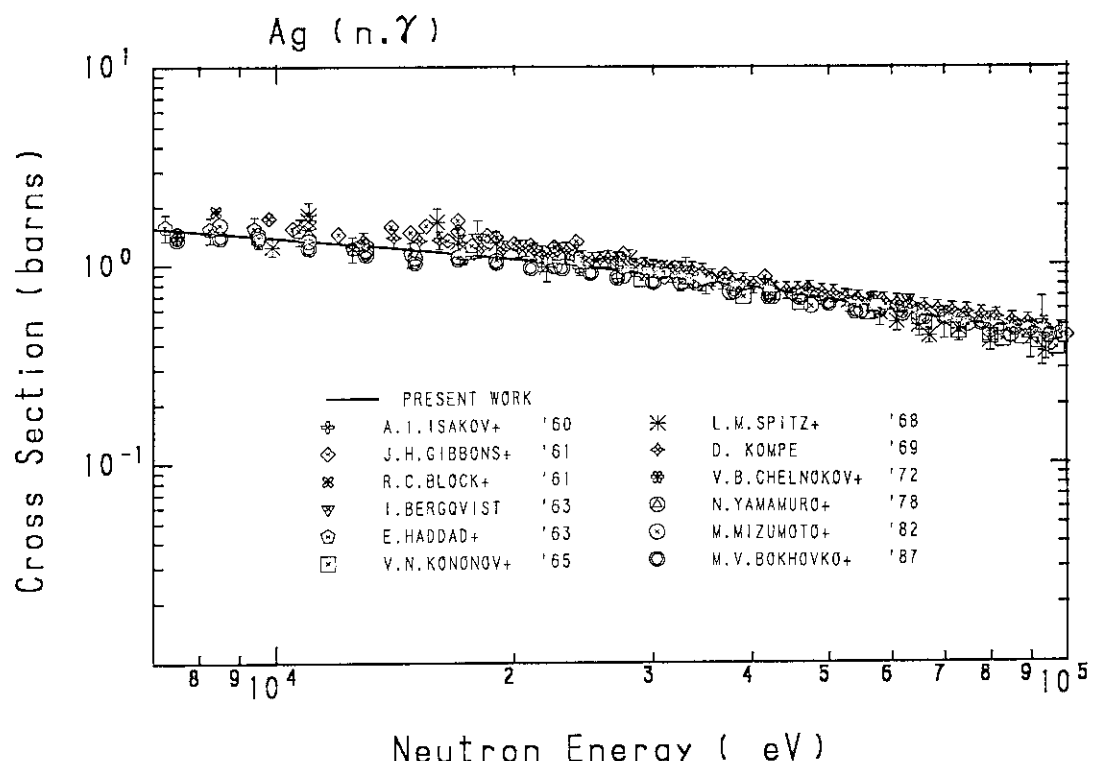
Fog. 29(e) Capture cross section of natural silver in the energy region from 1 keV to 3 keV.



Fog. 29(f) Capture cross section of natural silver in the energy region from 3 keV to 5 keV.



Fog. 29(g) Capture cross section of natural silver in the energy region from 5 keV to 7 keV.



Fog. 29(h) Capture cross section of natural silver in the energy region from 7 keV to 100 keV.

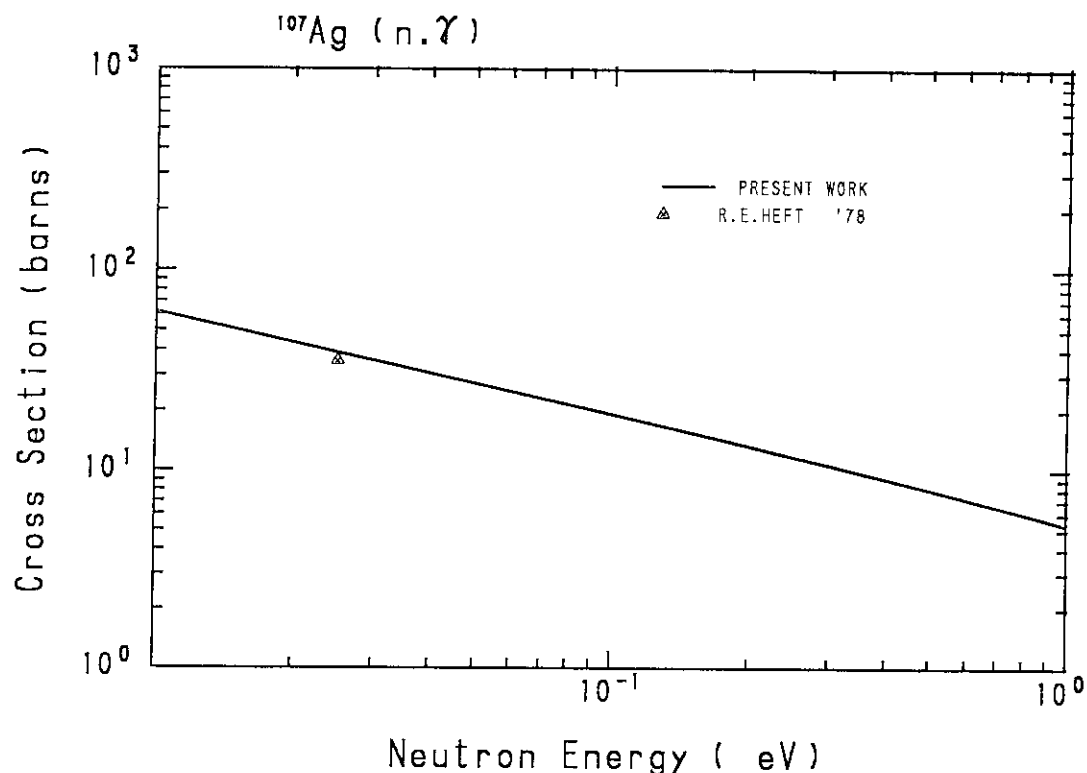


Fig. 30(a) Capture cross section of  $^{107}\text{Ag}$  in the energy region from  $10^{-2}$  eV to 1 eV.

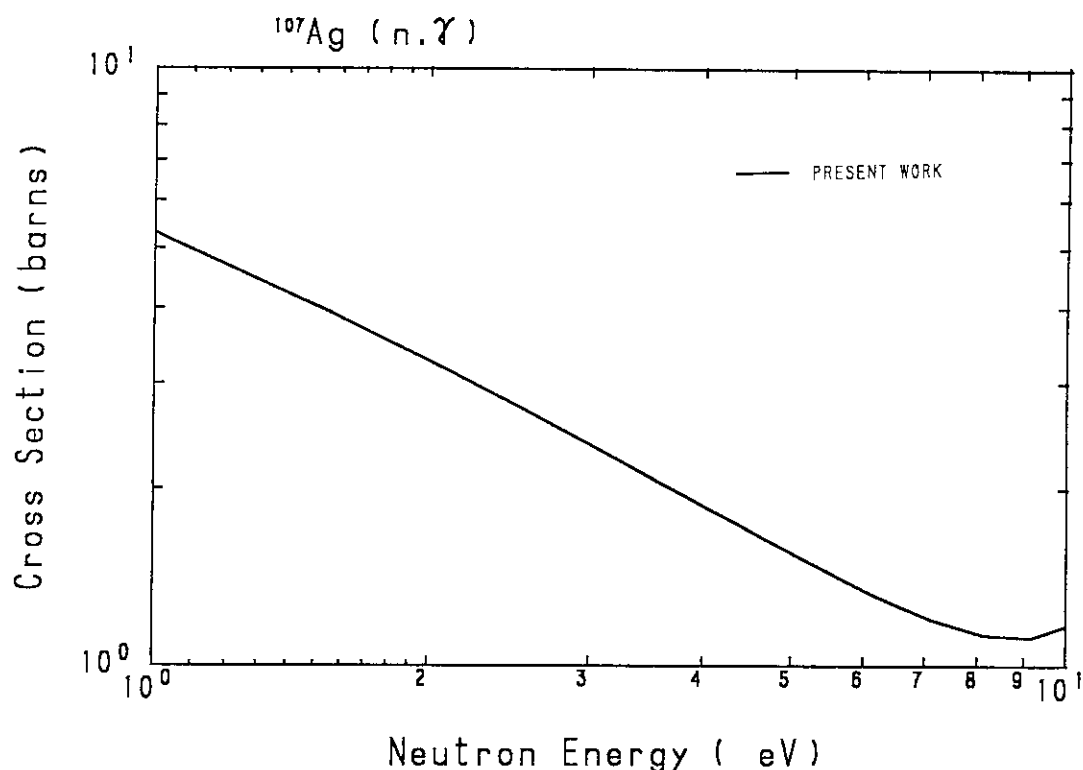


Fig. 30(b) Capture cross section of  $^{107}\text{Ag}$  in the energy region from 1 eV to 10 eV.

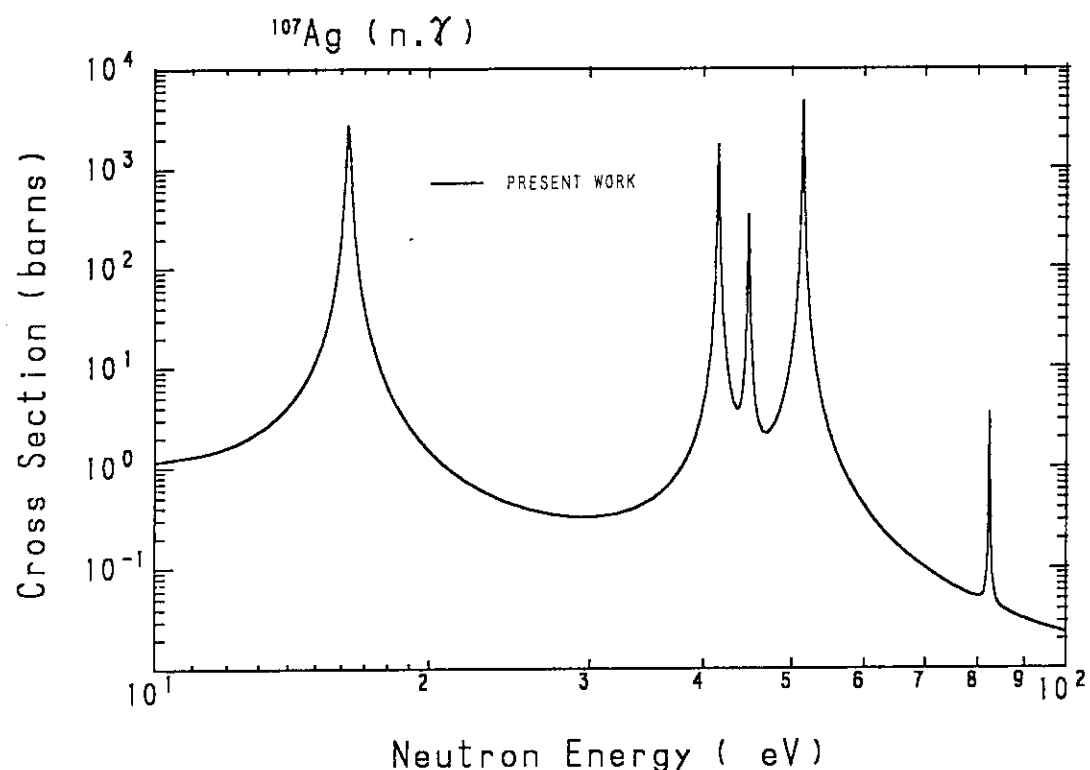


Fig. 30(c) Capture cross section of  $^{107}\text{Ag}$  in the energy region from 10 eV to 100 eV.

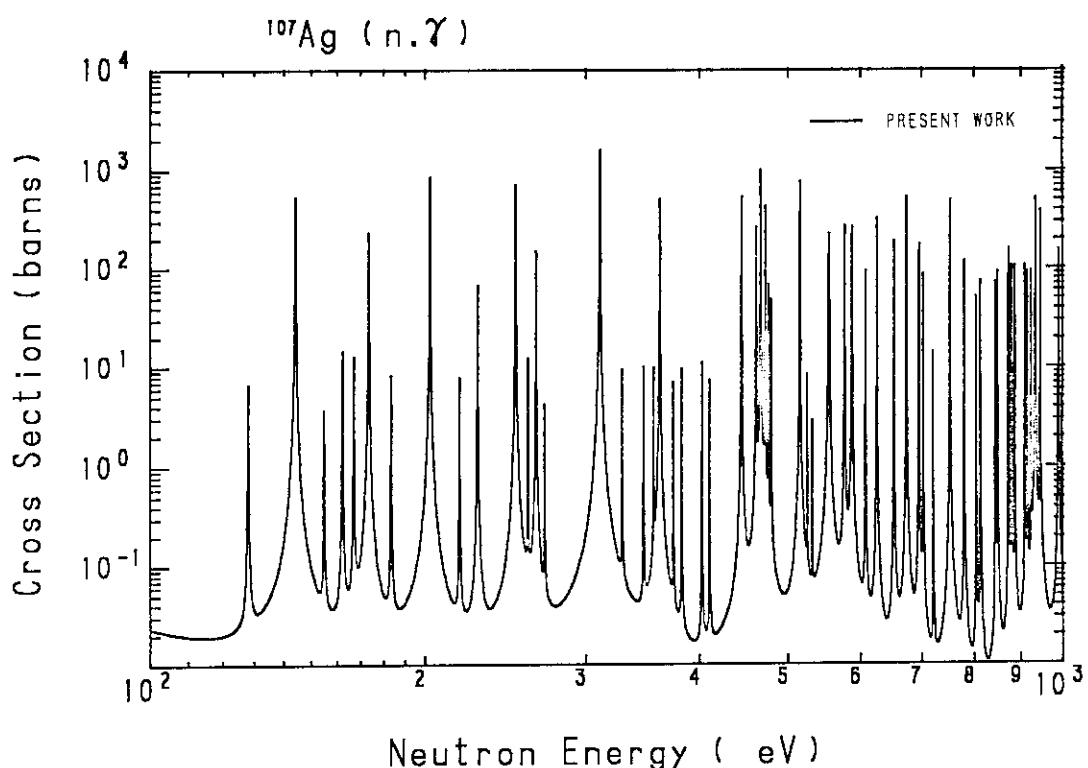


Fig. 30(d) Capture cross section of  $^{107}\text{Ag}$  in the energy region from 100 eV to 1 keV.

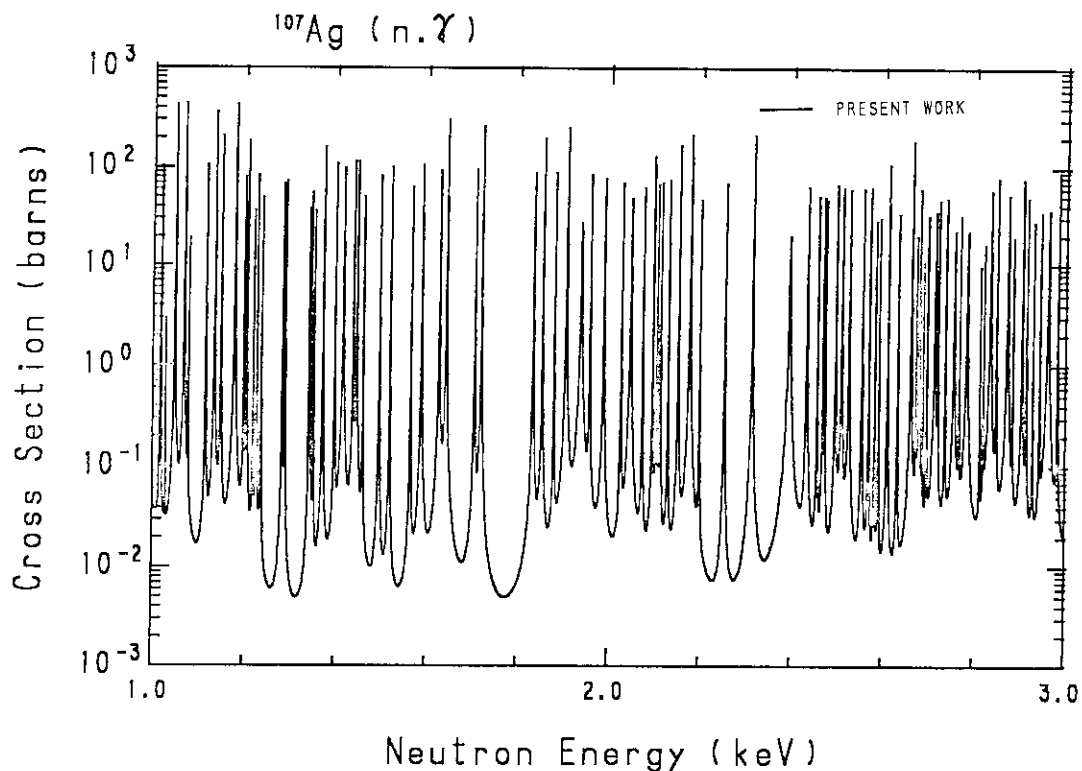


Fig. 30(e) Capture cross section of  $^{107}\text{Ag}$  in the energy region from 1 keV to 3 keV.

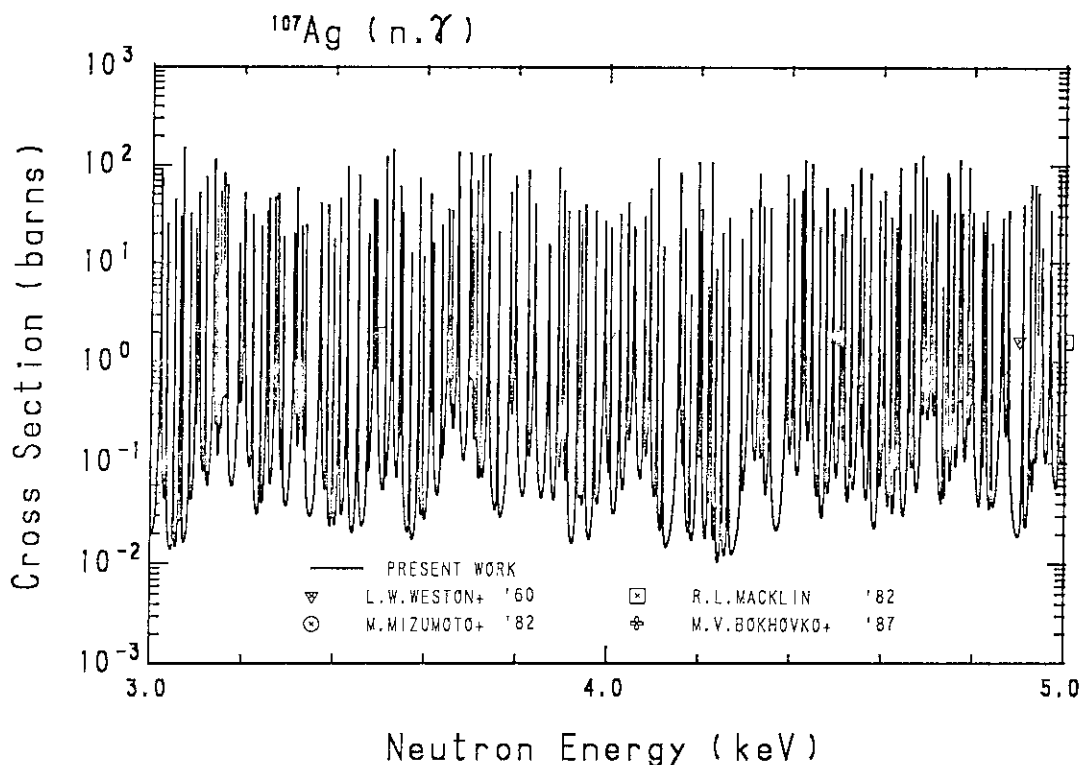


Fig. 30(f) Capture cross section of  $^{107}\text{Ag}$  in the energy region from 3 keV to 5 keV.

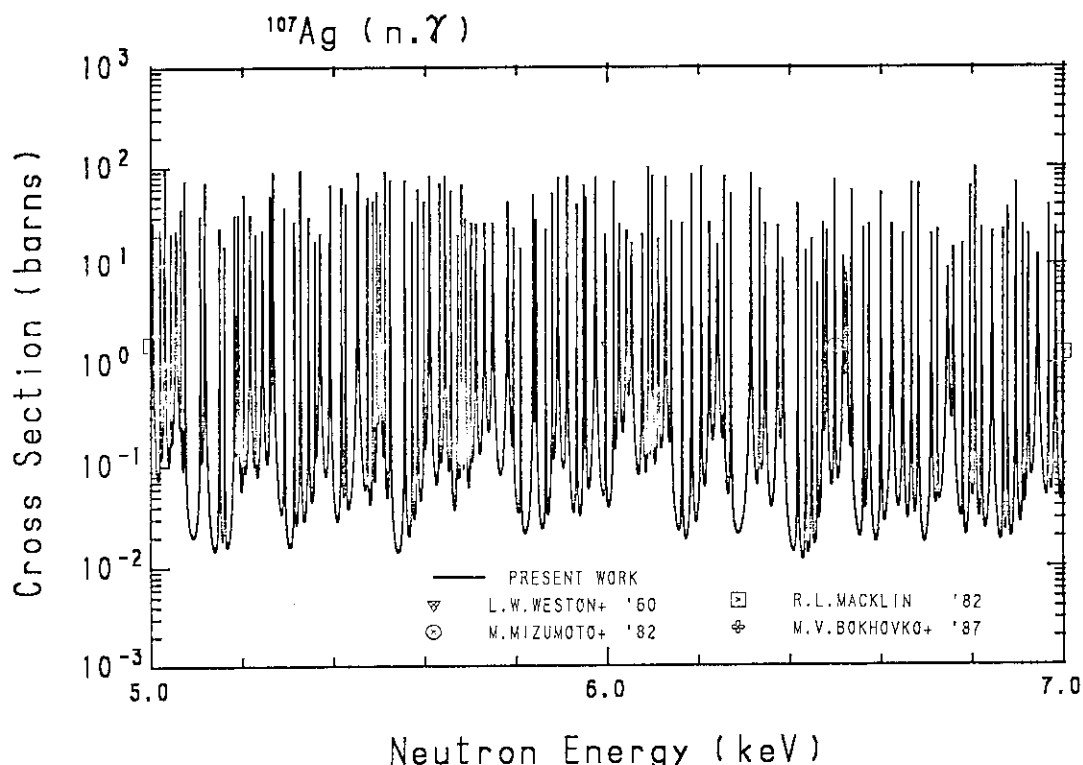


Fig. 30(g) Capture cross section of  $^{107}\text{Ag}$  in the energy region from 5 keV to 7 keV.

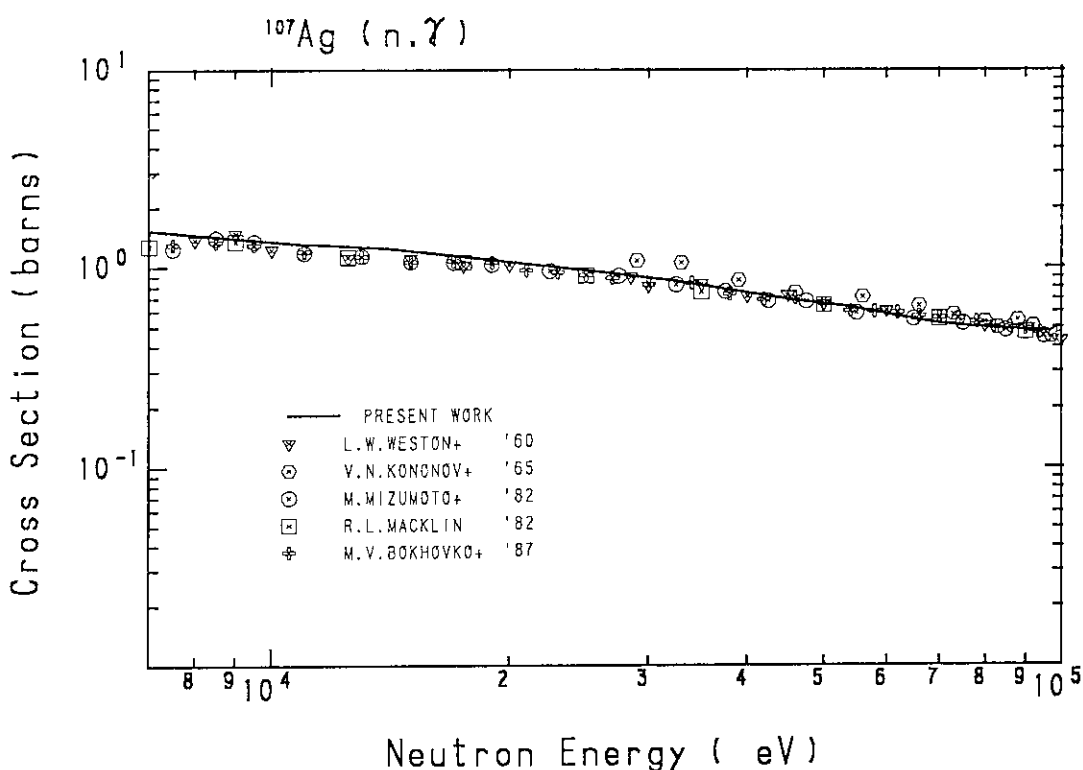


Fig. 30(h) Capture cross section of  $^{107}\text{Ag}$  in the energy region from 7 keV to 100 keV.

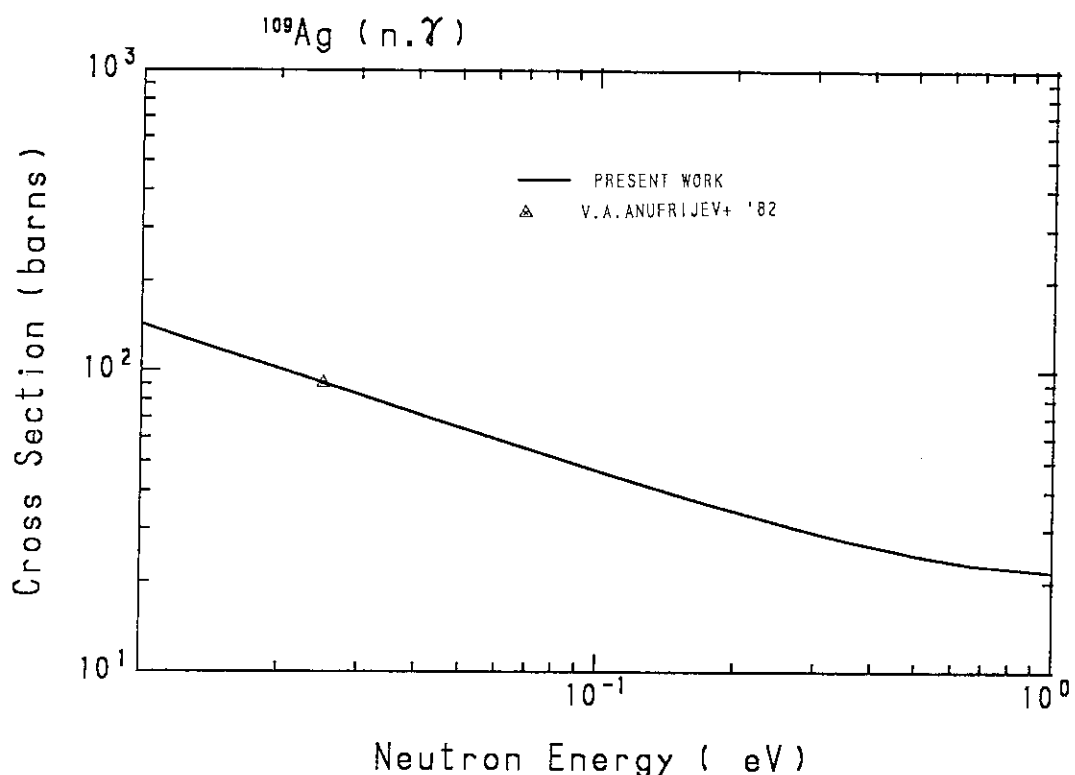


Fig. 31(a) Capture cross section of  $^{109}\text{Ag}$  in the energy region from  $10^{-2}$  eV to 1 eV.

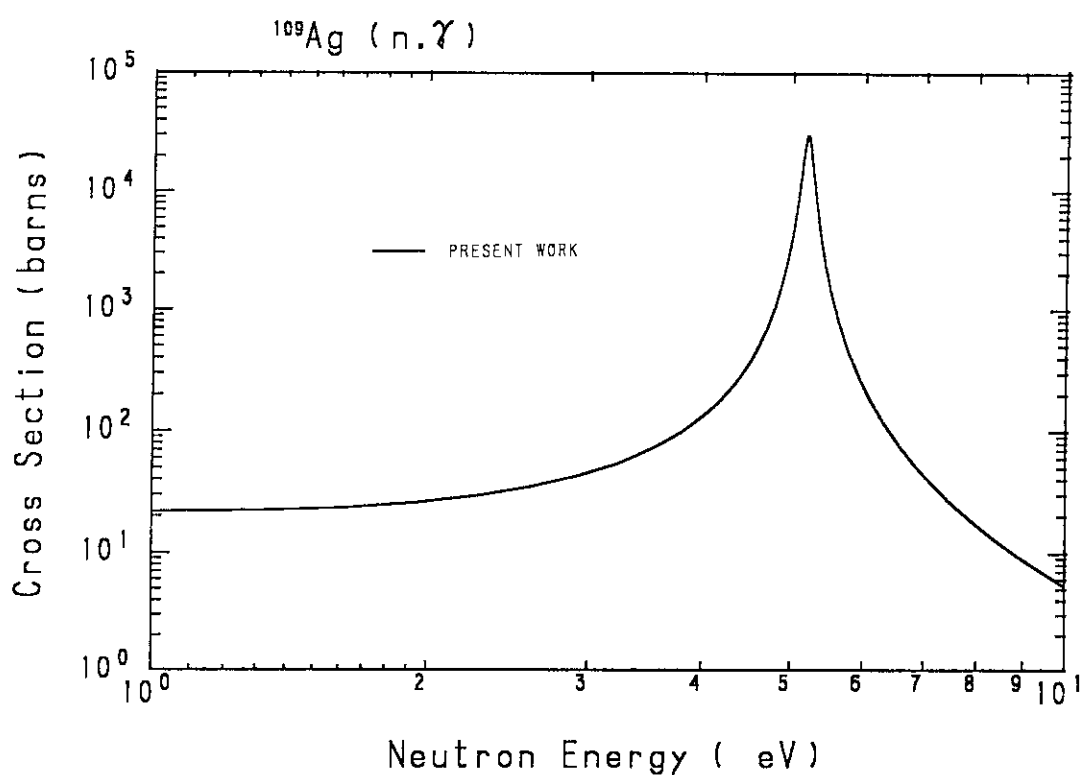


Fig. 31(b) Capture cross section of  $^{109}\text{Ag}$  in the energy region from 1 eV to 10 eV.

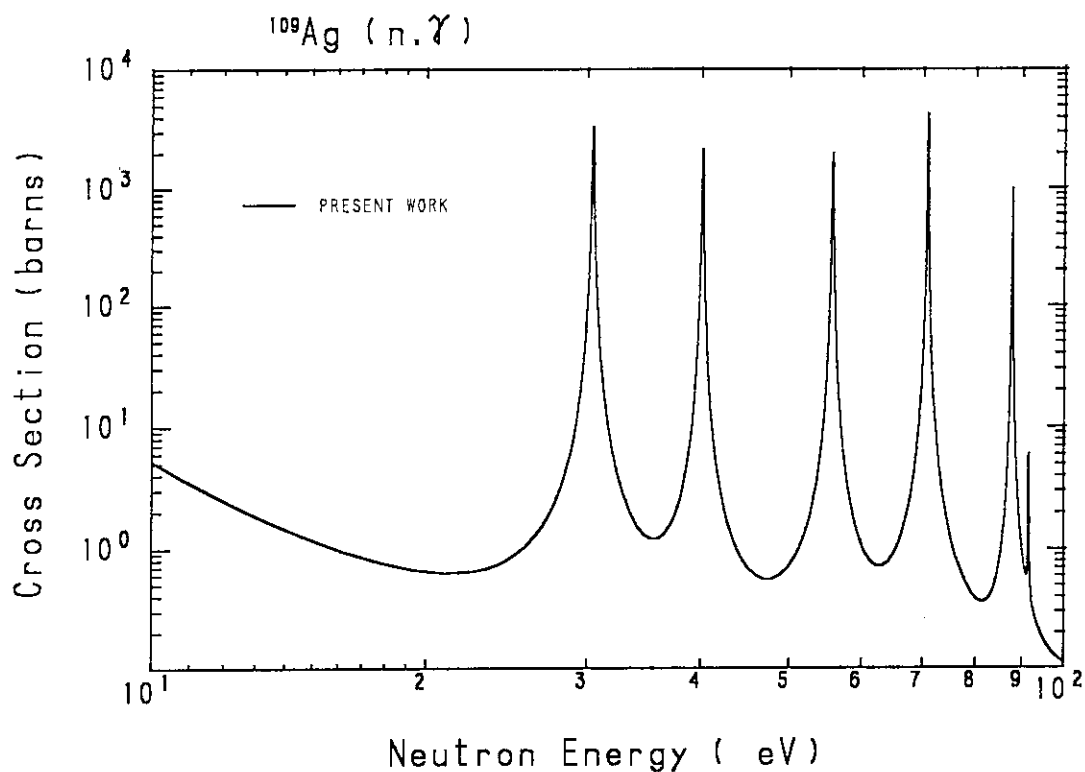


Fig. 31(c) Capture cross section of  $^{109}\text{Ag}$  in the energy region from 10 eV to 100 eV.

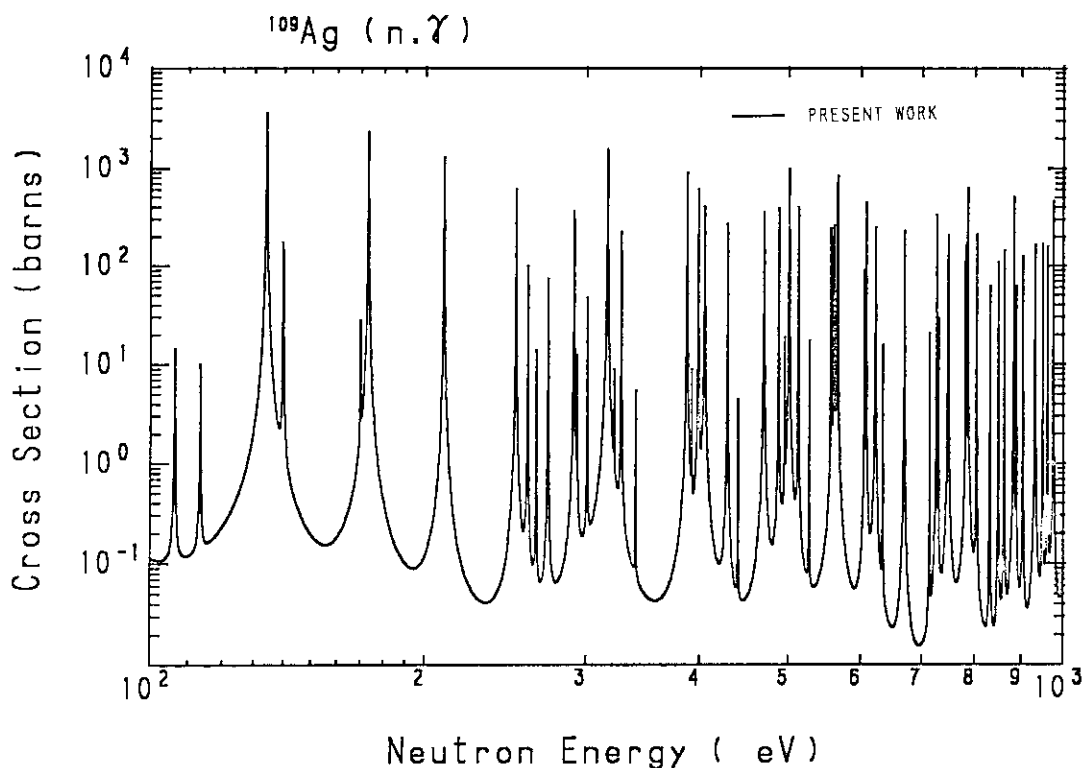


Fig. 31(d) Capture cross section of  $^{109}\text{Ag}$  in the energy region from 100 eV to 1 keV.

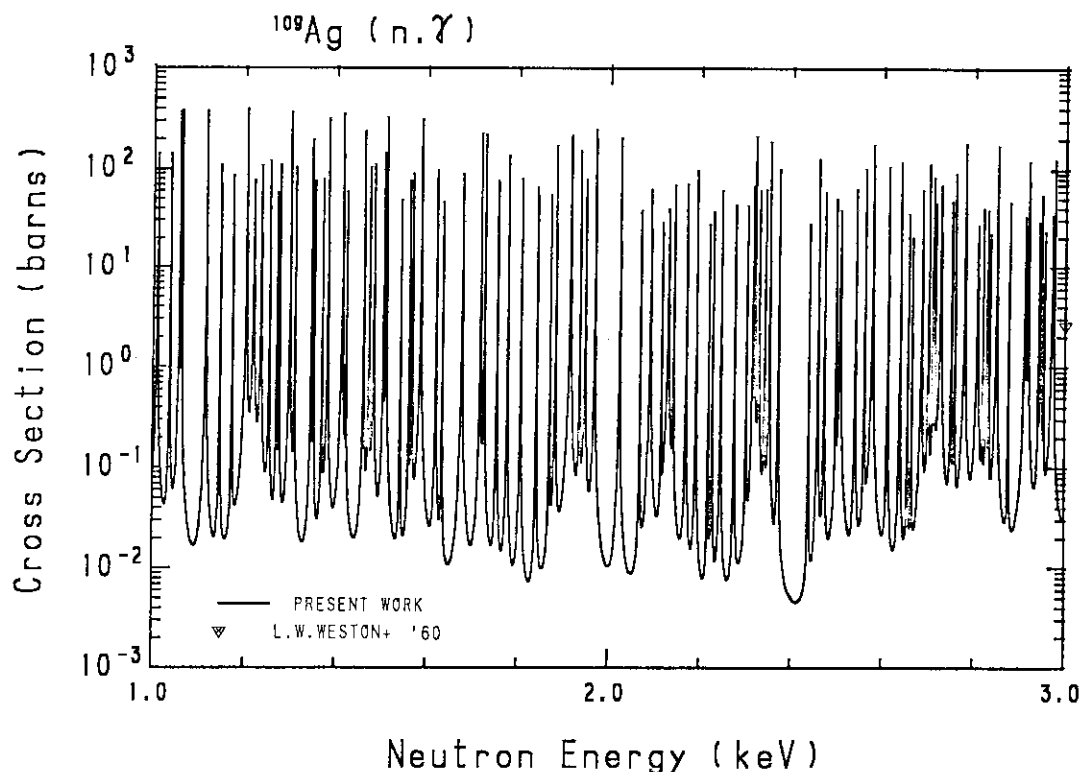


Fig. 31(e) Capture cross section of  $^{109}\text{Ag}$  in the energy region from 1 keV to 3 keV.

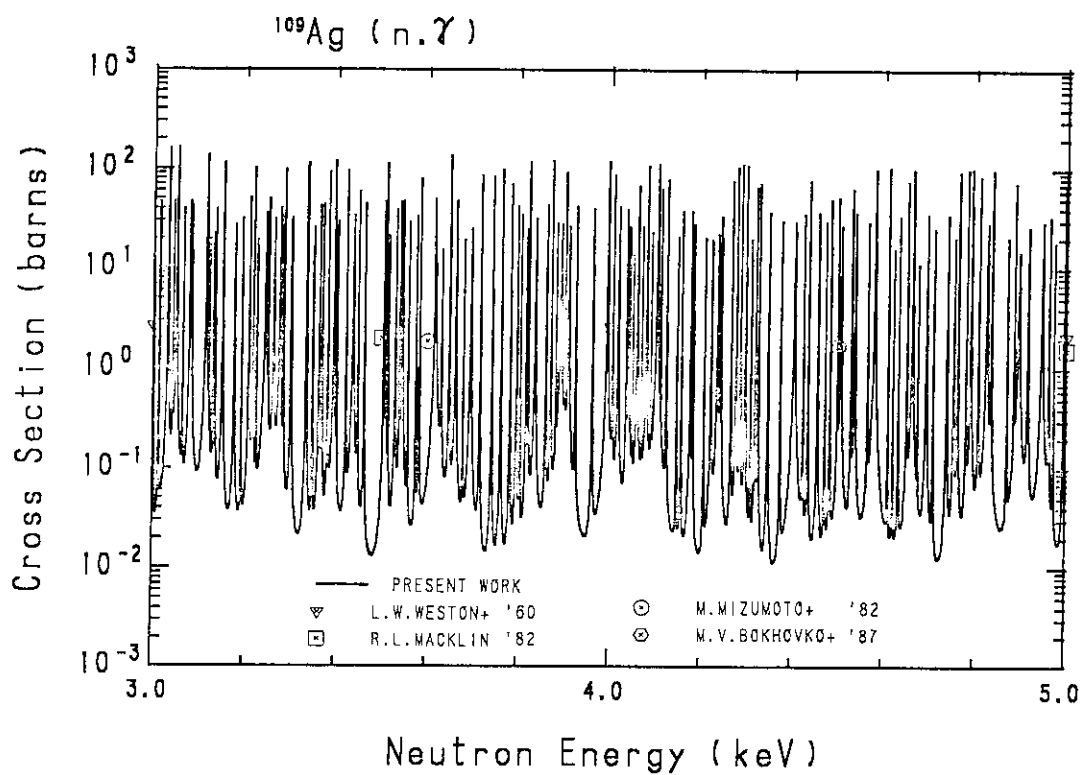


Fig. 31(f) Capture cross section of  $^{109}\text{Ag}$  in the energy region from 3 keV to 5 keV.

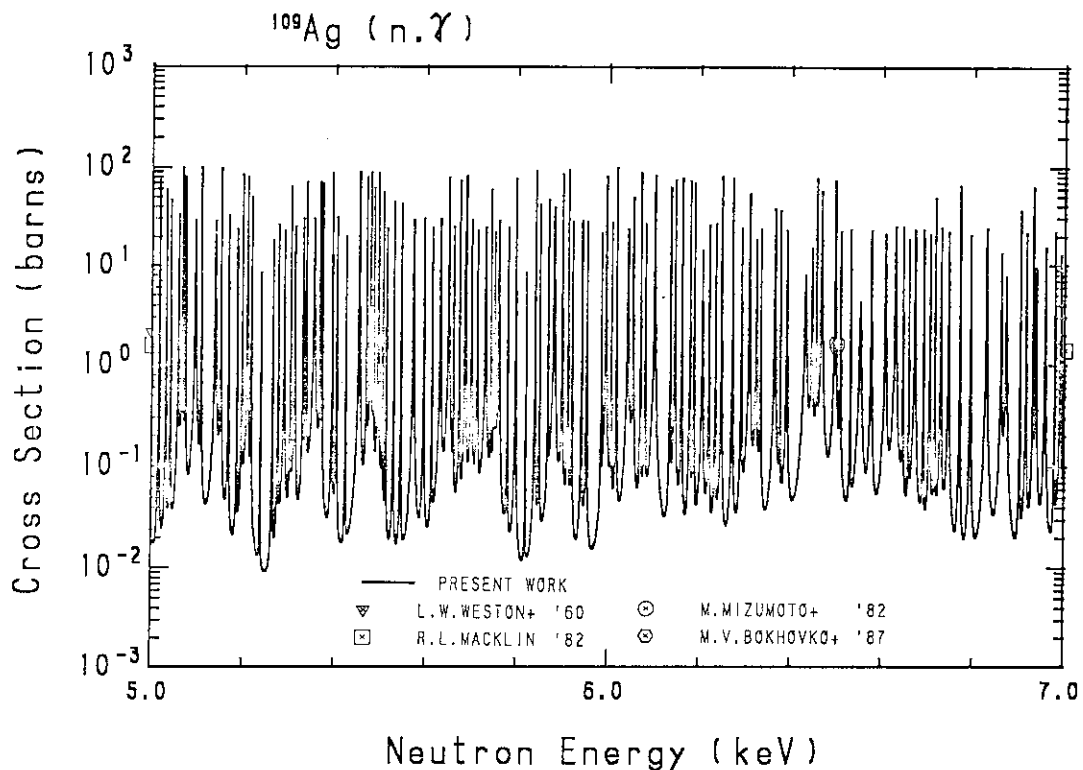


Fig. 31(g) Capture cross section of  $^{109}\text{Ag}$  in the energy region from 5 keV to 7 keV.

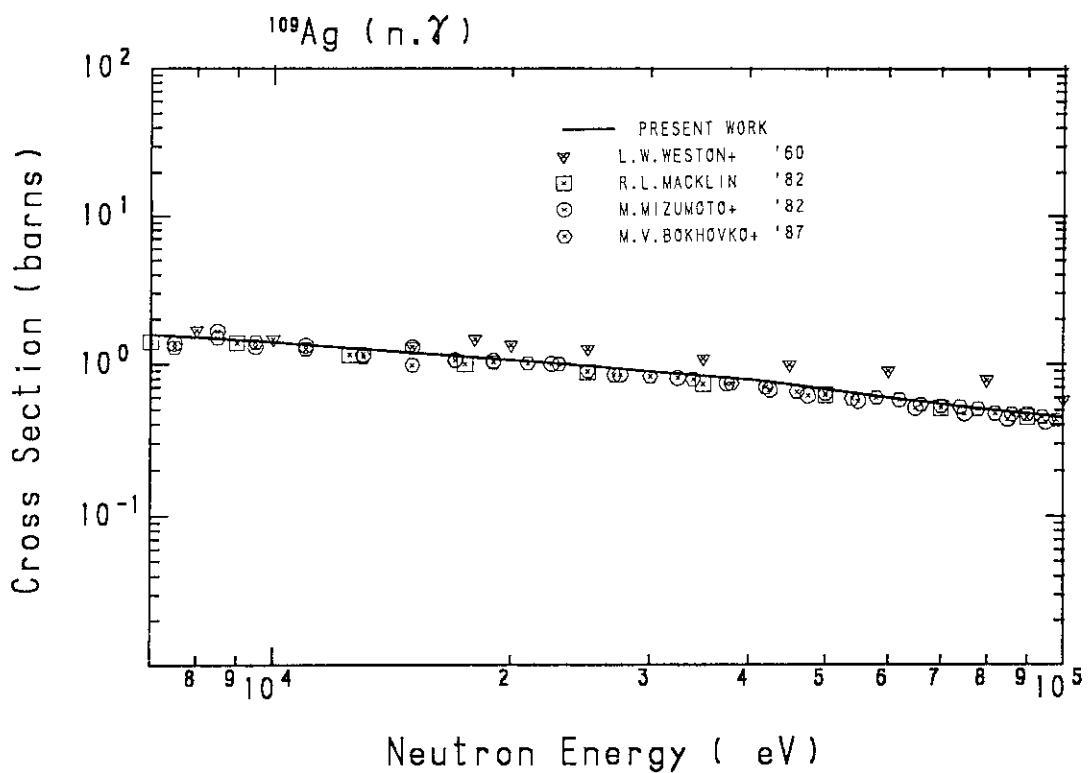


Fig. 31(h) Capture cross section of  $^{109}\text{Ag}$  in the energy region from 7 keV to 100 keV.

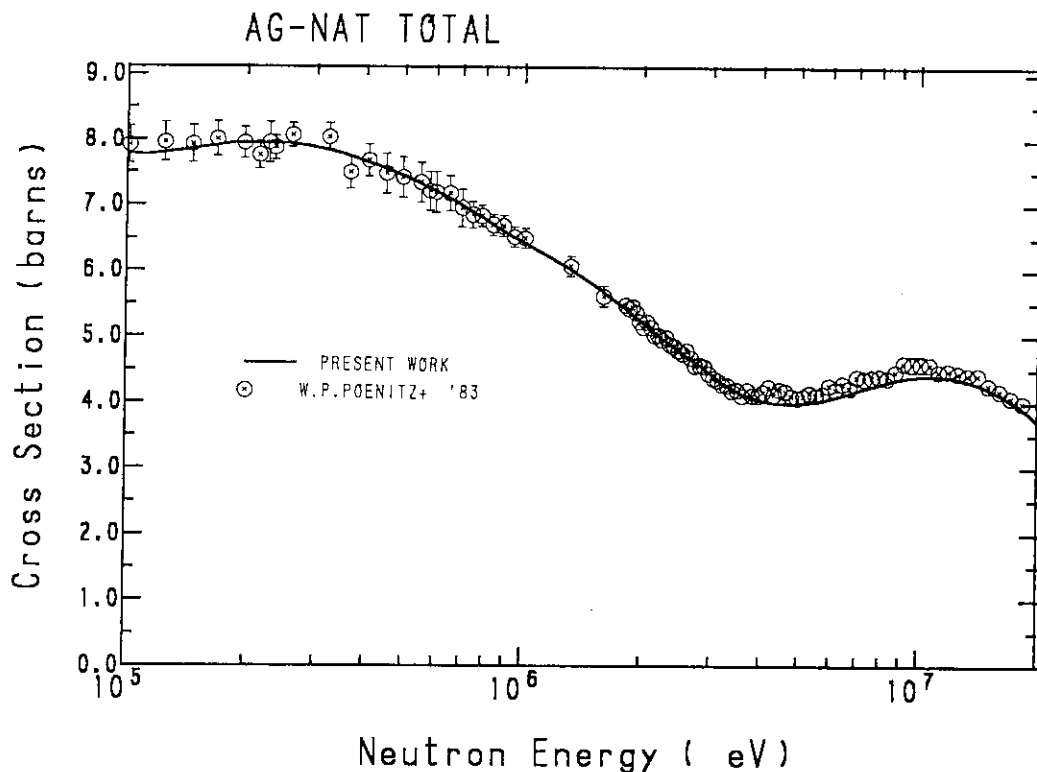


Fig. 32 Total cross section of natural silver above 100 keV.

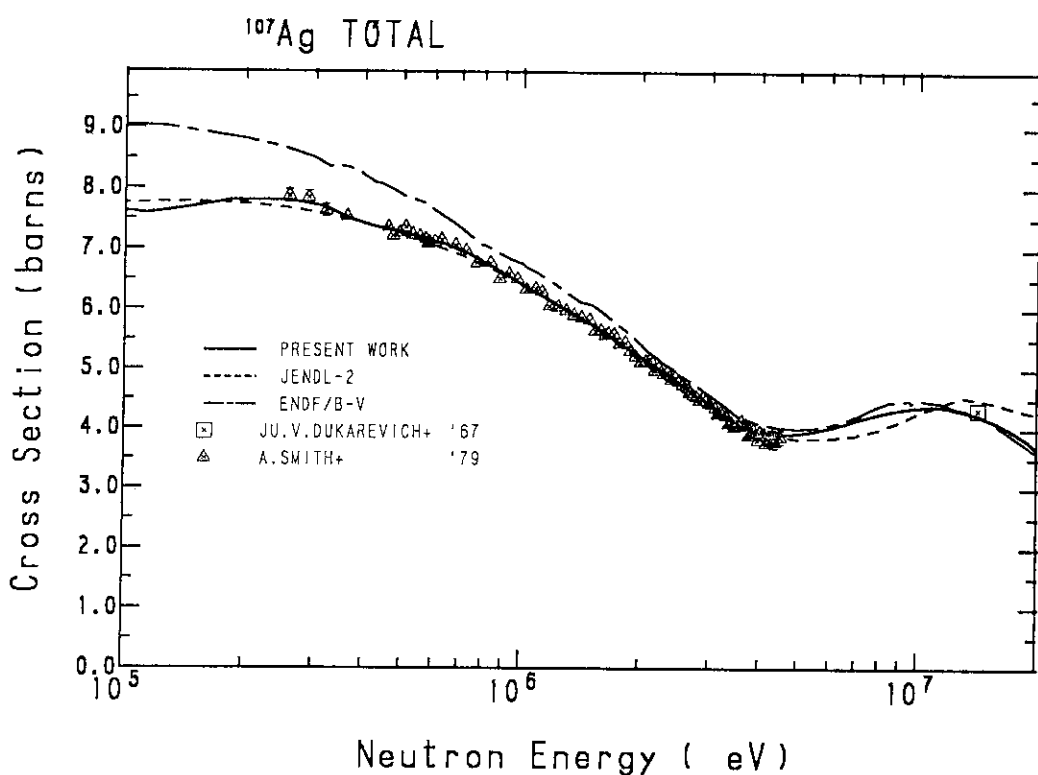


Fig. 33 Total cross section of <sup>107</sup>Ag above 100 keV.

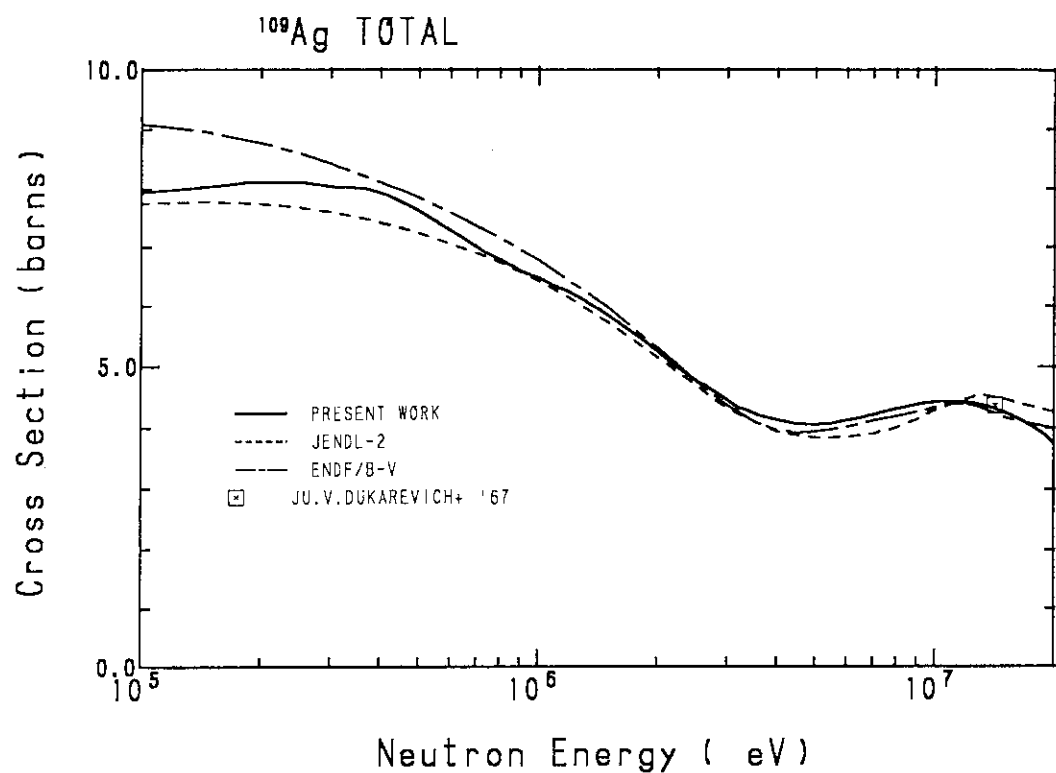
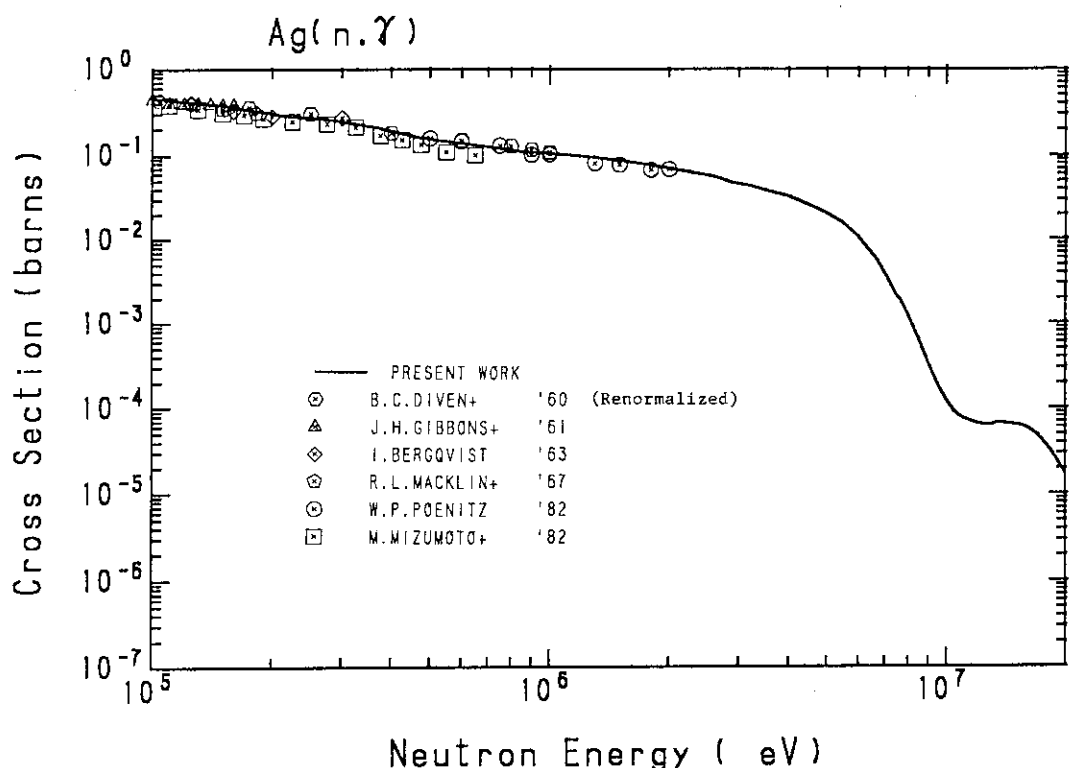
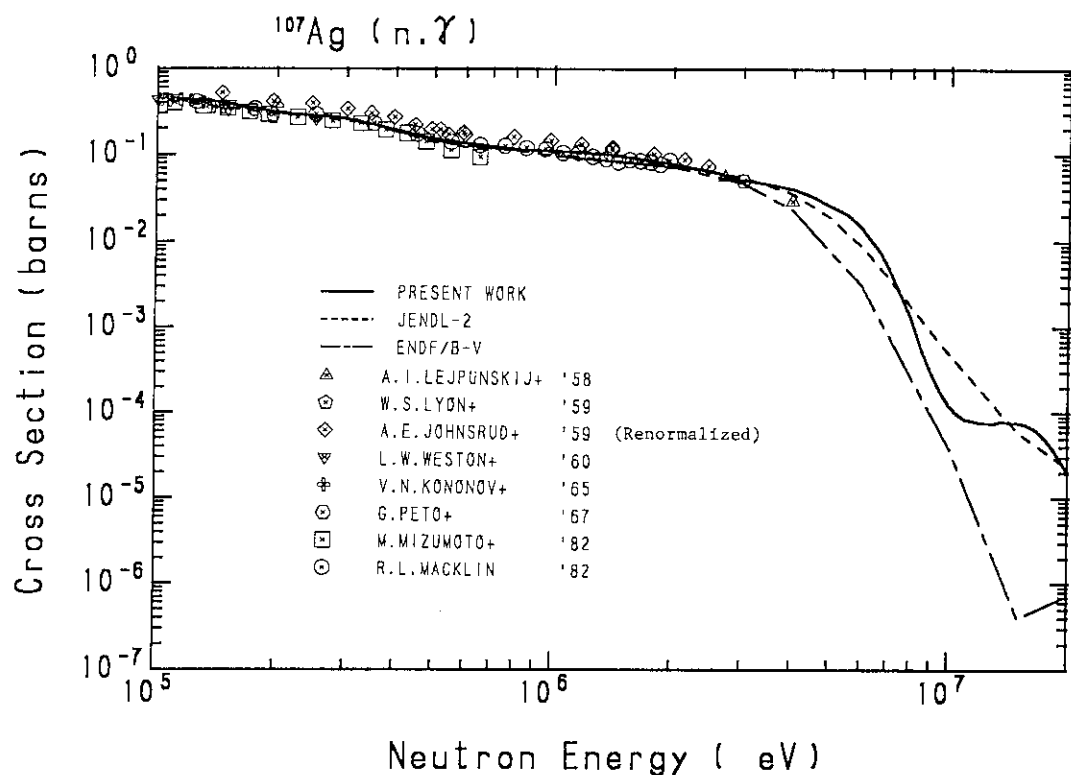
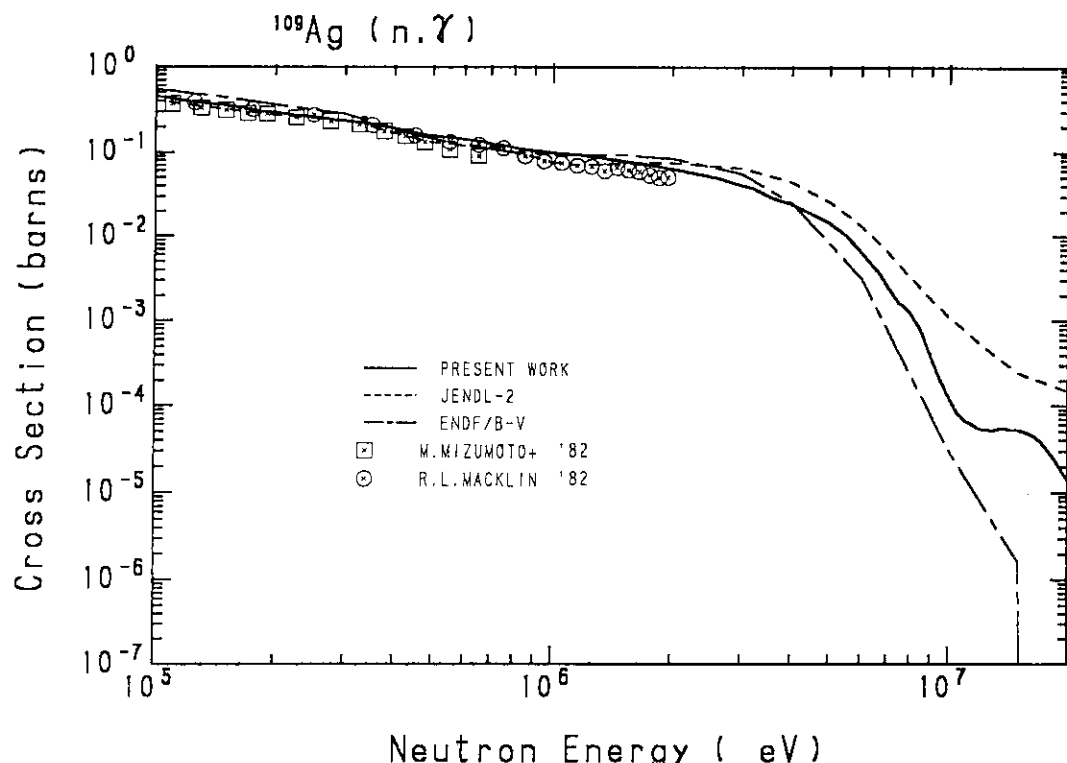
Fig. 34 Total cross section of  $^{109}\text{Ag}$  above 100 keV.

Fig. 35 Capture cross section of natural silver above 100 keV.

Fig. 36 Capture cross section of  $^{107}\text{Ag}$  above 100 keV.Fig. 37 Capture cross section of  $^{109}\text{Ag}$  above 100 keV.

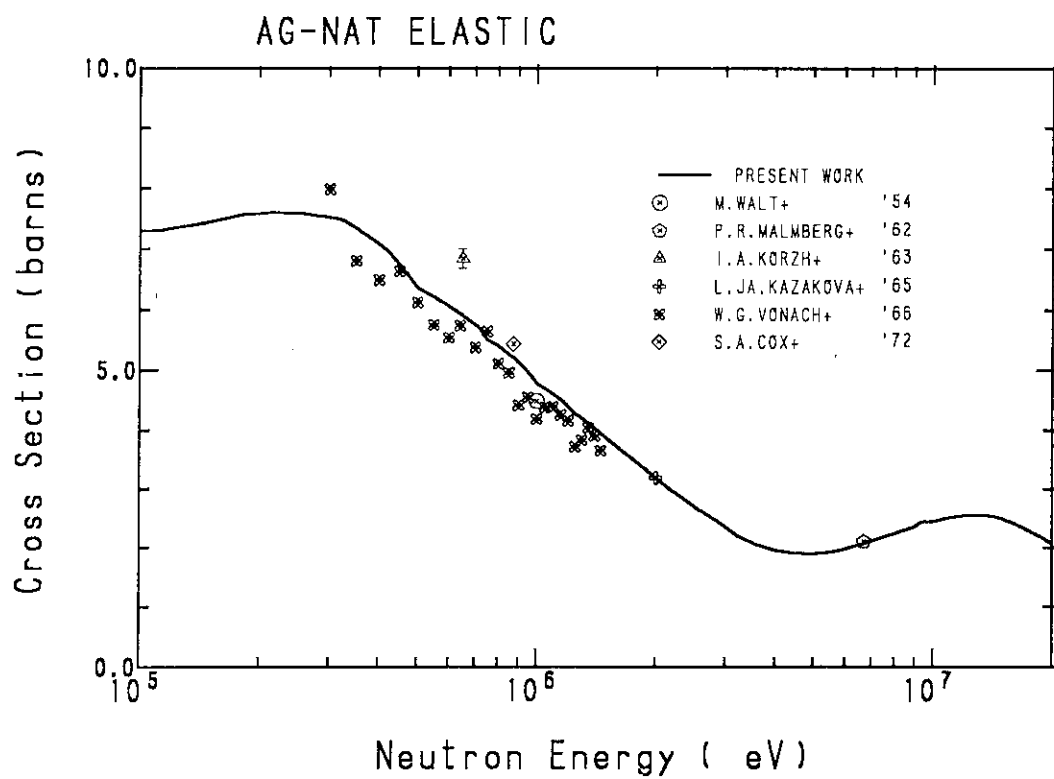


Fig. 38 Elastic scattering cross section of natural silver above 100 keV.

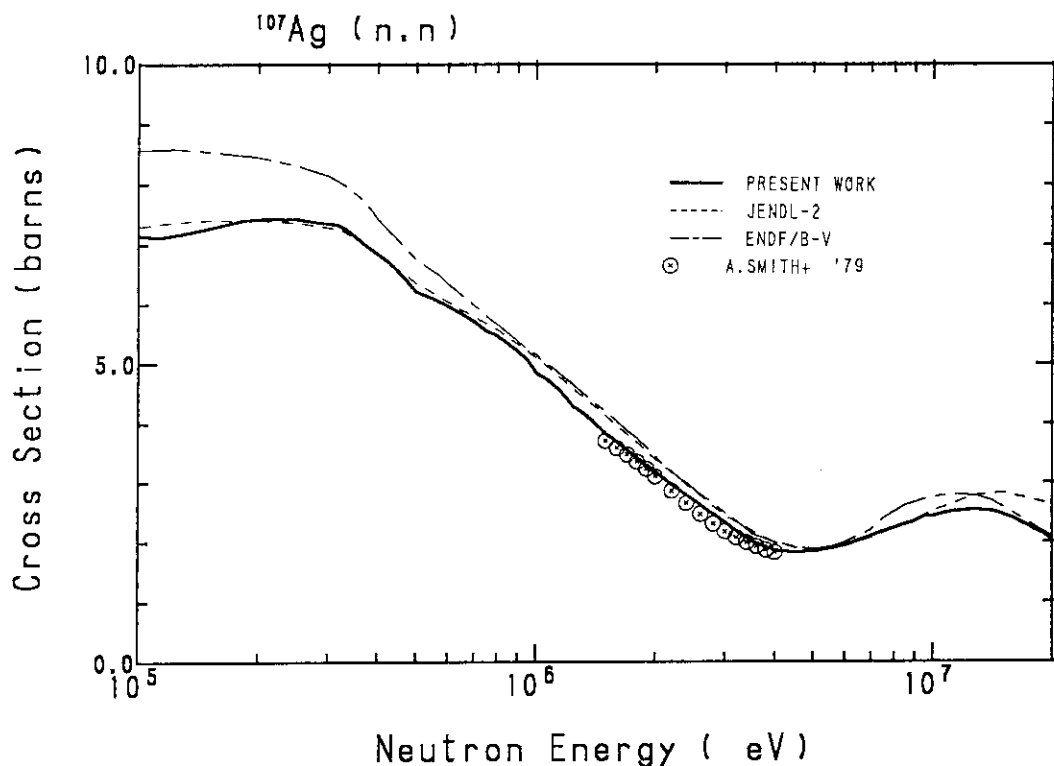


Fig. 39 Elastic scattering cross section of  $^{107}\text{Ag}$  above 100 keV.

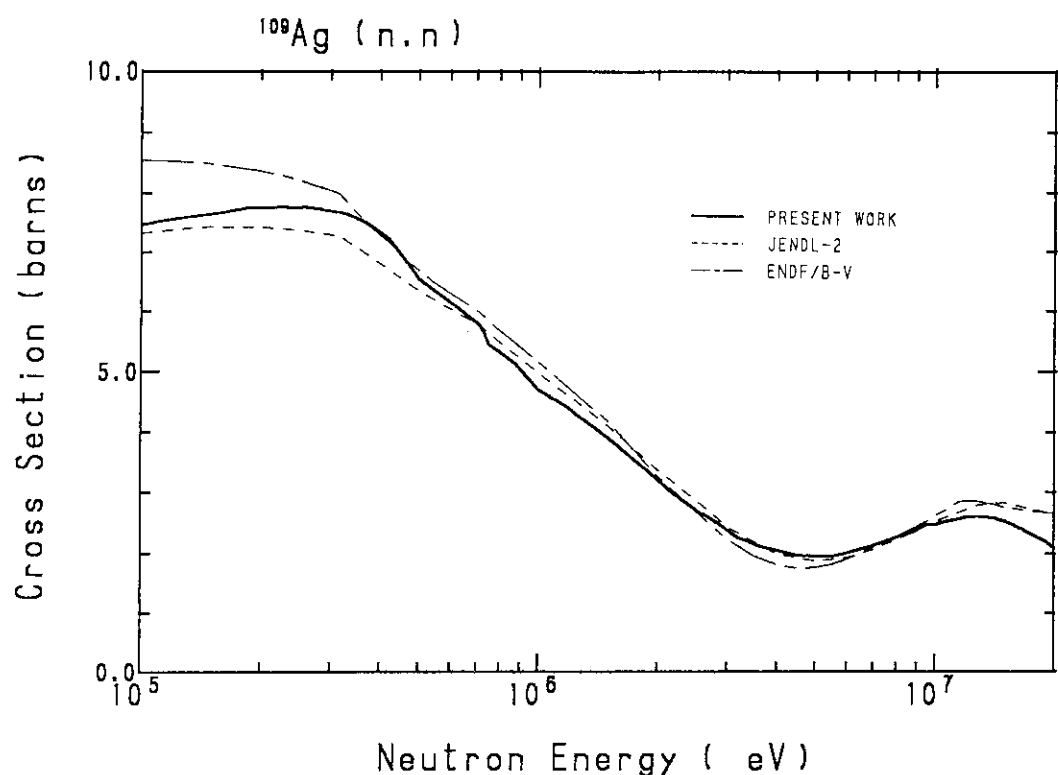


Fig. 40 Elastic scattering cross section of  $^{109}\text{Ag}$  above 100 keV.

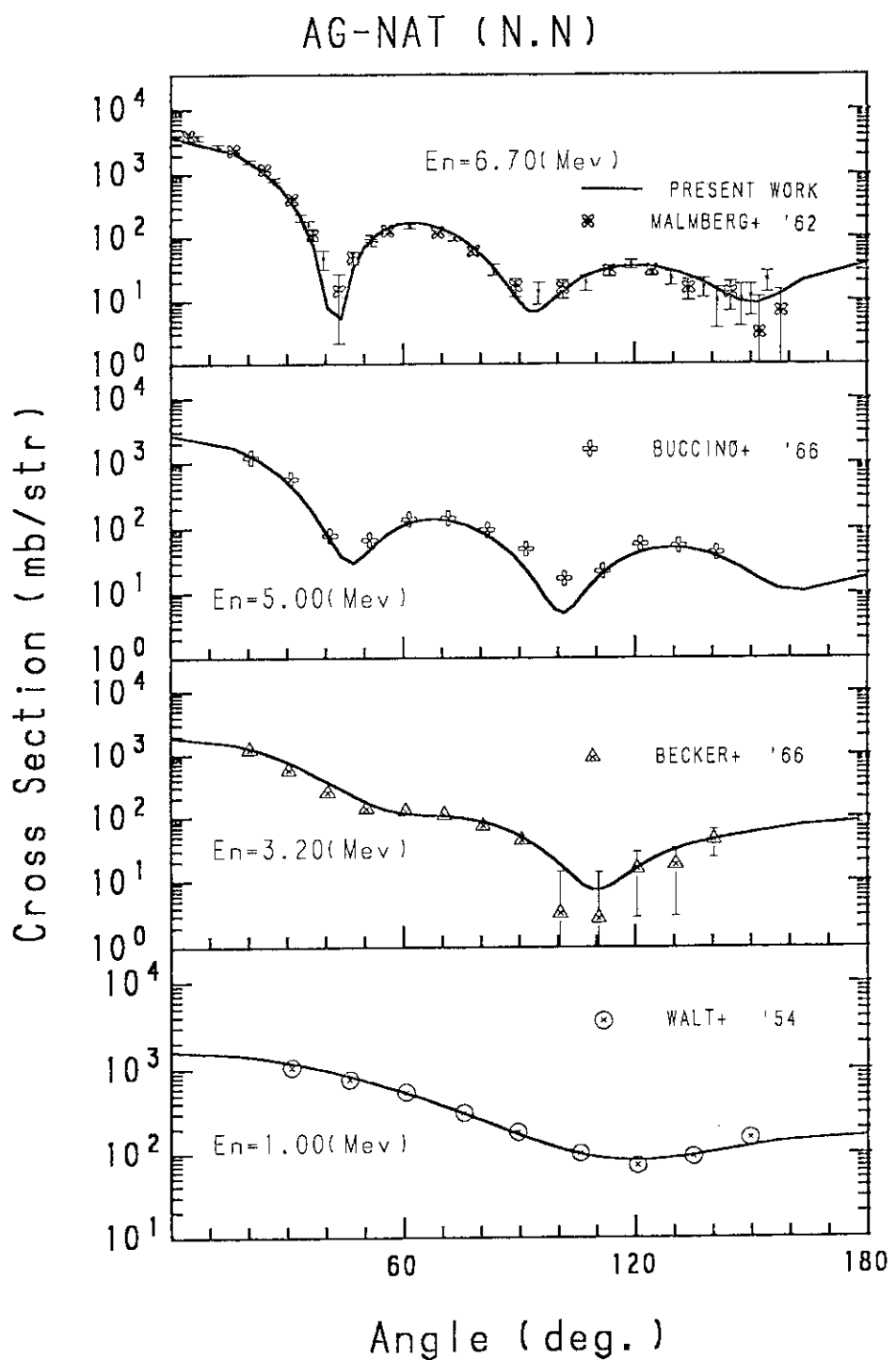


Fig. 41(a) Angular distributions of neutrons elastically scattered from natural silver at 1.0-6.7 MeV.

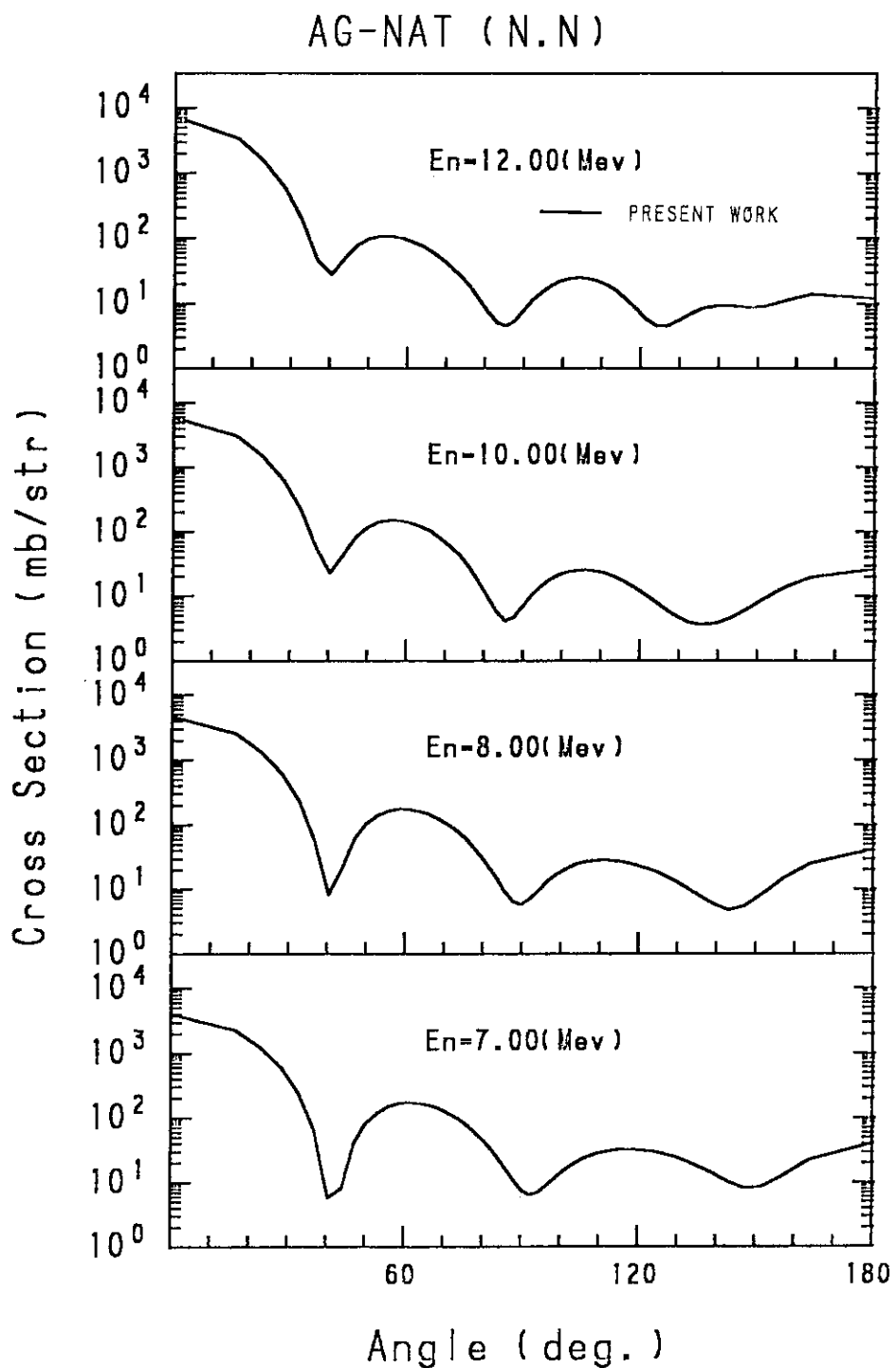


Fig. 41(b) Angular distributions of neutrons elastically scattered from natural silver at 7.0-12.0 MeV.

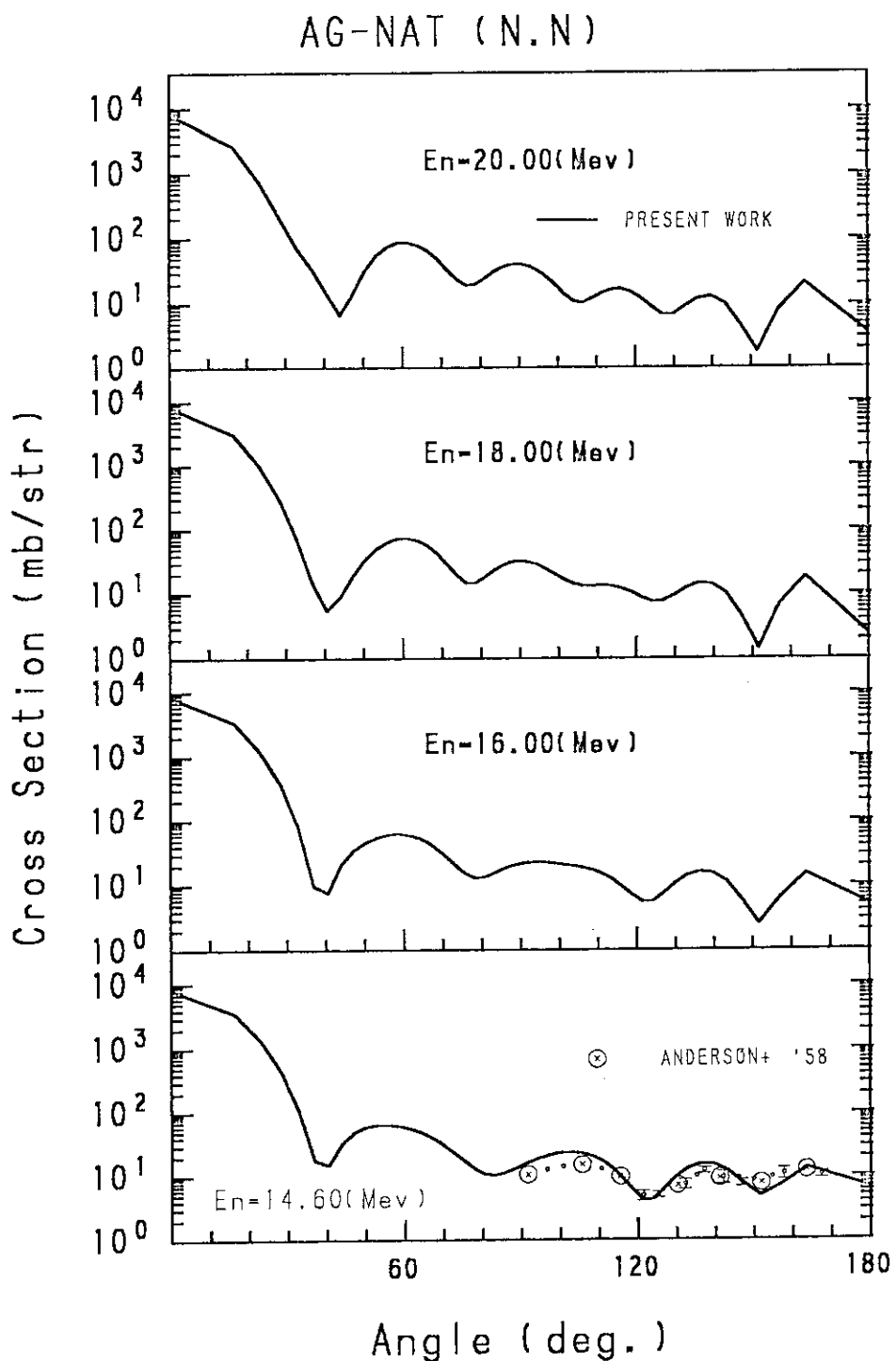


Fig. 41(c) Angular distributions of neutrons elastically scattered from natural silver at 14.6-20.0 MeV.

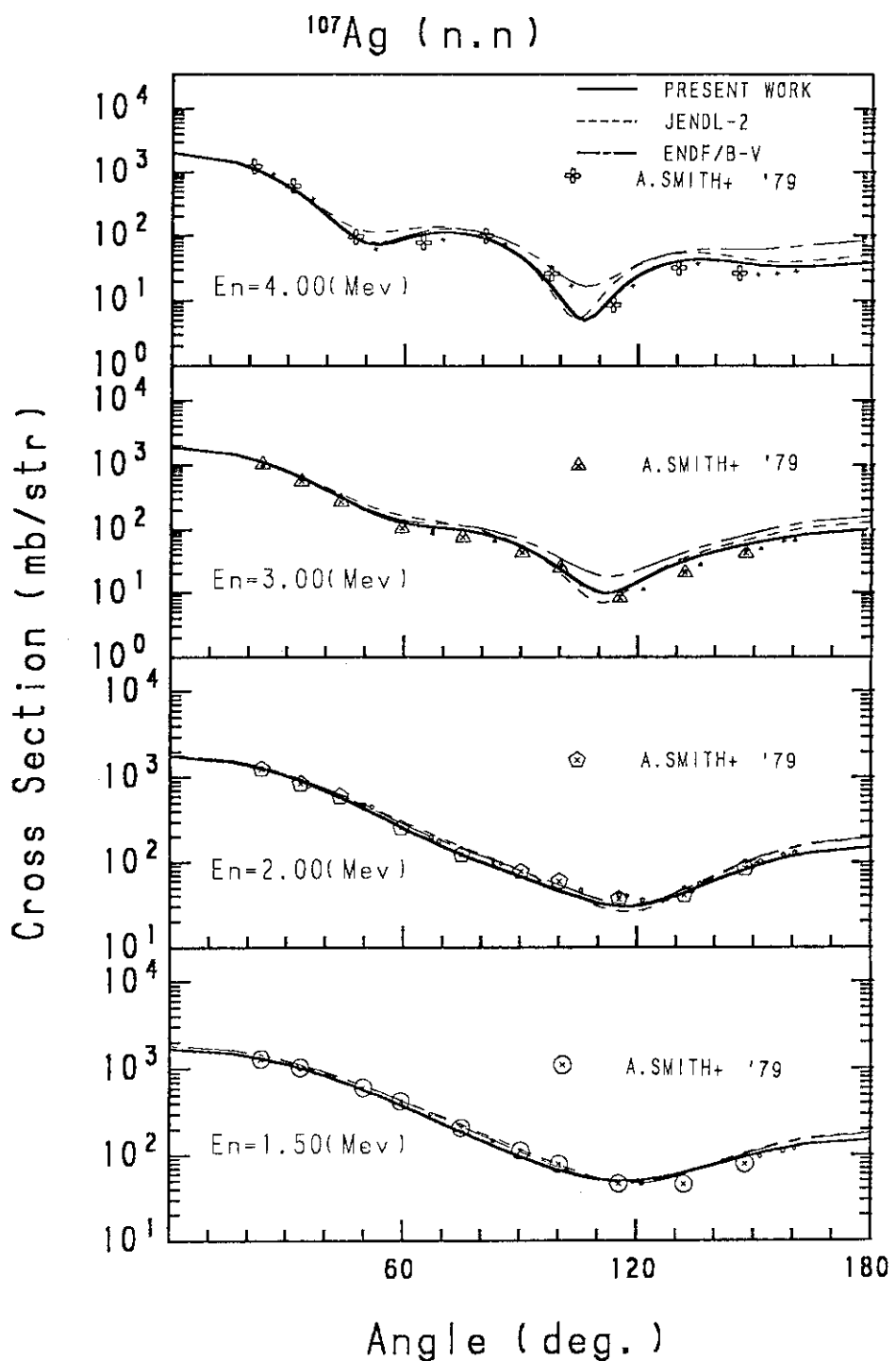


Fig. 42(a) Angular distributions of neutrons elastically scattered from  $^{107}\text{Ag}$  at 1.5-4.0 MeV.

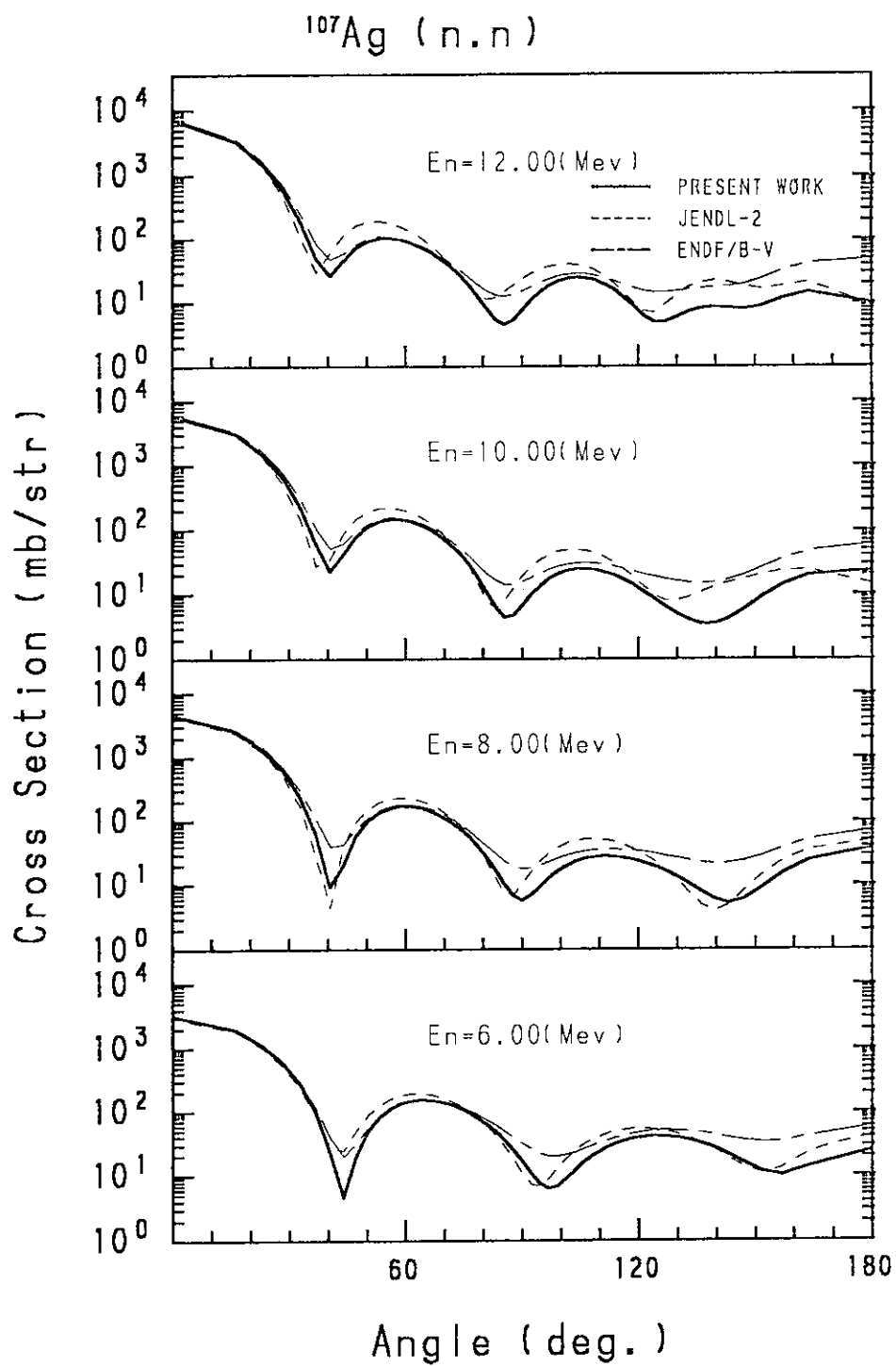


Fig. 42(b) Angular distributions of neutrons elastically scattered from  $^{107}\text{Ag}$  at 6.0-12.0 MeV.

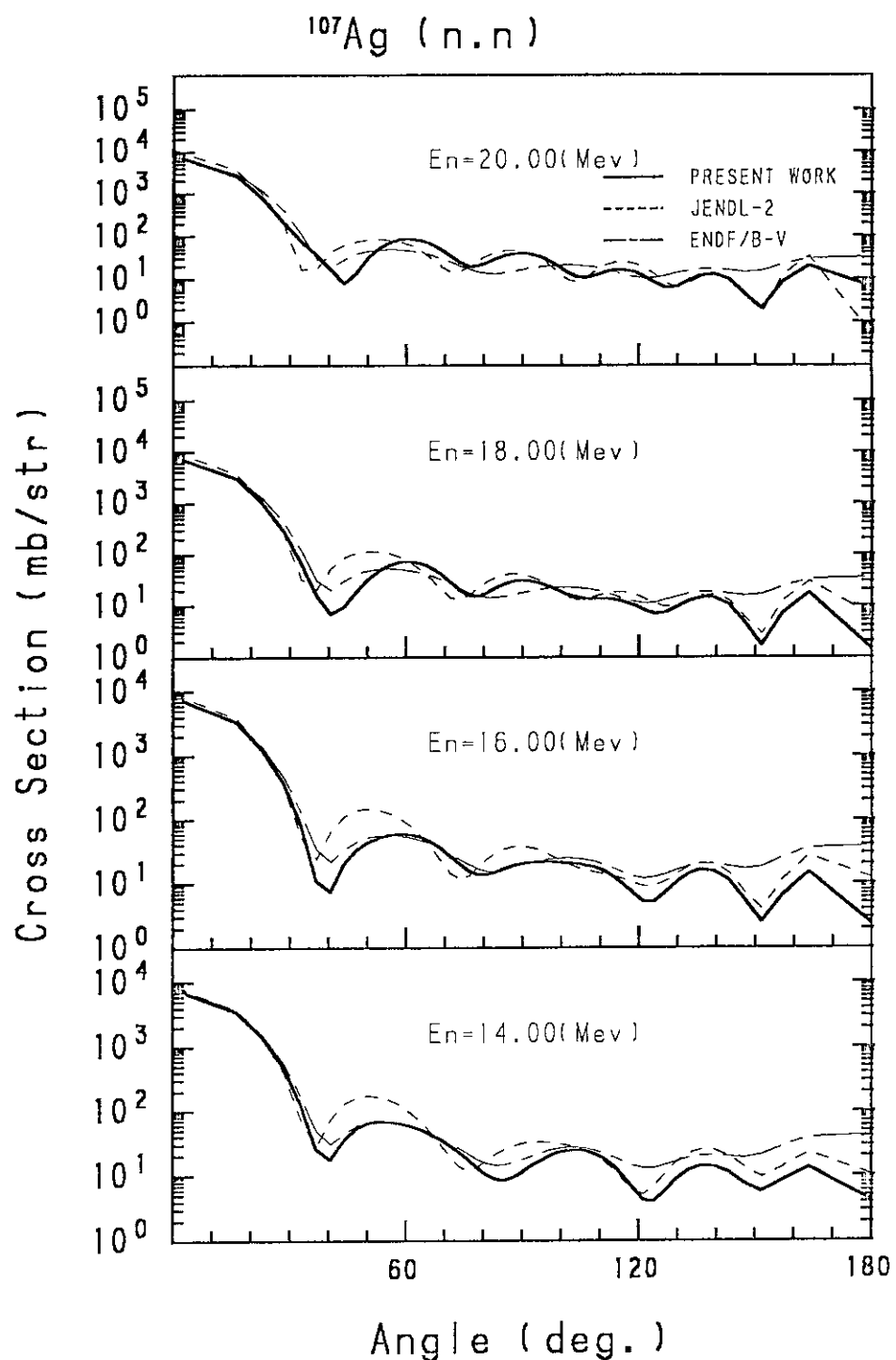


Fig. 42(c) Angular distributions of neutrons elastically scattered from  $^{107}\text{Ag}$  at 14.0-20.0 MeV.

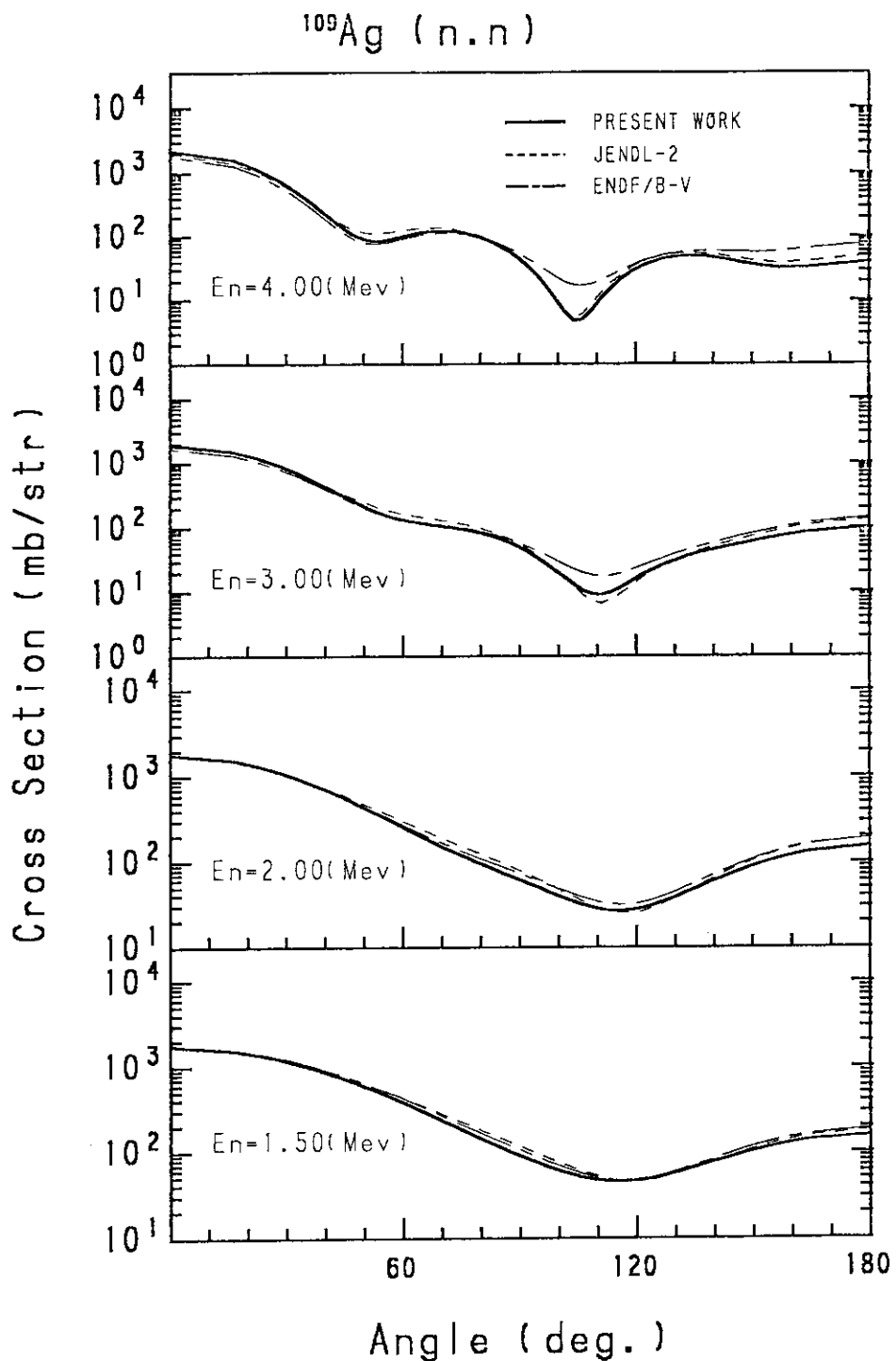


Fig. 43(a) Angular distributions of neutrons elastically scattered from  $^{109}\text{Ag}$  at 1.5-4.0 MeV.

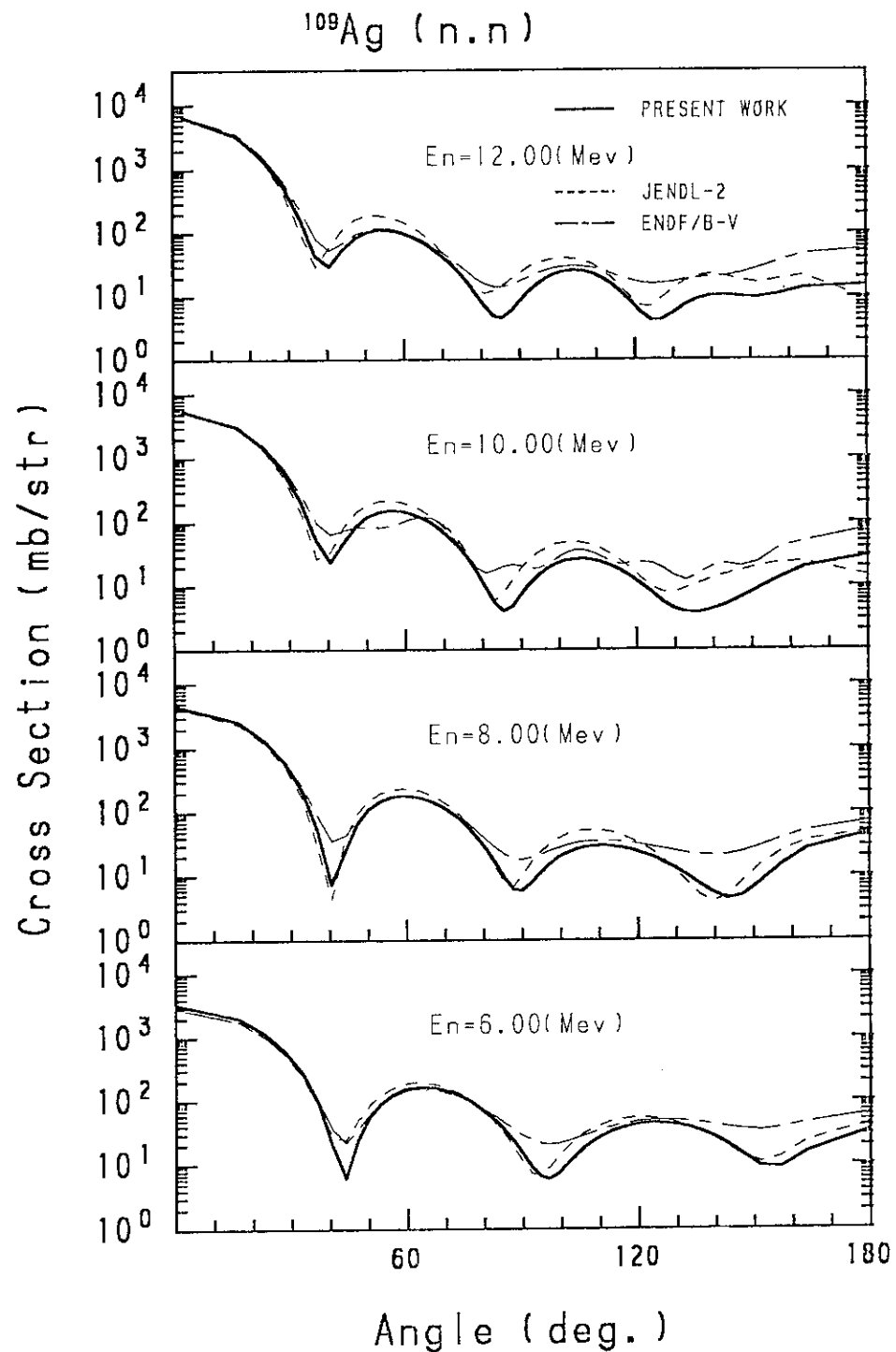


Fig. 43(b) Angular distributions of neutrons elastically scattered from  $^{109}\text{Ag}$  at 6.0-12.0 MeV.

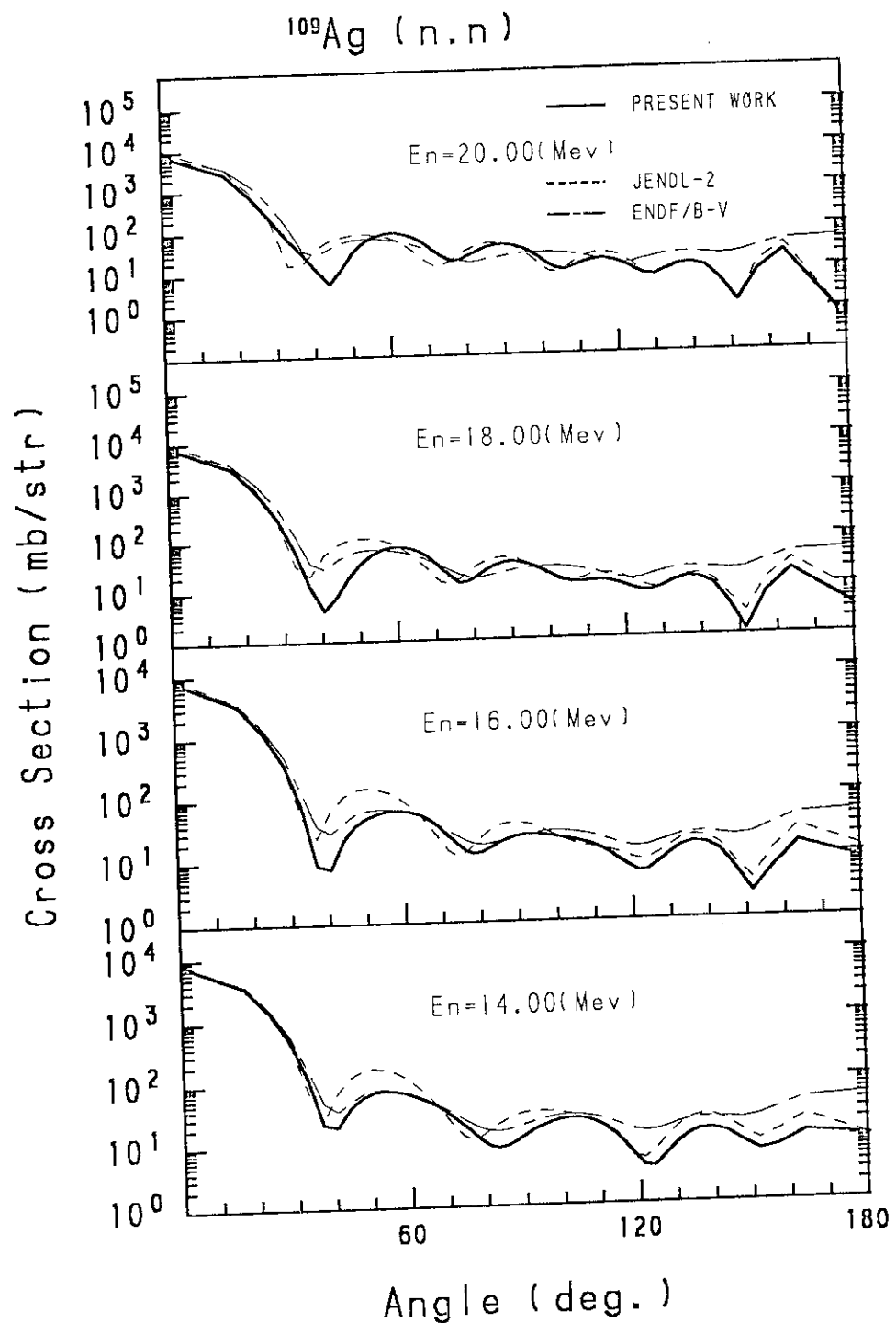


Fig. 43(c) Angular distributions of neutrons elastically scattered from  $^{109}\text{Ag}$  at 14.0-20.0 MeV.